UC Berkeley
UC Berkeley Electronic Theses and Dissertations

Title

Seismic Resilience of Regional Transportation Systems: Modeling Robustness and Rapidity

Permalink

https://escholarship.org/uc/item/2vv961n7

ISBN

9798293893058

Author

Virtucio, Michael Benedict

Publication Date

2025-08-01

Peer reviewed|Thesis/dissertation

eScholarship.org Powered by the California Digital Library
University of California

Seismic Resilience of Regional Transportation Systems: Modeling Robustness and Rapidity

by

Michael Benedict Virtucio

A dissertation submitted in partial satisfaction of the

requirements for the degree of

Doctor of Philosophy

in

Civil and Environmental Engineering

and the Designated Emphasis

in

Global Metropolitan Studies

in the

Graduate Division

of the

University of California, Berkeley

Committee in charge:

Professor Kenichi Soga, Chair
Professor Joan Walker
Professor Daniel Rodriguez

Summer 2025

Seismic Resilience of Regional Transportation Systems: Modeling Robustness and Rapidity

Copyright 2025
by
Michael Benedict Virtucio

Abstract

Seismic Resilience of Regional Transportation Systems: Modeling Robustness and Rapidity

by

Michael Benedict Virtucio

Doctor of Philosophy in Civil and Environmental Engineering

and the Designated Emphasis in

Global Metropolitan Studies

University of California, Berkeley

Professor Kenichi Soga, Chair

Seismic events can severely disrupt regional transportation systems, compromising mobility, economic activity, and emergency response. While the resilience of transportation infrastructure has been widely studied, most existing work focuses either on system robustness or on rapidity of recovery, often using static or small-scale models that limit the spatial and temporal resolution of the analysis. This dissertation addresses these limitations by developing a flexible, regional-scale framework to evaluate the seismic resilience of transportation systems along the dimensions of robustness and rapidity, incorporating both system performance and user-level impacts.

The study adopts a mesoscopic, semi-dynamic, agent-based traffic model designed to balance spatial and temporal detail with computational feasibility. The model simulates individual-level vehicle movements across large urban regions using 15-minute time steps and disaggregated origin-destination demand, enabling the capture of dynamic congestion effects and evolving network conditions during and after seismic events. This traffic simulation is embedded within broader resilience assessment frameworks that quantify degradation in system functionality (robustness) and characterize network recovery trajectories over time (rapidity), using performance indicators such as total travel time, vehicle hours traveled (VHT), and recovery curve metrics including area under the curve (AUC) and skewness.

Two case studies are used to demonstrate the utility and flexibility of the proposed frameworks. The first assesses the robustness of the Southern California transportation network under a hypothetical magnitude 7.4 earthquake along the Palos Verdes Fault. A hybrid bridge damage modeling approach was used to generate input fragility curves, and economic losses were estimated based on simulated travel delays and trip loss. Results show pronounced spatial

heterogeneity in impacts, with disproportionately high delays and losses concentrated near the Ports of Los Angeles and Long Beach. These findings suggest that resilience planning should be guided not only by exposure and structural vulnerability but also by functional importance at the system level and within regional economies.

The second case study focuses on rapidity, evaluating the recovery of the Tokyo Metropolitan Area highway system under multiple coordination strategies between two major expressway operators: the Metropolitan Expressway Company (MEX) and East Nippon Expressway Company (NEXCO). A scenario-based coordination framework was introduced to model varying levels of inter-agency coordination, including information sharing, strategy alignment, and pooled resource allocation. Results show that higher levels of coordination significantly improve recovery performance, as measured by both AUC and skewness, and help mitigate spillover congestion onto local roads. These outcomes highlight the importance of governance structures, institutional interoperability, and collaborative response protocols in post-disaster recovery.

This dissertation makes three key contributions: (1) it proposes scalable, semi-dynamic traffic modeling frameworks for regional seismic resilience analysis; (2) it operationalizes robustness and rapidity through integrated metrics and simulation outputs; and (3) it provides empirical insights into the spatial distribution of disruption and the value of inter-agency coordination in recovery. Together, these contributions support more targeted investment planning, cross-agency coordination, and data-driven decision-making for hazard mitigation and emergency response.

Para sa mga Pilipinong nangangarap ng ginhawa't sagana

Contents

Contents **ii**

List of Figures **iv**

List of Tables **vi**

1 Introduction **1**
1.1 Seismic hazards and transportation systems 1
1.2 Vulnerability and resilience 2
1.3 Research hypothesis, questions, and objectives 6
1.4 Dissertation outline 7

2 Literature review **8**
2.1 Infrastructure damage assessment 8
2.2 Traffic Modeling under Seismic Hazard Scenarios 10
2.3 Resilience and Performance Assessment 12
2.4 Summary of Research Gaps 21

3 Regional semi-dynamic agent-based traffic model **22**
3.1 Overview 22
3.2 Model description 24
3.3 Conclusion 32

4 Assessing robustness of regional transportation systems to seismic hazards: Southern California case study **34**
4.1 Introduction 34
4.2 Framework for robustness studies 34
4.3 Southern California (Ports of Los Angeles and Long Beach): case study . . . 41
4.4 Results and discussion 47
4.5 Conclusion, limitations, and suggested future work 57

5 Assessing rapidity of recovery of regional transportation systems to seismic hazards: Tokyo case study **60**

5.1 Introduction . . . 60
5.2 Rapidity metrics . . . 62
5.3 Coordination modeling . . . 66
5.4 Tokyo case study formulation . . . 69
5.5 Case study results . . . 77
5.6 Discussion . . . 80
5.7 Conclusion, limitations, and recommendations . . . 85

6 Summary and conclusions **87**
6.1 Overview of seismic resilience of transportation systems . . . 87
6.2 Mesoscopic traffic model for resilience assessment . . . 88
6.3 Robustness framework and Southern California case study . . . 89
6.4 Rapidity framework and Tokyo case study . . . 90
6.5 Institutional and policy implications . . . 91
6.6 Limitations and future directions . . . 92

Bibliography **94**

A MEX and NEXCO route groupings **103**
A.1 MEX routes . . . 103
A.2 NEXCO routes . . . 104
A.3 Grouping criteria . . . 105
A.4 MEX groups . . . 106
A.5 NEXCO groups . . . 107

B Recovery/reopening sequences **108**

C Coordination scenario recovery curves **120**

List of Figures

1.1 Dimensions of resilience (from Nozhati [77]) 3

3.1 Traffic assignment flowchart 28
3.2 Sample trips without highway closure 33
3.3 Sample trips with highway closure 33

4.1 Framework flowchart 35
4.2 Sample earthquake visualization (from Cetiner [15]) 43
4.3 Fragility functions computed for two of the modeled bridges 44
4.4 Road closure map, which includes the damaged bridges and connecting road/bridge segments assumed to also be closed for inspection. 45
4.5 Travel demand data 46
4.6 Travel time variation over 10 runs 48
4.7 Assessing impacts to transportation networks 50
4.8 Simulation results 51
4.9 Travel time distribution of port area trips 52
4.10 Change in VHT (overall area vs port area) 53
4.11 Cost per origin TAZ 55
4.12 Indirect cost and road closures 56
4.13 Cost estimate visualization 58

5.1 Resilience as area under the recovery curve (AUC) (from Frangopol and Bocchini [40]) 63
5.2 Tokyo highway network: MEX (purple) and NEXCO (green) 70
5.3 MEX route groupings 71
5.4 NEXCO route groupings 71
5.5 Hourly distribution of people outside their area of residence 72
5.6 Hourly distribution of car trips outside area of residence 72
5.7 Traffic model flowchart 74
5.8 Comparison of recovery curves 75
5.9 Scatter plot of normalized AUC vs. skewness 77
5.10 AUC-Skewness scatter plot (zoomed in) 81
5.11 Highway congestion (orange) versus local road congestion (purple) at timestep 5 83

5.12 Highway congestion (orange) versus local road congestion (purple) at timestep 15 83
5.13 Highway congestion (orange) versus local road congestion (purple) at timestep 20 84
5.14 Percentage of congested local roads across time steps 84

A.1 MEX routes 104
A.2 NEXCO routes 106

C.1 Recovery curves for Scenario 1 120
C.2 Recovery curves for Scenario 2 121
C.3 Recovery curves for Scenario 3 121
C.4 Recovery curves for Scenario 4 121
C.5 Recovery curves for Scenario 5 122
C.6 Recovery curves for Scenario 6 122
C.7 Recovery curves for Scenario 7 122
C.8 Recovery curves for Scenario 8 123
C.9 Recovery curves for Scenario 9 123
C.10 Recovery curves for Scenario 10 123
C.11 Recovery curves for Scenario 11 124
C.12 Recovery curves for random scenarios 124

List of Tables

2.1 Review of robustness studies 14
2.2 Review of rapidity studies (part 1) 18
2.3 Review of rapidity studies (part 2) 19

3.1 Comparison of traffic modeling approaches across key dimensions. 24
3.2 Node headers 25
3.3 Edge headers 25
3.4 Aggregation categories from Tokyo Person Trip Survey 26
3.5 Demand headers 27
3.6 edge_vol headers 31
3.7 trip_info headers 31

4.1 Travel demand summary 44
4.2 Port area measures 49

5.1 Coordination scenarios 76
5.2 Final coordination scenarios 78
5.3 Normalized AUC and skewness (mean and standard deviation) for each scenario 79
5.4 Normalized AUC and skewness for random scenarios 80
5.5 Percentage of total congested road length on local roads 82

Acknowledgments

It's been quite a ride, and I still can't quite believe I'm here at the end. It's been six years since I started my journey here in Berkeley, and so much has happened and changed since that wide-eyed, naïve, ambitious guy got off that 51B bus at College Ave. and Bancroft Way on a fantastically foggy morning. Since then, I've lived through a global pandemic and lockdowns, unbelievable political seesaws across the world, and, well—just growing up. Now, standing at the finish line with this finalized dissertation in hand, I'm happy and proud.

Back in 2018, after attending my first academic conference in Tokyo, my eyes were opened to the possibilities of technology and research—particularly in transportation and mobility—which served as the catalyst that pushed me to apply to graduate school. To the people who helped me with my applications back then—Christine, Abby, Keziah, and Ralen—I'm grateful for your encouragement and support. I hope you're as happy as I am to see this journey finally come to a close.

To the people and institutions that made this journey possible in the first place: my deepest gratitude to the Department of Science and Technology's Science Education Institute for funding me throughout my PhD. A special shoutout to Dr. Joel Marciano for helping me secure this support from the get-go.

To my academic supervisors and colleagues—thank you. The biggest thank you to Prof. Kenichi Soga and Bingyu Zhao for sticking with me through the ups and downs, the starts and stops, of this long journey. I share this achievement with you. A huge thank you as well to members of the Soga Research Group, particularly Nanda, Paola, and Pengshun—thank you for the advice, the conversations, and the company. To Prof. Steve Glaser, Prof. Joan Walker, Prof. Daniel Rodriguez, and Prof. Desiree Fields—thank you for your guidance, feedback, and kindness as I navigated this rollercoaster. To CEE staff—Shelley, Robbie, and Sara—thank you for helping me through all the administrative hoops and logistics of grad life.

None of this would've been remotely possible without my friends and community. Through the uncertainty, the anxiety, the listlessness, and the depression, I'm endlessly grateful for the people who lifted me up when I was down and kept me company when I couldn't handle the isolation. To my early friends that first year at I-House, particularly Allen, Hans, Gavin, and Meghna—thank you for the friendship during that time of beginnings and uncertainty. To the most fabulous community I've ever been part of—Convent in the Fall of 2020—thank you for making me feel so loved and at home, especially Holly, Tanner, and Vincent, whose friendship and support I still cherish to this day. To those I've met at and through Convent since—Sarina, Raquel, Ellis, Jules, Adesewa, Yakira, Dom, Liam—thank you for truly seeing and rooting for me. To my badminton buddies through the years—Lincoln, Ming, Harry, and Koki—thank you for being a constant presence throughout this journey, letting me smash my stress away and keep alive a hobby I've loved for close to a decade now. To my Filipino friends through the years—Mar, Fredmar, Joy, Alben, and Renz—thank you for the support and sense of community I can only find with people who share my culture and lived experience.

To classmates turned friends I've met along the way—Alex, Alden—thank you for choosing to continue hanging out with me outside the classroom.

To the counselors at the Tang Center—particularly Paige and Mar—thank you so sincerely. Your support helped me survive the hardest emotional stretches. To the libraries across campus and the staff who keep them running: thank you. Special shoutout to the dissertation writers' room, Main Stacks, and the Art History and Classics Library, where I wrote much of this dissertation.

Finally, to my dearest family—whose physical presence I still continue to crave—I would not have made it without your prayers and company. Thank you for your love; thank you for being there whenever I had no one else. Mom and Dad, Patricia and Renzo, Kuya Jason, Gab, and Sam, I love you dearly.

At some point during my PhD, I realized that the experience is different for everyone. It's a fool's errand to stack yourself against others—to wonder why it seems so easy for them and so difficult for you. That said, I've come to embrace and accept everything about this ride. If at any point during this journey I've been your collaborator, your classmate, your friend, your teacher, or just your acquaintance—thank you for enriching this experience in one way or another.

There's still so much life to live and so many lessons to learn as I enter this next phase of my life. With much anxiety but also excitement as I leave this chapter to start a new one—thank you so much, UC Berkeley, for the ride!

Chapter 1

Introduction

1.1 Seismic hazards and transportation systems

Natural hazards pose a significant risk to the critical infrastructure of an area, and each area may be more prone to certain hazards than others. For example, places like California are more prone to earthquakes and wildfires due to their geographic location, whereas states in the Southeast and Midwest of the United States are more prone to flooding. Some hazards are easier to forecast and, consequentially, to prepare for, while others are more unpredictable and, therefore, can cause more damage and losses. Earthquakes are a good example of the latter. A report by FEMA estimates that the US incurs a minimum Annual Earthquake Loss (AEL) of $6.1 billion, not yet including losses due to damage to lifeline infrastructure and indirect economic losses; it further indicates that 55 metropolitan areas account for 85% of this AEL [51]. With urbanization concentrating population and infrastructure in cities, areas with high seismic hazard and high building exposure—such as Los Angeles and San Francisco Bay—rank high on AEL at over $100 per capita [51].

The US Cybersecurity and Infrastructure Security Agency (CISA) defines critical infrastructures as systems that are key to society's daily operations and any impairment, disruption, or destruction of which can have significant to devastating impacts on physical or economic security, public health, or safety [96]. An example of this is transportation infrastructure, which this study focuses on. Transportation systems provide mobility to people, goods, and services that are vital to society's daily operations, making them even more important in times of crisis [63] for scenarios like evacuation. These infrastructure systems are built based on standards established at the time of construction, ensuring a level of quality for a set amount of time. However, various factors, such as a lack of funding or oversight, can lead to the upkeep of these infrastructures being overlooked. For example, bridges are considered one of the more vulnerable parts of a transportation system, as they connect two points while hanging over land or water. In the US, the average age of bridges is 43 years, very close to the typical 50-year design life [3], and ASCE estimates that $123 billion (2017 values) are needed to rehabilitate all US bridges. Discussions on transportation systems' vulnerability

and resilience therefore become very crucial.

With these risks in mind, this study aims to better understand various aspects of the resilience and recovery of regional transportation systems under seismic hazards, particularly how they can be measured and improved with an increased focus on the impacts on their users, both on the individual level and on the system level.

1.2 Vulnerability and resilience

Definition and dimensions

Before proceeding, it is necessary to first define resilience and vulnerability of transportation systems. A quick look at previous literature shows that these terms have been defined across different disciplines. For example, Goldberg [41] defined resilience in socio-ecological systems as "the size of the perturbation that the system can withstand and still retain its essential characteristics". This definition transfers well into civil infrastructure systems, as Berdica's landmark study more than a decade ago similarly defines reliability in road transportation systems as the complement of vulnerability—"a susceptibility to incidents that can result in considerable reductions in road network serviceability" [7]. Reductions in road network serviceability are the most direct impact of a lack of resilience in the transportation infrastructure; however, impacts can have more far-reaching implications than just a longer travel time. Disruptions to the connectivity of the transportation system can result in economic losses for a variety of sectors [24]. Given the unpredictability of a large earthquake and its potentially devastating impacts in certain areas, it is important to adopt a holistic definition of resilience that encompasses the direct and indirect impacts of seismic hazards on the transportation system and the economy at large.

In broad strokes, the landmark work by Bruneau et al. [11] started to define which areas to focus and conduct research on to develop a more well-rounded view of resilience, particularly seismic resilience of communities. They defined four dimensions, namely:

- robustness, defined as "strength, or the ability of elements, systems, and other units of analysis to withstand a given level of stress or demand without suffering degradation or loss of function",
- redundancy, defined as "the extent to which elements, systems, or other units of analysis exist that are substitutable, i.e., capable of satisfying functional requirements in the event of disruption, degradation, or loss of functionality",
- resourcefulness, defined as "the capacity to identify problems, establish priorities, and mobilize resources when conditions exist that threaten to disrupt some element, system, or other unit of analysis; resourcefulness can be further conceptualized as consisting of the ability to apply material (i.e., monetary, physical, technological, and informational) and human resources to meet established priorities and achieve goals", and

- rapidity, defined as "the capacity to meet priorities and achieve goals in a timely manner in order to contain losses and avoid future disruption".

These dimensions are shown in Figure 1.1 from Nozhati [77]. Bruneau et al. [11] note however, that while all dimensions of resilience are important, robustness and rapidity are seen as key in measuring system and community resilience. Figure 1.1 shows that robustness and rapidity are consistent with the functionality and time axes, respectively, while resourcefulness and redundancy have more to do with the shape of the recovery curve. Changes in the shape of the recovery curve can be captured by the robustness and rapidity dimensions. Intuitively, setting robustness and rapidity as the key dimensions makes sense, since the two questions typically asked about the resilience of transportation systems are: (1) how much damage is expected to be incurred by the system, and (2) what is the best strategy to recover the quickest. This is evident in prior research in this space that can be divided into those that either look at robustness or those that look at rapidity, as will be discussed in Chapter 2.

Therefore, in this study, resilience is interpreted to mean the capacity of a system to retain functionality after experiencing an extreme event and to quickly recover from it.

Resilience analysis of transportation systems

In the context of this dissertation, the term "transportation systems" refers exclusively to road-based networks, encompassing private automobiles and freight vehicles. Public transit modes (e.g., bus, rail) are excluded from the scope of analysis due to their distinct infrastructural and operational characteristics, as well as limited data availability necessary

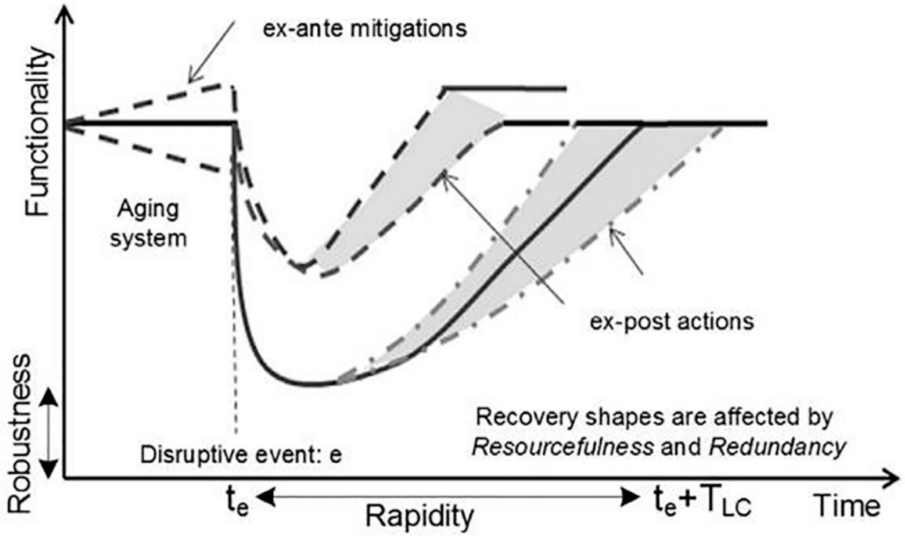


Figure 1.1: Dimensions of resilience (from Nozhati [77])

for consistent integration within the modeling framework. In order to analyze the resilience of transportation systems, a specific traffic model has to be chosen to represent the traffic conditions for the time and area of study. Traffic models in resilience analysis studies have evolved over the years. In previous decades with less data and computing resources, it was common to simply use aggregate numbers for traffic flow, volume, etc. to represent the traffic conditions over specific time periods. However, as newer data and technology have arisen, it has become the trend to model traffic down to the individual with as high spatial and temporal resolution as possible to more accurately replicate reality. Regardless of whether the study being conducted is for robustness or rapidity, different temporal and spatial resolutions can affect the quality of the results, analysis, and discussion that can be extracted from the work.

Different levels of temporal and spatial resolution can be mapped onto different types of traffic models—whether they are static or dynamic traffic models [23], or whether they are macroscopic or microscopic ones. Static traffic models are time-independent, meaning they assume that traffic conditions are in a steady state and do not vary over time. These models assign flows across a network based on average conditions, typically assuming user equilibrium without capturing dynamic congestion effects. They are commonly used for long-term or strategic planning. For example, a static model might compute the shortest travel time between zones based on average traffic levels across the network. On the other hand, dynamic models are time-dependent and capture the changes in traffic conditions over time. For example, a dynamic model can simulate the movement and behavior of cars/drivers as they react to a sudden roadblock over time. In terms of the difference between macroscopic and microscopic traffic models, macroscopic (or link-based) models treat traffic as a fluid instead of vehicles and tend to use aggregate variables for flow, density, and speed for each link. This is common in large-scale simulations where only the changes in flow are being tracked. Microscopic (or agent-based) models simulate individual vehicles and track the changes in their status over time. Although this is more detailed, realistic, and provides a granular understanding of traffic dynamics, it is computationally expensive.

Most traffic models in older studies are static and link-based [91, 57, 72] and therefore, do not update over time. This leads to simulations that do not necessarily capture driver behavior very accurately, if at all, and thereby make the results less intuitive. More recent studies are starting to take a dynamic, agent-based approach to traffic modeling to account for changes in individual movement or behavior in the hopes of also making results more realistic and understandable [18, 37]. However, this comes with a higher requirement for computational power and storage.

This raises a practical challenge: how can transportation systems be modeled with high temporal and spatial resolution while keeping computational and storage demands manageable? While this dissertation does not provide a formal comparison of model efficiencies, it adopts mesoscopic models as a pragmatic approach that balances detail and computational feasibility. Mesoscopic models simulate individual vehicle behavior but do so using simplified rules and aggregated movement patterns within groups. This allows them to capture behavioral dynamics with more realism than macroscopic models, while avoiding the intensive

computational demands of fully microscopic, agent-based simulations.

One such example is the semi-dynamic agent-based model introduced by Zhao et al. [104]. This approach is semi-dynamic in the sense that traffic conditions are updated at fixed intervals (e.g., every fifteen minutes), rather than continuously as in fully dynamic models. This discretization in time reduces computational load while still allowing the model to capture key changes in traffic patterns and driver behavior over time. The model was shown to perform efficiently and yield reliable results in a case study of San Francisco.

This combination of regional coverage, individual vehicle representation, and moderate computational requirements makes the semi-dynamic mesoscopic model well-suited for seismic resilience analysis, where traffic conditions can rapidly change following a disruption. This study adopts such a model as a core component of the proposed frameworks for both robustness and rapidity assessment.

Another important consideration is the spatial scale of resilience. The impact of seismic hazards, in particular, can span multiple cities or counties; therefore, resilience analysis must be conducted on a similar, regional scale. For robustness studies, a regional scale of analysis would allow analyzing system or sector interdependencies when it comes to cascading impacts (e.g., breakdown of transportation system leading to restriction of the flow of goods, further leading to business impacts). For rapidity studies, using a regional scale will also allow for the analysis of the impacts of regional factors on how quickly functionality is restored. For example, as different agencies or organizations across a region manage various parts of the transportation infrastructure, how much impact can their level of coordination among each other have on the rapidity of recovery of the transportation system?

The possibilities opened up by applying a regional scale stands in contrast with some previous studies that conduct resilience analysis on a local scale [68, 18]. While smaller scale studies allow for faster experimentation, testing, or optimization of recovery strategies (e.g., ranking all links in the network to determine the optimal repair sequence), they do not necessarily translate to the larger scale as computational expediency is chosen over incorporating different characteristics and redundancies of regional road and highway networks into the traffic model.

An example of a good regional study is done by Wein et al. [100] as part of USGS's "HayWired" scenario study that looks into the potential impacts of an earthquake along the Hayward fault in California. Their work focuses on a spatial analysis of industries, employment, and commute flows in areas of concentrated damage. For example, some of their results include a breakdown by county of damage to non-residential versus residential buildings, and an analysis of impacted industries also broken down by county. Another example is an analysis showing employed residents and workers in concentrated-damage areas, broken down by county. It also shows the effects across counties, since it also shows whether people live and work in the same area or not. This level of analysis is only possible with a regional scale and high temporal and spatial resolution, as they are able to highlight which areas are more severely impacted than others. This study therefore adopts a regional scale of analysis with high temporal and spatial resolution in constructing frameworks for robustness and rapidity studies of transportation systems.

1.3 Research hypothesis, questions, and objectives

This study aims to better understand the resilience of regional transportation systems under seismic hazards, particularly how resilience can be measured and improved with greater attention to impacts on both individual users and the system as a whole. It identifies robustness and rapidity as two key dimensions of resilience and develops corresponding analytical frameworks for each. These frameworks incorporate, among other components, a mesoscopic traffic model applied at a regional scale. They are demonstrated through two case studies: a robustness analysis conducted on the road and highway network in the Southern California area, and a rapidity analysis on the road and highway network in the Tokyo Metropolitan Area.

Hypothesis

Regional-scale transportation resilience frameworks that integrate seismic damage modeling, agent-based traffic simulation, and performance-based metrics can reveal new insights into the spatial, temporal, and institutional drivers of network performance under disruption and recovery.

Research Questions

1. What modeling strategies balance temporal and spatial resolution, behavioral realism, and computational scalability in large-scale traffic simulations of disrupted networks?
2. Which performance metrics best capture system robustness and rapidity, and how well do they reflect spatial and institutional variation in transportation resilience?

Research Objectives

1. Develop a mesoscopic, semi-dynamic, agent-based traffic model tailored for regional-scale analysis of transportation systems under seismic disruption.
2. Establish a modeling framework and define metrics for robustness to quantify immediate system degradation and economic impact after seismic events.
3. Establish a modeling framework and define metrics for rapidity to evaluate system recovery trajectories and assess the role of coordination in recovery.
4. Demonstrate the utility of the frameworks through application to two regional case studies.
5. Evaluate how geographic, structural, and institutional factors influence transportation system performance and resilience.

1.4 Dissertation outline

Chapter 2 presents a review of related literature across three key domains that inform this study: (1) infrastructure damage assessment under seismic events, (2) traffic modeling in the context of seismic hazard, and (3) resilience and performance assessment.

Chapter 3 introduces a mesoscopic, semi-dynamic, agent-based traffic model that is used throughout the study. It outlines the rationale for this modeling approach, describes the model's structure, parameters, and flexibility, and discusses how it can be adapted to different applications, along with its limitations.

Chapter 4 presents the proposed framework for robustness analysis and demonstrates its application to a deterministic hypothetical earthquake scenario near the Ports of Los Angeles and Long Beach in the Southern California region.

Chapter 5 presents the proposed framework for rapidity analysis and applies it to a case study involving hypothetical highway closures in the Tokyo Metropolitan Area following an earthquake. This chapter also explores the effects inter-agency coordination between highway operators with jurisdiction over Tokyo's interconnected highway network.

Finally, Chapter 6 summarizes the key findings of the study, discusses its limitations, and outlines directions for future research.

Chapter 2

Literature review

Seismic resilience studies of transportation systems are typically structured around three core components [58]: infrastructure damage assessment, traffic modeling, and resilience or performance assessment.

Infrastructure damage assessment involves modeling how various components of the transportation network, such as roads, bridges, highways, and tunnels, respond to a specific hazard. For example, bridges are often characterized by fragility curves, which relate structural properties (e.g., span length, construction material) to the probability of reaching different damage states. These damage estimates inform post-event functionality levels and expected recovery timelines.

The next step is to simulate traffic under both pre- and post-disaster conditions. Once the functionality of infrastructure components has been estimated, traffic models are used to analyze how disruptions affect flows across the network. Studies have employed a range of modeling approaches, from static to dynamic and from macroscopic to microscopic. These models enable estimation of key performance indicators such as changes in flow, travel time, trip completion, and network accessibility.

The final step pertains to resilience or performance assessment. This may focus on how system functionality evolves over time or extend further to capture downstream social and economic impacts. The specific metrics used often depend on which dimension of resilience, such as robustness or rapidity, is being analyzed.

This chapter reviews prior work across these three key domains. It highlights how existing studies have approached each component and identifies limitations, particularly in integrating them at the regional scale with sufficient spatial and behavioral resolution. These gaps directly motivate the modeling strategies and analytical frameworks developed in the chapters that follow.

2.1 Infrastructure damage assessment[1]

[1]Portions of this section draw from a published version of this work in the *International Journal of*

While transportation infrastructure has many components, many previous studies have focused on the impact that seismic hazards have on bridges in particular. This is because bridges and other elevated structures are particularly vulnerable to seismic damage by design. Furthermore, damages to bridges (or their failure) can have larger consequences on public safety, emergency response, and the economy at large. This section thus focuses on previous work in bridge modeling for predicting seismic damage.

Bridge modeling for predicting seismic damage

Assessing the seismic vulnerability of bridges consists of two main tasks. The first is the hazard characterization (e.g., the magnitude and epicenter of an earthquake, as well as the intensity or ground motion that characterize the severity of the probabilistic hazard at a location). The second task is the development of models or relationships that establish a connection between the hazard characteristics (e.g., an earthquake intensity measure) and the severity of the damage to the bridge. Previous work on resilience assessment has used different approaches in modeling the effects of seismic hazards on bridges. Some focus on analyzing past earthquake scenarios and therefore use historical data collected on bridge damage to aid in quantifying costs and resilience [19]. For those more concerned with predicting the effects of future or hypothetical scenarios, a popular way to model bridges' behavior under seismic hazards is through the use of fragility curves that take into account different types of bridge material and composition and their historical behavior under earthquake scenarios [76]. HAZUS developed by FEMA has a database, including those from the National Bridge Inventory (NBI), of such curves that have been used extensively by prior studies [40]. NBI has a comprehensive database of bridges, including information like year built, year reconstructed, material type, functional classifications, etc. Works like Padgett, DesRoches, and Nilsson [81], which sought to model 375 bridges for South Carolina, simplified classifications using two characteristics: span configuration and girder material type, leading to 11 bridge types. However, a common method employed by some studies is to assume that bridges in an area have the same structural type, mostly modeled as multi-span simply supported (MSSS) reinforced concrete or steel bridges to simplify bridge modeling and analysis [74, 37, 18]. Although this makes modeling simpler and easier, it can fail to incorporate certain characteristics that are structure-specific or site-specific.

Recently, new data sources have been explored to inform the development of more detailed and granular structural models for bridges: Google Street View and satellite images are just a few of these new data sources that are also openly available. Their use cases have been demonstrated in Cetiner [15] and Cetiner et al. [16], where highly accurate models for individual bridges are constructed in a semi-automated image-based process. This focus on structure- and site-specific bridge modeling is in line with the emphasis on Chapter 1 regarding higher temporal resolution of the transportation system modeling, and is therefore incorporated later in this study.

Disaster Risk Reduction [99].

Furthermore, although bridges are more vulnerable to seismic hazards, other studies have also pointed out the importance of also understanding seismic impacts on regular road networks. This is also very relevant when it comes to understanding road closures, when they happen, and how long these closures last, especially when it comes to studies on rapidity. Pioneering work by Misra et al. [67] presents empirical data they were able to collect through an expert opinion survey that can lead to more accurate models and estimates of road and bridge closure times based on their level of damage. This can be explored in more detail in future work.

2.2 Traffic Modeling under Seismic Hazard Scenarios[2]

Traffic simulation models are widely used in various applications to understand the effect of different circumstances or interventions on the status quo. These models can be categorized into two. The first is macroscopic modeling, in which traffic flow is represented in terms of aggregate measures like flow, space-mean speed, and traffic density. Payne [83] states that these models sacrifice detail for efficiency and the ability to analyze problems of much larger scope. Microscopic models, on the other hand, perform simulations at the level of individual vehicle movement [83]. The main drawback of microscopic models is the high computational demands required to run simulation models, especially for large networks. For example, Wu, Hou, and Chen [102] used microscopic models to simulate traffic flows of a very small transportation network with only around 30 links and 20 nodes. Some studies have tried to find the middle ground between macroscopic and microscopic models to find a good balance between granularity and simplicity.

Another way to categorize traffic models is to determine whether they are static or dynamic. Static traffic models, such as the all-or-nothing or user equilibrium assignment methods, are time-independent—they assume that traffic conditions represent an average or steady state over a defined period, such as the peak hour. These models incorporate congestion through volume-delay functions, but do not capture how traffic evolves over time [68, 72, 24]. This allows for the analysis of slightly larger networks with Modarres and Zarei [68] analyzing 534 links and Cho et al. [24] analyzing up to 20,000 links. Alipour and Shafei [1] used static traffic assignment but operated at the traffic analysis zone (TAZ) level with 1,527 TAZs representing Los Angeles and Orange Counties—an approach that sacrifices a considerable amount of spatial resolution as each TAZ covers 4 square miles on average. Zhou, Banerjee, and Shinozuka [106] used traffic assignment at the node level but condensed the origin-destination (OD) pairs to only 148 representative nodes in the network.

Unlike static models, dynamic models explicitly take into account temporal changes in travel demand and network conditions [18, 76]. They are able to model how traffic builds up, propagates, and dissipates across the network over time, making them more suitable for analyzing phenomena such as queueing and the effects of signal timing or incidents. They

[2]Portions of this section draw from a published version of this work in the *International Journal of Disaster Risk Reduction* [99].

resemble reality more closely but take more time and computational resources to execute compared to static models. Chang, Elnashai, and Spencer Jr [18] for example only analyzes 25 nodes and 75 links while Nojima and Sugito [76] analyzed 100 links and 30 nodes.

The above traffic models are then applied to a study network, which can vary in size. Previous studies have used these traffic models on varying spatial scales to analyze seismic resilience. For example, Chang, Shinozuka, and Moore [20], Nojima and Sugito [76], and Cho et al. [24] all study regional networks while Modarres and Zarei [68] and Chang, Elnashai, and Spencer Jr [18] study a smaller and more local setting. However, as mentioned in Chapter 1, seismic hazards can have regional impacts, and so it is appropriate to also use a regional scale in resilience analysis.

Tables 2.1, 2.2, and 2.3 enumerate a select list of resilience studies over the past couple of decades. These studies illustrate a trade-off between choosing a regional scale with low temporal and/or spatial resolution—typically involving static or macroscopic traffic models, or none at all—as seen in Chang, Shinozuka, and Moore [20], Chang and Nojima [19], Padgett, DesRoches, and Nilsson [81], Kilanitis and Sextos [56], and Barati, Yazici, and Almotahari [6]. In contrast, other studies adopt higher temporal and/or spatial resolution using dynamic or microscopic traffic models, but are limited to a local scale, as in Modarres and Zarei [68], Chang, Elnashai, and Spencer Jr [18], Nakanishi, Matsuo, and Black [72], and Sohouenou and Neves [88]. The former is not able to capture changes in traffic conditions, especially in time-sensitive applications like evacuations, and is not able to distinguish the variation in spatial impacts. The latter, while good for testing and experimenting strategies, does not necessarily scale as they fail to capture regional characteristics that may not be present in local networks alone (e.g., local roads as redundancies to highway networks). Furthermore, as mentioned in Chapter 1, the impacts of seismic hazards span multiple cities/counties and therefore require a regional view of the system; likewise, the traffic model used for such work must match the intended area of study. Wein et al. [100] provides a good example of work done on a regional scale, albeit not solely transportation-focused. They study what they dub the "HayWired" scenario, which investigates the potential impacts of an earthquake along the Hayward fault in California, looking specifically at industries, employment, and commute flows in areas of concentrated damage. For example, they are able to generate results that include a breakdown by county of damage to residential versus nonresidential buildings, or a breakdown by county that shows employed residents and workers in concentrated-damage area. This further shows cross-county impacts as the results include whether people work in the same area or not. This level of analysis is possible only by using a regional scale.

However, there is currently a gap in applying mesoscopic traffic models at regional scale with high temporal and spatial resolution in the context of seismic hazards. While such models offer a promising balance between behavioral realism and computational efficiency, their use in post-disaster or infrastructure disruption scenarios remains limited. For example, Zhao et al. [104] developed a semi-dynamic agent-based traffic model for the San Francisco Bay Area, where traffic conditions are updated every fifteen minutes to reduce computational demand. Although their model was not designed for hazard applications, they demonstrated that it could produce reliable outputs by benchmarking results against those from the

Metropolitan Transportation Commission's (MTC) regional models. This study builds on their approach by adapting the semi-dynamic mesoscopic modeling structure for use in post-earthquake simulations, enabling the analysis of disruption and recovery dynamics in large-scale transportation networks. The model is introduced in the following chapter.

2.3 Resilience and Performance Assessment

As mentioned in Chapter 1, resilience can be viewed as having four dimensions: robustness, redundancy, resourcefulness, and rapidity. Of these four, robustness and rapidity are identified as the key dimensions, as both redundancy and resourcefulness can typically be factored into studies of the former dimensions. This section goes through previous work on both dimensions, especially as it relates to the use of infrastructure damage assessment, traffic models, and the metrics/indicators they use to quantify resilience.

Robustness studies[3]

Robustness is defined as the ability of the system to withstand impacts without suffering loss or degradation of performance or functionality. Measurement of a transportation network's performance under seismic hazards can generally be divided into two types: those pertaining directly to transportation effects and those that pertain to external and indirect impacts. Direct transportation impacts include metrics such as the total number of fulfilled trips (which indicates the connectivity of the post-earthquake network), travel times, and travel distances [20, 102, 18, 76, 37]. These metrics are typically defined by estimating the drop in performance of the system from pre-disaster to post-disaster. Table 2.1 shows that most previous studies incorporate some level of direct transportation impact measurement.

However, damages to the transportation system can have cascading impacts to other interdependent sectors, which are referred to as external or indirect impacts. Examples of these indirect performance metrics include measures of safety [102], accessibility of hospitals [37] and businesses, and economic losses [24]. Many studies focus on rehabilitation strategies or prioritization of bridge retrofitting based on importance [8, 102, 40, 30] without explicitly considering economic impacts or the time and financial constraints. Translating direct transportation impacts into economic losses helps to understand the more far-reaching implications of damaged transportation infrastructure. Having a monetary estimate of the impact enables a more direct comparison between the cost of preventive measures (e.g., seismic retrofits) versus the cost of repairing damaged highways or roads combined with the losses incurred by interdependent sectors. In other words, these results help to weigh the risks associated with delaying highway and bridge restoration or maintenance in the event of an earthquake. This, in turn, informs the formulation of more realistic budget proposals and

[3]Portions of this subsection draw from a published version of this work in the *International Journal of Disaster Risk Reduction* [99].

policy recommendations, such as bridge repair prioritization, seismic retrofits, or improvement of hospital and emergency response capacity.

Among studies that have investigated economic impact estimation, a popular method is the use of input-output (I-O) analysis as popularized by Leontief [59]. This method uses an input-output table that summarizes all interactions between each pair of sectors in a given region. This can then be used to show how any change in economic activity in one sector can result in ripple effects on others [10]. Another method of quantification is to measure the overall economic impacts using integrated transport networks and multi-regional trade models [46]. This entails collecting commodity flow data to and from each zone of analysis. While the US Bureau of the Census and the Bureau of Transportation Statistics collect this data between the 50 states and smaller regional economic units, the spatial resolution may not be high enough if the objective is to assess the local economic impacts of an earthquake.

Another popular way of measuring economic impacts is the use of Computable General Equilibrium (CGE) models. CGE models incorporate the behavior of producers and consumers to price signals, on top of allowing nonlinearities as opposed to I-O models. However, the same data availability issues hinder the use of CGE models as employed in Tatano and Tsuchiya [92]. While these methods offer comprehensive analyses, it is difficult to develop an understanding of more specific effects on individual sectors like transportation. Furthermore, the spatial resolution of results from impact analyses at this overall regional level of abstraction is not high enough to make specific conclusions, actionable items, and strategies at the transportation sector level.

Bhattacharjee and Baker [8] provides a third, simple, and compact example of a cost model in relation to transportation impacts. This model breaks down costs between direct costs, which pertain to the repair costs for all the damaged bridges, and indirect costs, which pertain to the delays and unsatisfied demand multiplied by respective values of time. A similar model is adopted in this study.

Finally, of the three mentioned components of resilience analysis of transportation networks to seismic hazards (bridge modeling, traffic modeling, and performance/resilience assessment, including economic losses), different studies have not applied all three consistently, as can be observed in Table 2.1. Cho et al. [24] is the best example of applying all these steps, but each step, particularly that of the transportation network model and economic model, is still wanting in terms of spatial resolution. Therefore, a gap also exists in estimating the economic impact on the transportation sector with high spatial resolution.

Table 2.1: Review of robustness studies

Author/s	**Hazard**	**Traffic Model Used**	**Scale of Study & Network Size**	**Indicators Used**
Chang, Shinozuka, and Moore [20] (2000)	47 scenario earthquakes in Los Angeles	None (link damage states only)	Regional; 133 nodes, 202 links on LA highway network	System performance degradation based on change in minimum travel distance
Nojima and Sugito [76] (2000)	Ten damage rate scenarios	Static, link-based, node-level	Regional; 100 links, 30 nodes (Japan highway)	Flow, system travel distance, system travel time
Cho et al. [24] (2001)	M_w 7.1 Elysian Park fault	Static, zone-level	LA Metro; 19,601 links, 1,534 TAZs	Structural/business loss, network costs
Chang and Nojima [19] (2001)	Loma Prieta, Northridge, Kobe EQs	Topological + historical ADT	Regional; Hanshin: 63 nodes, 62 links	Total length of network open, total distance-based accessibility, distance-based accessibility ratios
Modarres and Zarei [68] (2002)	None	Topological only	Rasht, Iran street network; 353 nodes, 534 links	Accessibility (time/safety)
Suarez et al. [91] (2005)	Flooding scenarios	Static, link-based, trip-based	Boston Metro; 986 TAZs, 22,000 links	Links flooded, VHT, VMT, trip loss, avg. speed change
Kiremidjian et al. [57] (2007)	M_w 7.0 Hayward fault	Static, link-based, trip-based	Bay Area; 1,120 zones, 26,522 links	Damage cost, system functionality loss
Padgett, DesRoches, and Nilsson [81] (2010)	M_w 4.0–7.0 Charleston scenarios	None (link damage only)	Charleston, SC; 375 bridges	Direct economic loss (repair cost)

Author/s	**Hazard**	**Traffic Model Used**	**Scale of Study & Network Size**	**Indicators Used**
Chang, Elnashai, and Spencer Jr [18] (2011)	M_w 8.0 scenario in Sioux Falls	Static	Sioux Falls; 24 nodes, 75 links	Congestion (V/C), total system travel time
Wu et al. [101] (2012)	2008 Wenchuan earthquake	None	Regional (Sichuan Province)	IO tables, CGE economic impact
Nakanishi, Matsuo, and Black [72] (2013)	2011 East Japan earthquake + tsunami	Static, OD-level	Ishinomaki City & periphery	Total/avg. travel distance and time
Alipour and Shafei [1] (2016)	47 scenario earthquakes for Los Angeles and Orange counties	Static, link-level	LA & Orange Counties; 3,133 bridges, 1,527 TAZs	Direct (repair) + indirect (delay) losses
Kilanitis and Sextos [56] (2019)	Probabilistic seismic scenarios	Static	Greece; 12 nodes, 34 links	Delay cost, cancelled trips
Koc et al. [58] (2020)	M_w 7.3 Palos Verdes fault	Static (varying time scenarios)	Southern California network	VHT, delay
Wein et al. [100] (2020)	M_w 7.0 Hayward Fault	None; spatial demographics only	SF Bay Area	Spatial analysis of industries, employment, commute flows
Feng, Li, and Ellingwood [37] (2020)	M_w 8.0 earthquake	Dynamic, agent-based	Tangshan; 216 nodes, 750 links	Congestion, travel speed change

Rapidity studies

Studies focused on rapidity ensure that the identification of how to restore service and performance in a timely fashion is just as important as identifying what the losses are. Tables 2.2 and 2.3 list a select number of rapidity studies over the past decade. As can be observed in these tables, many rapidity studies talk about a ranking of links that could then be extended to a restoration or repair sequence that leads to the fastest improvement in service or performance [40, 30, 48, 88, 6]. Interestingly, Table 2.2 shows that many rapidity studies describe themselves as hazard-independent or generalizable across different types of disruptive events. This is largely because their analyses focus on the relative importance of network links—often measured by the amount of traffic a link can service or its contribution to connectivity—rather than modeling the specific physical impacts of a particular hazard. These metrics are typically structural or functional in nature and are applied uniformly across the network, regardless of whether the disruption stems from an earthquake, flood, or other event. While many studies adopt a hazard-independent perspective, this study focuses specifically on seismic hazards.

Tables 2.2 and 2.3 also show that recent rapidity studies either do not define a specific time horizon or rely on generalized time units in their analyses. This time-agnostic approach implies that the total recovery duration is determined solely by the assumed rate of repair, which can vary widely depending on the level of resources (e.g., funding, labor) allocated after a disruption. As such, the actual time horizon becomes effectively out of scope, since it is not explicitly modeled but rather embedded in assumptions about repair speed and resource availability. One possible reason for this modeling choice is the limited availability of empirical data on the actual time frames associated with road and highway repair, closure, and restoration following major disruptions. For example, Misra et al. [67] have begun to address this gap by surveying experts to identify realistic timelines for these processes as a function of damage severity. Still, detailed and consistent datasets remain scarce.

Another important consideration is that total recovery may not always be the desired outcome. In some cases, permanently removing a damaged link may support broader urban, environmental, or social goals. A well-known example is the Embarcadero Freeway in San Francisco, which was irreparably damaged in the 1989 Loma Prieta earthquake and subsequently demolished rather than rebuilt—an action that spurred waterfront revitalization and improved urban connectivity [14]. This suggests that restoration planning should not assume a return to the pre-disruption network as inherently optimal.

While a time-agnostic approach offers flexibility, it may fall short in situations where time-critical decisions—such as evacuation planning or staged road reopening—must be made. In these contexts, understanding not just which links are critical, but when they become available, is essential. Despite these limitations, this study adopts a time-agnostic framework due to the lack of detailed repair time data and the need to maintain generalizability across different scenarios. This abstraction allows for a focus on relative importance and sequencing of link recovery, with the understanding that specific timelines can be incorporated when more data becomes available.

Another notable pattern from Table 2.2 is that rapidity studies tend to use smaller networks compared to robustness studies. This is largely a consequence of the methodologies employed. Many of these studies simulate single-link closures—where one link is removed at a time—to estimate each link's contribution to overall system performance, typically in terms of travel time [88, 6]. This approach naturally leads to a ranking of links by relative importance.

However, such strategies do not account for the interdependencies among links that arise from network connectivity. In reality, the impact of a given link may depend on the status of other links, and these compound effects cannot be captured by analyzing single-link failures alone. Some studies address this by simulating multi-link failures (e.g., combinations of 2, 3, 4, or even 5 links), but the number of combinations grows exponentially with the size of the network. As a result, most rapidity studies limit their analyses to simplified bridge networks or small sub-networks of a larger system.

Nevertheless, as discussed in Chapter 1, it is essential for resilience studies to operate at regional scales and incorporate both high spatial and temporal resolution. This highlights a gap in the literature: the need for methodologies that can account for interconnectivity and cascading effects without being limited to small-scale networks.

Furthermore, while studies such as Dong, Frangopol, and Saydam [30] and Merschman et al. [65] have begun to incorporate social and environmental metrics into the development of post-disaster recovery strategies, much of the earlier work does not account for factors external to transportation system costs and performance or functionality when generating repair sequences.

In summary, similar to the previous section on robustness, rapidity studies that address regional-scale networks with high spatial and temporal resolution remain underexplored and warrant further attention.

Table 2.2: Review of rapidity studies (part 1)

Author/s	**Hazard**	**Traffic model used**	**Scale & size of network**	**Time horizon**
Frangopol and Bocchini [40] (2011)	Magnitude 7 earthquake in Lehigh Valley, Pennsylvania	Static	13 bridge network in Lehigh Valley, Pennsylvania	24 months
Dong, Frangopol, and Saydam [30] (2014)	Monte Carlo simulation of different seismic events	Static, high-level (damage, topology, and average daily traffic)	10-bridge highway network in Orange County, CA	30 years
Hu et al. [48] (2016)	General hazard	Purely topological	Square lattices with up to 2500 nodes	No time horizon
Zhang, Wang, and Nicholson [103] (2017)	General hazard	Purely topological	Hypothetical road network with 37 links and 30 nodes	24 months
Merschman et al. [65] (2020)	Not hazard specific	Purely topological	Mobile County, Alabama road network (4 bridges)	No time horizon
Sohouenou and Neves [88] (2021)	General hazard	Static	Sioux Falls network with 24 nodes, 76 links	Not time dependent
Bhattacharjee and Baker [8] (2021)	Seismic hazards	Static, zone-level (1156 OD pairs)	San Francisco Bay Area road network	Not time dependent
Pan et al. [82] (2022)	Generalized disruptive events	Grid-based GPS vehicle data model	Chengdu, China	Generalized time units
Barati, Yazici, and Almotahari [6] (2024)	Generalized disruptive events	Purely topological	Sioux Falls network (24 nodes, 76 links, 528 OD pairs)	No time horizon

Author/s	Hazard	Traffic model used	Scale & size of network	Time horizon
Chen et al. [22] (2024)	Generalized disruptive events	Intercity multi-modal public transport network	Guanzhong Plain agglomeration (90 districts in 4 provinces)	Generalized time units
Ma et al. [60] (2024)	Generalized disruptive events	Multi-modal traffic assignment	Beijing-Tianjin-Hebei-Shandong region	Generalized time units

Table 2.3: Review of rapidity studies (part 2)

Author/s	Indicator/s used	Strategy used
Frangopol and Bocchini [40] (2011)	Functionality over time (damage level, rehabilitation cost)	Optimization to determine bridge repair sequence (maximize resilience, minimize cost)
Dong, Frangopol, and Saydam [30] (2014)	Total retrofit cost, expected economic loss	Optimization to minimize retrofit and expected economic, social, environmental cost
Hu et al. [48] (2016)	Recovery level, AUC, edge recovery percentage	Compare 4 strategies (random, greedy, preferential, periphery) under localized/random/malicious attacks
Zhang, Wang, and Nicholson [103] (2017)	Recovery time, trajectory skew, weighted average number of reliable independent pathways between all OD pairs	Sequencing to minimize recovery time and skew
Merschman et al. [65] (2020)	Social vulnerability, travel time/distance to hospitals	Scenario testing to determine repair sequence based on smallest AUC and equity

Author/s	**Indicator/s used**	**Strategy used**
Sohouenou and Neves [88] (2021)	Travel time change, robustness, unsatisfied demand	Link criticality via multi-link failure combinations
Bhattacharjee and Baker [8] (2021)	Retrofit cost	Sensitivity analysis for bridge prioritization
Pan et al. [82] (2022)	Resilience (loss/recovery ratio, AUC)	Optimization of recovery sequence and resource allocation
Barati, Yazici, and Almotahari [6] (2024)	Network Efficiency Index-based metrics under link failure combos	Link criticality ranking based on Network Efficiency Index and shortest path
Chen et al. [22] (2024)	Connectivity, capacity, resilience score	Optimal node recovery sequencing to maximize resilience
Ma et al. [60] (2024)	Normalized performance, total travel cost, demand served	Link recovery sequencing and capacity upgrades

2.4 Summary of Research Gaps

This chapter has reviewed the state of knowledge across three domains central to this dissertation: infrastructure damage assessment, traffic modeling under disruption, and performance-based approaches to transportation resilience. While each of these domains is well-developed individually, there remain significant limitations in how they are connected and applied at a regional scale.

In the domain of seismic damage modeling, much of the literature has focused on generalized fragility curves and probabilistic assessments at the component level (e.g., bridges). However, these approaches often fall short in capturing the site-specific and structural nuances that influence damage outcomes in real events. Newer data sources, such as satellite imagery and Google Street View, present opportunities for developing more individualized and spatially granular damage models that can better inform system-level impact assessments.

In traffic modeling for resilience analysis, a persistent gap lies in the ability to represent regional-scale systems while maintaining sufficient spatial and behavioral resolution. Although dynamic and agent-based models have grown more common, many studies continue to rely on static or macroscopic models that oversimplify congestion dynamics and user response. Mesoscopic approaches offer a promising middle ground, capable of simulating individual behavior within a scalable framework. However, their application in post-disaster contexts remains limited, in part due to a lack of integrated modeling frameworks and established practices for incorporating infrastructure disruption and recovery processes.

In the assessment of transportation resilience, robustness and rapidity are often analyzed using different models or approaches, each tailored to specific aspects of system performance. However, there remains a persistent tradeoff between achieving regional coverage and maintaining high spatial resolution in traffic modeling. This limits the ability to analyze how disruptions and recovery processes unfold across heterogeneous geographies. A regional lens enables a better understanding of not only the spatial distribution of impacts and recovery rates, but also how broader structural or institutional factors may influence resilience outcomes. These considerations motivate the development of separate, but complementary, frameworks for evaluating robustness and rapidity at regional scale.

These research gaps underscore the need for scalable, behaviorally realistic, and regionally focused modeling approaches that can trace the impacts of seismic hazards to transportation networks and evaluate both robustness and rapidity using interpretable metrics. This study responds by developing and applying separate yet complementary frameworks for robustness and rapidity, each integrating seismic damage modeling, semi-dynamic mesoscopic traffic simulations, and performance-based resilience measures.

Chapter 3

Regional semi-dynamic agent-based traffic model

3.1 Overview

As mentioned in the previous chapter, different kinds of traffic models have been used and applied to different studies depending on their purposes. Different aspects of the model, such as scale and resolution, can be modified to fit research needs. This chapter makes an argument for a regional semi-dynamic agent-based traffic model to be used in studies related to seismic hazards.

Spatial resolution

In the context of seismic hazards, it is important to consider things in a regional scale, as fault lines can extend up to a thousand kilometers long, and thus can have impacts that span multiple cities or counties. Furthermore, these studies are focused on an instance in which there can be significant changes in travel demand and network capacity or performance. In that sense, it is important to capture the changes in traffic behavior that occur as a result. In a spatial resolution sense, this can mean that people have to be diverted or choose to divert from their original route due to closures or traffic congestion. For example, a sudden closure of certain roads or highways means that vehicles have to reroute. It is therefore important to have a fine spatial resolution that includes these alternative links to which traffic will be diverted due to closures or congestion. This study therefore proposes the use of a regional scale in seismic resilience assessment studies that also has a high spatial resolution, which means that the study network must include both highways and local roads. Previous seismic resilience assessment studies listed in Chapter 2 have a tendency to:

- **Include local roads but have a local scale:** These studies typically test an algorithm or methodology to optimize recovery efficiency (e.g., generating the optimal repair sequence of closed highway links to speed up recovery). They test the methodologies

on a small test network (that is sometimes removed from seismic hazard contexts) to demonstrate its efficiency. While this is good for proof-of-concept studies, it is necessary to extend the work to realistic scenarios and places that have high risks of the specific hazard.

- **Have a regional scale but only include highway networks:** While a regional scale helps develop a fuller perspective on the impacts of an earthquake, having a low spatial resolution (i.e., not including local roads) can generate results that do not take into account the redundancies inherent to the transportation network.

In this sense, a traffic model with a regional scale and high spatial resolution (i.e., includes both local roads and highways) is recommended for studies on the seismic resilience of transportation networks.

Temporal resolution

The following are key dichotomies that characterize different types of traffic models:

- **Static versus dynamic:** Static traffic models are typically defined over a relatively long time period where each link's congestion properties are described by a volume-delay function that expresses the steady-state travel time as a function of the volume of traffic on the link [23]. This is in contrast with dynamic traffic models that focus on capturing real-time changes in traffic over time (i.e., no steady-state assumptions). This is typically realized by modeling individual vehicles and their routes and allowing vehicles to respond to these changes as they happen.
- **Macroscopic (link- or flow-based) versus microscopic (agent- or vehicle-based):** Macroscopic models are typically link-based models that treat traffic as continuous flow. These models also use aggregated measures (e.g., vehicle density, flow, speed). This makes it good for large-scale analysis and has high computational efficiency, but trades it off with lower spatial resolution. On the other hand, microscopic models follow individual vehicles and models their interaction with each other. This makes this very computationally intensive.

In terms of temporal resolution, macroscopic and static traffic models operate with coarser granularity compared to dynamic and microscopic models, which require finer temporal detail. Static, macroscopic models have long been used in transportation planning to support policy and project decisions [23]. However, when evaluating the seismic resilience of transportation networks, understanding how traffic responds to changes in travel demand or network performance is critical——for both short- and long-term resilience assessments.

Dynamic models are particularly useful in this context, as they track individual agents or vehicles along their routes, offering greater behavioral realism and interpretability. Yet, the computational demands of dynamic, microscopic models, especially at regional scales, can be prohibitive, often requiring hours of simulation time.

To balance realism with efficiency, a mesoscopic or semi-dynamic approach is proposed. This model retains the use of volume-delay functions to characterize link congestion but introduces time-sensitive updates: link travel times are recalculated at smaller intervals to reflect evolving traffic conditions more accurately. Depending on the application, this also enables agents to adapt their routes in response to changing congestion levels. A detailed discussion of this semi-dynamic agent-based model follows in the next section.

To motivate the use of a semi-dynamic, mesoscopic agent-based model in this study, Table 3.1 summarizes the strengths and limitations of common traffic modeling approaches across four key dimensions: spatial resolution, temporal resolution, behavioral realism, and scalability. The selected modeling strategy aims to strike a balance across these criteria, offering enough fidelity to simulate disruption and recovery dynamics while maintaining tractability at a regional scale.

Table 3.1: Comparison of traffic modeling approaches across key dimensions.

Model Type	**Spatial Resolution**	**Temporal Resolution**	**Behavioral Realism**	**Scalability**
Static macroscopic	–	–	–	✓
Dynamic macroscopic	–	✓	∼	✓
Semi-dynamic mesoscopic	∼	∼	✓	✓
Dynamic microscopic	✓	✓	✓	–

3.2 Model description

The proposed model framework is made up of three parts: collecting regional travel demand data and the regional travel network, traffic assignment, and customizing the output. This section discusses each step of the model framework. While the general steps of the framework are fixed, different modifications can be implemented depending on the needs of the research.

Travel demand and network

1. **Get network data from OpenStreetMap**

   After the region of study is set, the highway and road network can be extracted from OpenStreetMap using OSMnx [9]. The network is processed to have separate files for the nodes and edges. The nodes have the following headers shown in Table 3.2 while the edges have the following headers shown in Table 3.3.

Table 3.2: Node headers

Headers	Description
node_id	Unique identifier of node in the network
osmid	Unique identifier of node in the OSM network
signal	Indicator of whether there is a signal at the node
lon	Longitude of the node
lat	Latitude of the node

Table 3.3: Edge headers

Headers	Description
start_nid	Unique identifier of start node
end_nid	Unique identifier of end node
length	Length of edge
lanes	Number of lanes in edge
geometry	Line geometry of the edge
maxmph	Maximum speed on the edge
oneway	Indicator of whether edge is oneway
type	Type of edge (e.g., motorway, primary, secondary, tertiary, residential)
capacity	Capacity of edge
crossings_stops	Indicator of whether there are crossing or stops at the edge
traffic_signals	Indicator of whether there are traffic signals at the edge
fft	Free flow travel time of the edge

2. **Get zonal demand data from relevant government agencies or other sources**

   Travel demand for the region of study is required to conduct traffic analysis. Most government or government-attached agencies in different countries or regions run travel surveys every several years. This travel demand data is typically aggregated over defined traffic analysis zones (TAZs). For example, Japan runs a Nationwide Person Trip Survey every 10 years. They have the following data available for use shown in Table 3.4. For the purposes of this model, only demand data for modes that utilize the extracted road and highway network (e.g., cars, trucks, buses) are relevant. Modes such as trains, bicycles, and walking are not incorporated into the model.

3. **Finalize number of interzonal trips**

   Since the survey data typically contains more data than is necessary for the scope of the research, it has to be processed further to make the data quantity more manageable. For example, information on mode splits or trip activity can be incorporated to finalize

Table 3.4: Aggregation categories from Tokyo Person Trip Survey

Category	**Description**
Origin/Destination Zones	Spatial aggregation level of data (e.g., large, middle planed basic, small zones)
Gender	Men/Women
Age group	Five-year age ranges from 5–9 to 85 or older
Occupation	Three categories (primary, secondary, or tertiary industry workers)
Employment status	Nine categories (self-employed, employees, temporary, part-time, students, etc.)
Driver's license	Whether person has driver's license or not
Availability of a car at your disposal	Whether person has a car or not
Physical difficulties in going out	Whether person is able to go out alone or needs assistance
Annual household income	Five income ranges from less than 2 million yen to over 15 million yen
Facilities	Housing, schools, medical facilities, etc.
Time	Hour of the day
Parking space	What type of parking space is used
Bicycle parking area	What type of bicycle parking is used
Means of transportation	Up to 14 modes including railways, buses, cars, motorcycles, walking, etc.
Purpose type	Home to work, Home to school, Home to personal, etc.
List of cities, wards, towns, and villages included	List of prefectures and municipalities in Tokyo Metropolitan Area

the demand data. Furthermore, most travel demand data are typically aggregated by hours or range of hours, so assumptions have to be made so the data can be further processed on how to distribute the demand over the hour, if at all.

4. **Overlay TAZs onto OpenStreetMap network**

   The demand data has to be incorporated with the OpenStreetMap network. Shapefiles for the TAZ geometries or boundaries have to be located and overlaid onto the road and highway network. Once this is done, a list of nodes in each zone has to be generated.

5. **Assign trips to each node**

   Once the demand data is incorporated with the OpenStreetMap network, the trips for each TAZ origin-destination (OD) pair have to be assigned. The trips for each TAZ

OD pair are randomly assigned to the list of nodes for each TAZ. The final demand data is node-level OD and has the following headers shown in Table 3.5.

Table 3.5: Demand headers

Headers	Description
origin_nid	Unique identifier of origin node in network
destin_nid	Unique identifier of destination node in network
origin_TAZ	TAZ of origin node
destin_TAZ	TAZ of destination node
hour	Departure hour
quarter/tenth	More granular detail of departure time if available
cars	Indicator of mode of transportation (car, truck, etc.)

6. **Incorporate network revisions**

   Finally, the scenarios being tested may have modifications to the road or highway network. For example, certain highway links may be expected to be damaged or closed for inspection at the beginning of the time of study. A list of these scenarios have to be generated and can later on be programmed into the traffic assignment.

Traffic assignment

The traffic assignment has the following steps shown in Figure 3.1. These steps are elaborated below.

1. **Load travel demand and network**

   The study road and highway network, together with the corresponding travel demand for the time/s of study have to be loaded before starting the simulation. For the road and highway network, the opening and/or closing of certain links, together with the time of opening and/or closing, can be programmed into the simulation. Similarly, any refinement of the demand data can be done at this stage. These can include: (1) more granular demand distribution (e.g., distributing hourly demand into smaller time intervals like every 10 or 30 minutes), (2) incorporating relevant trip information (e.g., mode of transportation or trip activity).

2. **Initialization**

   The temporal granularity of the simulation—defined by the time step, substep count, and substep size—represents a key modeling decision that balances behavioral realism with computational tractability. In a mesoscopic simulation, microscopic behavior is approximated through the discretization of traffic updates within each time step.

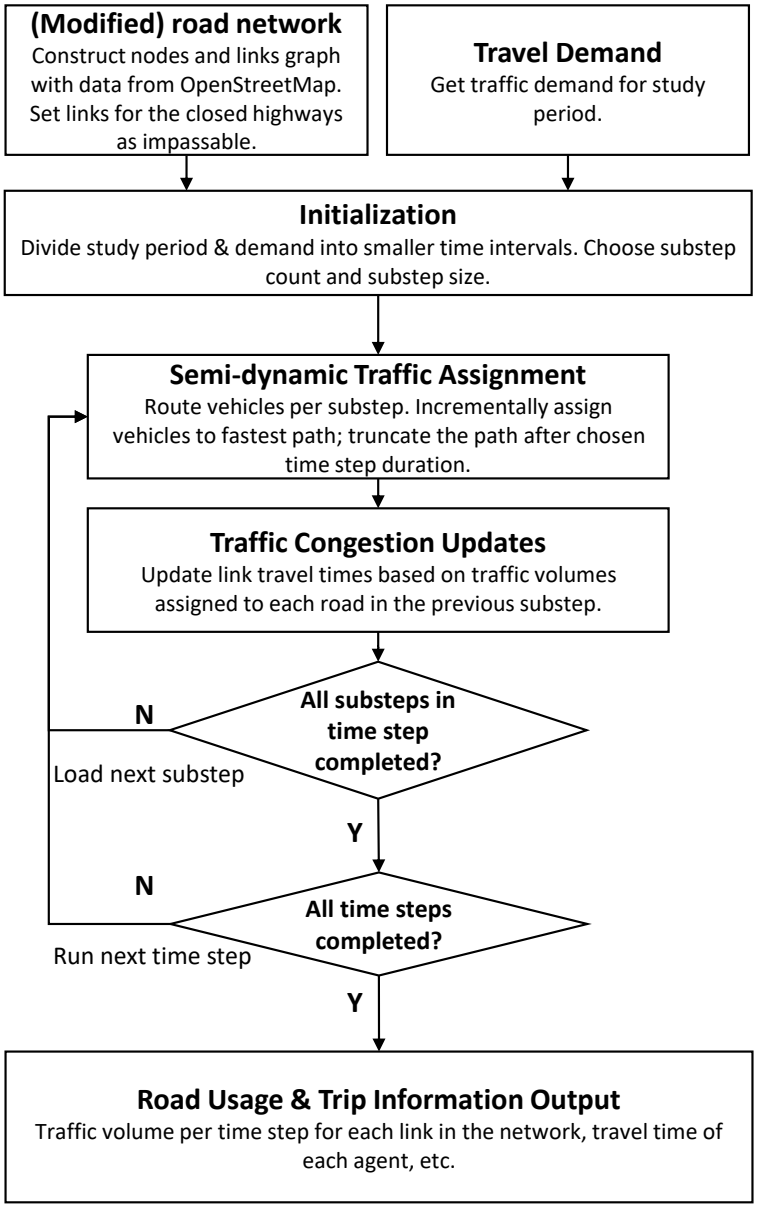


Figure 3.1: Traffic assignment flowchart

Substep count and substep size control how frequently link travel times are updated, effectively segmenting vehicle assignment into smaller batches. This is especially important in scenarios with high demand per time step. For instance, if a given time step contains 1 million trips, using a substep size of 30,000 results in approximately 30 substeps, where travel times are updated incrementally after each batch is assigned. This better captures the evolving congestion dynamics than assigning all 1 million trips simultaneously under the assumption of no mutual interference. These parameters must therefore be selected carefully to reflect the tradeoffs between accuracy and performance, particularly in large-scale simulations of disrupted networks.

3. **Semi-dynamic traffic assignment**

   For each substep and time step, the route of each agent has to be computed using the chosen method. For this study, the chosen method is the shortest path. The agents are then assigned to the fastest path which is truncated depending on the duration of the chosen time step.

4. **Traffic congestion updates**

   The link travel times are updated based on the traffic volumes assigned to each road in the previous batch. The traffic assignment follows the volume delay function in Equation 3.1 where t_i is the travel time on link i, $t0_i$ is the free-flow travel time on link i, v_i is the flow on link i, c_i is the capacity of link i, and α and β are calibration parameters set to the commonly used value of 0.6 and 4, respectively [25].

$$t_i = t0_i * \left(1 + \alpha * \left(\frac{v_i}{c_i}\right)^{\beta}\right) \tag{3.1}$$

5. **Road usage & trip information output**

   The output of the simulation is the road usage information for each link for each time step and the trip information for each agent as detailed in Tables 3.6 and 3.7. The following output can be generated from this proposed traffic model which can be further aggregated (e.g., spatially, temporally, by mode, by trip activity) depending on the needed applications. The most commonly used output are the total travel time and total travel distance per agent which can then be used to calculate the total system travel time and the total system travel distance. Furthermore, the path traversed by each agent can also be saved but may take too much storage space depending on the size of the travel demand being studied.

Possible modifications

There are several components of the traffic assignment that can be modified, including:

- **Choice of routing method and assumptions on driver behavior**

Different types of routing methods can be implemented using the above framework depending on what is being studied. For example, if the focus is to get people home in the shortest amount of time, the shortest path method can be used. If the goal is to minimize carbon emissions or environmental impact, eco-routing can be implemented instead. Furthermore, the chosen routing method can be applied once or multiple times throughout the simulation. For example, Chapter 4 shows a case where drivers are assumed to have complete knowledge of the condition of the network (as is the case when using a routing app) and they can choose to change their route every 15 minutes depending on the changing congestion levels on each link. This is assumed so because the study tries to assess long-term impacts of the seismic hazards to the recovery of the network, particularly by focusing on trips that would ordinarily have occurred in the absence of the disaster. On the other hand, Chapter 5 shows an example of a short-term assessment of the seismic hazard to the network. In this case, it is being tested how quickly people can return home after the event. For this case, the drivers are assumed to not know the condition of the network and therefore only follow a route they choose at the beginning of the simulation whether or not the congestion affects the initial estimated travel time.

- **Choice of time step, substep count, and substep size**

  Depending on the application, different choices for the time step, substep count, and substep size may be more appropriate. These define how frequently link travel times can be updated and by extension how frequently drivers can react to these changes in link travel times.

- **Choice of calibration parameters of volume-delay function**

  The calibration parameters of the volume-delay function can be changed depending on the specific characteristics of the city or region being studied. It is common to use default values of around 0.3 for α and 4 for β respectively, but if traffic data is available for the region of study, these parameters can be changed accordingly. Furthermore, the additional travel time introduced by traffic signals and pedestrian crossings can also be added either as a constant or a variable to the volume-delay curve to more closely approximate a dynamic model.

- **Choice of number of vehicles per agent**

  Each vehicle having its own origin and destination node is the ideal scenario when running traffic simulations. However over the course of using this model, it is found that this adds significantly to computational load when simulating around 5 million or more trips. To simplify this, some origin-destination pairs are collapsed by setting a number of vehicle per agent. The value used in the following studies is 5 vehicles per agent. The smaller this number, the closer it is to reality but more computational resources have to be used. Conversely, a higher number would simulate faster but may risk being too simplified.

Table 3.6: edge_vol headers

Headers	Description
start_nid	Unique identifier of start node in network
end_nid	Unique identifier of end node in network
vol_true	Current volume through the edge
vol_tot	Cumulative volume through the edge over the course of the simulation
flow	Flow through the edge (in vehicles per hour)
t_avg	Average travel time of the edge
type	Type of road of the edge (e.g., motorway, primary, secondary, tertiary, residential)

Table 3.7: trip_info headers

Headers	Description
agent_id	Unique identifier of agent
origin_nid	Unique identifier of origin node in the network
destin_nid	Unique identifier of destination node in the network
travel_time	Upper bound of travel time of agent
travel_time_used	Actual travel time of agent
travel_length	Total travel distance of agent
stop_nid	Unique identifier of stop node in the network (if unable to complete trip)
use_highway	Indicator whether agent used the highway
stop_hour	Time when the trip stopped in the simulation (if unable to complete trip)
stop_half	More granular time when the trip stopped in the simulation (if unable to complete trip)
stop_ssid	Substep when the trip stopped in the simulation (if unable to complete trip)

Verification

To validate the proposed traffic model, several test scenarios were conducted to ensure that its behavior aligns with the expected network responses under varying conditions. For example, for the case study centered on the Tokyo metropolitan area—discussed in detail

in Chapter 5—two key scenarios were evaluated: (1) a baseline condition with all highway links operational, and (2) a disruption condition in which all highway links were removed to simulate a severe post-earthquake scenario.

Two representative trips were selected for comparison: Trip A, a short-distance trip that generally does not use the highway network, and Trip B, a long-distance trip that typically depends on the highway network. To assess the model's accuracy under free-flow conditions, outputs were benchmarked against Google Maps travel time estimates. Google Maps was queried at 2 AM, when traffic is minimal, to approximate the same free-flow conditions assumed in the model.

Under the baseline scenario, Google Maps reports a travel time of 12 minutes for Trip A, and the simulation yields an identical estimate. For Trip B, Google Maps reports a travel time range of 2 hours and 10 minutes to 2 hours and 40 minutes; the simulation result is 2 hours and 9 minutes, very close to the lower bound of the estimated range.

Under the full highway closure scenario, Trip A remains unaffected, as expected, with both Google Maps and the model again reporting a 12-minute travel time. For Trip B, Google Maps estimates range from 3 hours and 10 minutes to 3 hours and 40 minutes. The simulation produces a travel time of 3 hours and 17 minutes, which falls squarely within this range.

These verification scenarios are illustrated in Figures 3.2 and 3.3.

While these preliminary comparisons support the plausibility of the model outputs, more rigorous calibration and validation could not be performed due to data limitations—particularly the scarcity of observed traffic patterns immediately following a seismic event. Moreover, most available data are derived from highway sensors, providing limited insight into traffic dynamics on local roads, further constraining validation efforts.

3.3 Conclusion

This chapter presented a regional semi-dynamic agent-based traffic model designed to evaluate the seismic resilience of transportation systems. By incorporating traffic assignment and link volume and travel time updates over shorter and regular time intervals, the model strikes a balance between computational feasibility and behavioral realism. Its flexibility makes it suitable for analyzing different resilience dimensions across different transportation systems. In the following chapters, the proposed model is embedded within broader frameworks to assess two key aspects of resilience: robustness in Chapter 4 and rapidity in Chapter 5. These applications demonstrate how the model enables more nuanced and scenario-sensitive evaluations of transportation network performance under seismic disruption.



Figure 3.2: Sample trips without highway closure



Figure 3.3: Sample trips with highway closure

Chapter 4

Assessing robustness of regional transportation systems to seismic hazards: Southern California case study

4.1 Introduction

Chapters 1 and 2 highlighted the need for a regional mesoscopic model to be embedded within resilience analysis frameworks for transportation systems, and Chapter 3 detailed the proposed traffic model. This chapter focuses on developing a framework for robustness analysis, structured around three main components: bridge model generation and damage assessment, traffic modeling, and economic impact estimation. The framework is then demonstrated through a case study involving a hypothetical earthquake near the Ports of Los Angeles and Long Beach in Southern California. A version of this work has been published in the *International Journal of Disaster Risk Reduction*, and portions of this chapter draw from that publication [99].

4.2 Framework for robustness studies

A four-part framework is adopted to facilitate the inclusion of highly granular infrastructure seismic performance in this study. Compared to existing methods reviewed in the literature, the adopted framework components have the advantages of being efficient and scalable, which facilitates the inclusion of detailed bridge- or road link-level results for large-scale system-level analysis. A detailed flowchart of this framework is shown in Figure 4.1. In this section, the focus is given to the latter three steps (bridge assessment, transportation network analysis, and economic impact analysis), highlighting their granularity and applicability to regional analysis. The hazard characterization method follows Koc et al. [58] and Cetiner

[15] where, for seismic hazards, a scenario earthquake is identified first, followed by the use of ground motion prediction equations (GMPEs) to get outputs such as the IMs peak ground acceleration (PGA), peak ground velocity (PGV), and peak ground displacement (PGD) which are then used as inputs to the subsequent bridge modeling methods.

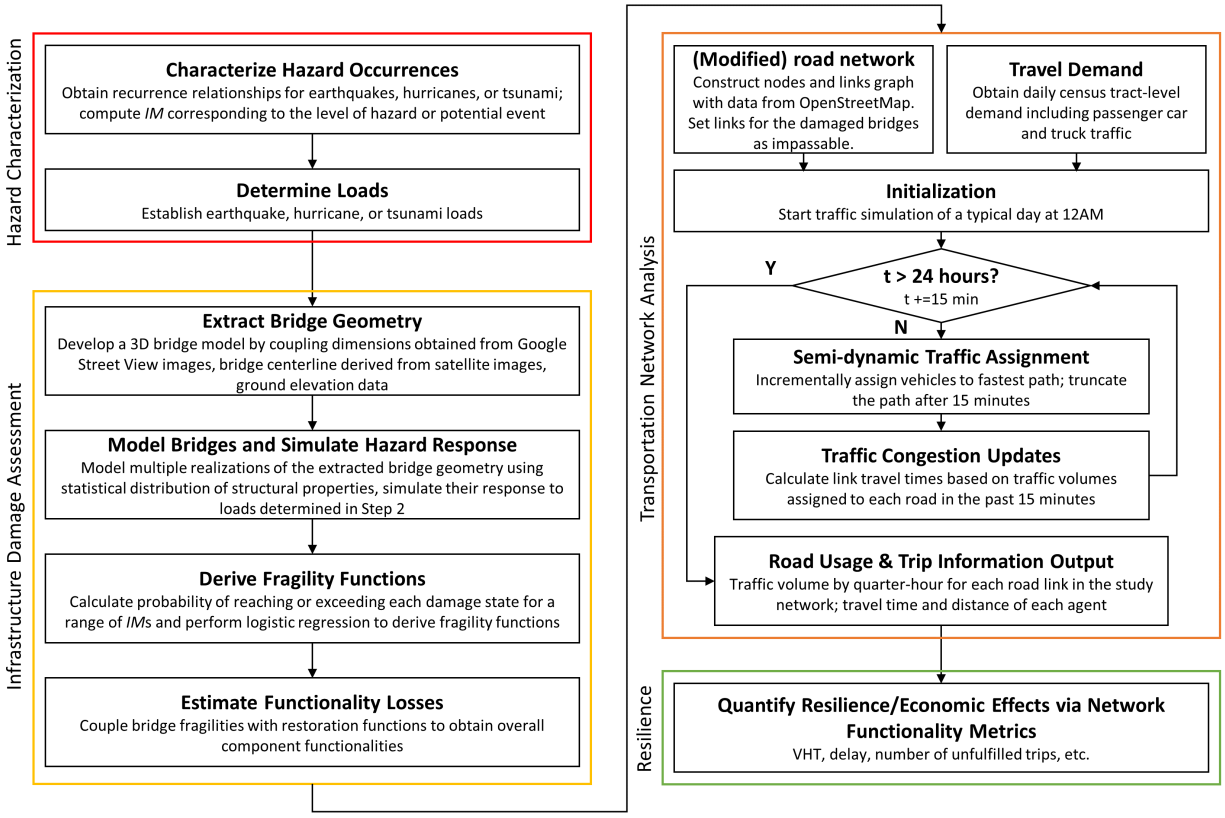


Figure 4.1: Framework flowchart

Bridge model generation and damage assessment

For this study, bridges are considered the only vulnerable components of the transportation network, given their higher likelihood of sustaining damage requiring extended time frames for full recovery, as evidenced by recent major seismic events [28, 53], and the limited disruption potential of the other transportation components, at least using HAZUS fragility functions [36]. In order to establish a detailed representation of the structural and seismic characteristics for individual bridges in a large geographical area, the image-based model generation methodology proposed by Cetiner [15] is used. This approach consists of five high-level steps:

1. Identifying tentative bridge locations for a region from National Bridge Inventory and refining this location information using an OpenStreetMap and routing APIs,

2. Downloading all street-level imagery associated with each detected bridge,

3. Reconstructing 3-D bridge geometry for each bridge using the downloaded imagery,

4. Populating these geometric shells with structural information using class statistics to develop nonlinear bridge models,

5. Calculating bridge fragility functions using component damage thresholds available in the existing literature.

The first step, identifying bridge locations and centerline geometry, begins with extracting approximate coordinate information available in the National Bridge Inventory (NBI) [38]. Once these coordinate values are obtained, all bridge centerlines that are within a mile radius of NBI coordinates are detected using OpenStreetMap (OSM)'s Overpass API [78], and the bridge geometries that match the route information stated in NBI are retained. Subsequently, to narrow down the query to a single unique matching centerline, a navigation query from the beginning and end vertices of each centerline curve is generated using Google Directions API [42], and the route/direction information for a bridge centerline that match NBI route and direction information is selected.

Benefiting from the unique strengths of each data source, this process results in accurate centerline extractions. NBI contains precise location and route information for every bridge in the US, but lacks the centerline information captured in OSM. OSM, on the other hand, has accurate centerline polygon and route information based on US Census Bureau [95] but lacks the direction information needed, e.g., northbound or southbound, to match these polygons to NBI bridges. Google Directions API provides detailed routing information between two points, but is somewhat limited in the accuracy of the path connecting these points. By combining these three sources, the centerline geometry of a bridge and the facility it carries are easily identified.

To download the street-level images for each bridge, two curves offset from the bridge centerline by a distance proportional to the NBI length of the bridge are computed. Next, all the Google Street View imagery on or near these curves is harvested, keeping track of the camera locations of images as they are obtained.

The street-level imagery for each bridge is semantically segmented using a deep learning model utilizing DeepLabV3 architecture [21] to identify all image regions containing bridge bent and deck elements. Then, the unique columns in each image and their locations are determined based on their order of occurrence and their linear distance along or offset from the bridge centerline. At this step, images for each unique column are grouped separately to determine column dimensions. By running the end-to-end wireframe parsing model by Zhou, Qi, and Ma [105] on column masks of segmented images, the vertical column lines are identified; counting the number of these vertical edges, column shapes are determined (e.g.,

two edges if circular, three edges if rectangular). Camera parameters at each column location are extracted using the multi-view automatic calibration pipeline developed by Vasconcelos, Barreto, and Boyer [98]. Subsequently, the heights and widths of each column are sampled at numerous intervals to determine the column dimensions. Superstructure depth is measured as the normal distance between the bottom and top faces of the superstructure. The top width of the bridge deck is read from the relevant NBI field, and the bottom is extracted from auto-calibrated images.

By the end of this step, a three-dimensional geometric model for each bridge is established. To convert these geometric models into structural models, the class statistics by Mangalathu [62] are utilized. For bridge columns, the longitudinal and transverse rebar locations, as well as concrete and steel strength properties, are computed based on the era-specific rebar ratios and strength distributions (where the construction year of a bridge is obtained from NBI). Then, using this cross-sectional information and era-specific standard connection details, columns are modeled using force-based formulation as discussed by Neuenhofer and Filippou [73]. Spreading of plasticity across column cross-section and length due to flexure is computed using a beam-column element with fiber sections where moment-curvature and axial force-deformation characteristics and their interaction are explicitly considered. Column shear behavior is considered by combining this beam-column element in series with the limit-state uniaxial material suggested by Elwood [33].

Abutments are modeled as zero-length elements that are assembled differently based on the abutments' construction type. The longitudinal behavior of integral abutments is modeled using springs with a tri-linear force-deformation relationship for the contribution of abutment piles, as presented by Mangalathu [62], and a Generalized Hyperbolic Force–Displacement (GHFD) backbone curve for the passive resistance of the abutment backfill, as proposed and described by Khalili-Tehrani et al. [55]. In seat-type abutments, the lateral resistances of the abutment back wall and elastomeric bearings are also factored into the longitudinal resistance of the abutment. The seat back wall is modeled using the simplified impact model proposed by Muthukumar [71], and the bearing pads are assumed to follow the elastic-perfectly plastic behavior suggested by Caltrans [13]. The transverse behavior of a diaphragm abutment is assumed to comprise the lateral resistance of abutment piles alone, with the pile behavior defined as identical to the longitudinal behavior. In defining the abutment resistance in the transverse direction for seat-type abutments, however, the resistances of elastomeric bearings and shear keys are also considered. Bearings are assumed to follow the elastic-perfectly plastic force-deformation relationship identical to that prescribed in the longitudinal direction. The transverse resistance of each shear key is defined as the shear resistance from the shear key reinforcing steel and concrete combined in parallel as per Silva, Megally, and Seible [86] and connected in series to an elastic no-tension material to account for the gap between the deck and shear keys. Similar to the application for bridge columns, the statistical properties of all the lateral pile, elastomeric bearing, and soil resistances required to define the described abutment models were obtained from Mangalathu [62].

The superstructure is assumed to remain elastic under earthquake shaking. Hence, elastic properties based on the gross area of the superstructure are assigned to line elements

representing the superstructure. For scalability of this nonlinear modeling approach, all bridge models are established using OpenSees [64] through custom-built automation scripts.

The relationship between the probability of each bridge reaching or exceeding different damage states for an earthquake intensity measure (IM) is defined using fragility functions. In certain situations, to account for different seismic conditions, multiple sets of fragility functions may be derived for different IMs (e.g., to account for ground shaking and ground failure-induced damages to bridges, two sets of fragility functions may be defined in terms of the IM's 1-second spectral acceleration and peak ground deformation, respectively). Following performance-based earthquake engineering (PBEE) methodology [70], fragility functions are prescribed as lognormally distributed functions and are generated for four distinct damage states: slight (ds_1), moderate (ds_2), extensive (ds_3), and complete (ds_4). Each fragility function is characterized by a median value IM (M), and a lognormal standard deviation value (β). The general form of a fragility function according to Baker, Bradley, and Stafford [4] is

$$\Pr(D^k \geq \mathrm{ds}_j | \mathrm{IM} = x^k) = \Phi_j^k \left(\frac{\ln(x^k/M)}{\beta} \right) \tag{4.1}$$

where k is the index of the IM for which the fragility function is established (e.g., for the case study discussed in the following section, only one IM is utilized; hence, the superscript k can be ignored in defining fragility functions), j is the PBEE damage state index, D^k is the damage state of a network component due the kth IM being equal to x^k, x^k is the value of the kth IM at the site of the network component, and Φ is the normal cumulative distribution function. Here, the no damage state is denoted as ds_0. The component threshold values required to develop these fragility curves were defined as outlined by Ramanathan, Padgett, and DesRoches [84]. The fragility functions were computed via multiple-stripe analysis [52] using the ground motion record sets developed for the Pacific Earthquake Engineering Research Center, Transportation Research Program [5].

To calculate the total functionality level of a network component, it is necessary to determine the probabilities of this component being in each of the five damage states for a set of IMs (P_j^k) as below.

$$\mathrm{P}_j^k = \begin{cases} \Pr(D^k \geq \mathrm{ds}_j) - \Pr(D^k \geq \mathrm{ds}_{j+1}) & j = 0, 1, 2, 3 \\ \Pr(D^k \geq \mathrm{ds}_4) & j = 4 \end{cases} \tag{4.2}$$

where $\Pr(D^k \geq \mathrm{ds}_0) = 1$.

Once these P_j^k values are combined with the restoration functions suggested by FEMA [36] for each damage state (RC_j) as follows, the total functionality level (FL) of a network component due to the kth IM can be computed.

$$FL^k = \sum_{j=0}^{4} \mathrm{P}_j^k \cdot RC_j \tag{4.3}$$

Traffic modeling

To capture the effects of bridge damage on the traffic network performance on a large geographic scale, an open-source agent-based semi-dynamic traffic assignment model developed at UC Berkeley (`https://github.com/cb-cities/residual_demand`) is adopted [104, 17]. The traffic model takes in two types of inputs: On the road network supply side, the base road network information is downloaded from OSMnx [9]. The network structure is represented by the nodes (i.e., road intersections) and links (i.e., stretches of road between two intersections). Various traffic-related attributes are attached to the road links, such as the length, speed limit, and capacity. On the travel demand side, a list of time-stamped OD pairs is taken as the input, which can usually be obtained or extracted from local travel demand surveys or models.

The travel demand used in this study reflects pre-earthquake conditions and is held fixed in both the base and post-earthquake simulations. This assumption allows for a controlled comparison of network performance, enabling quantification of the impact of road network disruptions on trips that would have ordinarily occurred in the absence of the disaster. While real-world post-disaster behavior may lead to demand suppression (e.g., canceled trips due to school closures, fear, or uncertainty), such behavior-driven adaptations are intentionally excluded from the model scope. Instead, this study focuses on identifying trips that become infeasible due to physical disconnection in the network, labeled as "unfulfilled." As such, the results represent the loss of accessibility under infrastructure damage, not behavioral response. Future extensions of this framework could incorporate dynamic or scenario-based demand models that reflect post-disaster behavioral adaptation, trip suppression, or modal substitution.

Given the network supply and travel demand inputs, the traffic assignment module is then initialized: the simulation starts at 12 AM when there is relatively light traffic on the road network. With a time step of 15 minutes, vehicles (time-stamped OD pairs) with a departure time between 12 - 12:15 AM are incrementally assigned (100,000 ODs at a time) the initial fastest paths based on free-flow traffic conditions. The incremental assignment here increases the stability of the results by preventing all vehicles from being assigned to the same routes. After each increment, the traffic congestion status is updated for the network, and a new travel time is calculated for each link using the Bureau of Public Roads (BPR) volume-delay curves [97] as shown in Equation 4.4, modified to take into account traffic signal and crossing delays:

$$t_i = t0_i * \left(1 + \alpha * \left(\frac{v_i}{c_i}\right)^{\beta}\right) + \text{traffic signal delay} + \text{crossing delay} \tag{4.4}$$

where t_i is the travel time on link i, $t0_i$ is the free-flow travel time on link i, v_i is the flow on link i, c_i is the capacity of link i, and α and β are calibration parameters set to the commonly used value of 0.6 and 4, respectively [25]. Traffic signals and crossing delays are also taken into account, as this information is also provided by OSMnx.

An intermediate stopping location is determined for each vehicle that cannot finish the journey within the 15-minute interval. The intermediate stopping locations will then be set

as the new origin to allow vehicles to reroute (e.g., choosing a more optimal path) based on an updated traffic congestion status and finish the journey in the subsequent time steps. Such incremental assignment and residual demand calculation procedures are repeated for each 15-minute interval until 12 AM the next day. The outputs include both vehicle-level information (travel time) and link-level information (traffic volume per 15-minute interval). Many summary statistics, such as the Vehicle Miles Traveled (VMT) and Vehicle Hours Traveled (VHT) can thus be derived from this output.

Each agent is assumed to be selfish, i.e., choosing the path that would minimize their individual travel time, and having perfect information on the traffic conditions, which includes the changes in travel time on each link in the network due to congestion. This is possible due to the incremental loading (100,000 ODs at a time) of the network and the iterative calculation and link travel time and route choice every 15-minute interval. As such, user equilibrium is approximated in this model. While there are arguments that post-earthquake scenarios are not necessarily in equilibrium due to the uncertainty and the damage [75], it is adopted in this model as a conservative estimate of loss (i.e., assessing the impacts to trips that could normally have been fulfilled).

The traffic model has been adapted here to capture the effects of bridge damage. Specifically, for damaged bridges (and surrounding or underlying roads that cannot be accessed), the traffic model will label them as "closed links". For these closed links, they are assigned extremely small speed limits and capacity, which effectively leads to extremely high travel times (e.g., over 10 hours) for vehicles using them. In the simulation code, a supplementary logic is implemented to check the travel time of each assigned route. If the route travel time is over a certain threshold, the route must have gone through one of the closed links, and no faster path exists. The trip is then labeled as "unfulfilled". It is expected that more trips will be unfulfilled with increasing bridge damage severity.

If additional information, such as different trip activities and different vehicle types, is available, each agent can be labeled and restricted accordingly in the simulation for a richer analysis later on.

Economic impact estimation

The economic cost of damages in a transportation network is estimated by splitting it into two components: direct costs and indirect costs, as shown in Equation 4.5 [69].

$$C = C_{direct} + C_{indirect} \tag{4.5}$$

Direct costs associated with bridge b are computed based on the amount of resources needed to repair the damaged road components in the network as shown in Equations 4.6 and 4.7, where RCR is the repair cost ratio and A_b is the area of the bridge b [8]. The unit replacement cost is \$3,154 per square meter [35].

$$C_{direct} = \sum_{b=1}^{B} C_{direct}^{(b)} \tag{4.6}$$

$$C_{direct}^{(b)} = \mathbb{1}^{(b)} \times \text{RCR} \times A_b \times \text{unit replacement cost} \tag{4.7}$$

Indirect costs incurred over the disruption period are divided into two components: (1) additional travel time for trips that were still completed, and (2) productivity losses associated with unfulfilled trips—those that could not be completed due to network disconnection. Note that voluntarily canceled trips (e.g., avoided trips due to fear or closure of destinations) are not captured in the current framework, and thus the total indirect costs may be underestimated. Conversely, some assumptions about per-trip cost are intentionally conservative, as explained below. These indirect costs are shown in Equations 4.8 and 4.9 [8]:

$$C_{indirect} = C_{delays} + C_{connectivity} \tag{4.8}$$

$$= \alpha \Delta T + \gamma U P \tag{4.9}$$

where α is the value of travel time and γ is the value of productivity. ΔT is the change in total travel time, and U is the number of unfulfilled trips, both relative to the base pre-earthquake scenario. P is the number of productive hours assumed lost per unfulfilled trip, set to eight to reflect a full workday-equivalent loss. This does not imply that all trips are work-related. Instead, it serves as a proxy for forgone access to work, school, healthcare, or essential services, consistent with prior studies using full-day productivity losses for disrupted trips. This assumption provides an upper-bound estimate of per-trip loss, while the exclusion of voluntary trip suppression implies that overall losses are likely underestimated. α and γ vary for each region and can be computed using Equations 4.10 and 4.11 [8].

$$\alpha = \frac{\text{Median household income, USD}}{\text{2080 hours worked per year}} \tag{4.10}$$

$$\gamma = \frac{\text{Annual gross regional product}}{\text{Annual labor hours}} \tag{4.11}$$

Once cost estimates are obtained, they can be compared with other economic and financial measures such as the gross domestic product (GDP) of the area to get a sense of its scale compared to the economy at large, or the allocated budgets for bridge repair and restoration or seismic retrofitting by the Department of Transportation on the state or federal level.

4.3 Southern California (Ports of Los Angeles and Long Beach): case study

To more clearly highlight the contributions of the proposed framework, it is applied to a case study on the Southern California transportation system, particularly on the road and highway system.

Hazard Characterization and Infrastructure Damage Assessment

Nonlinear structural models were developed for 1,000 bridges around the Ports of Los Angeles and Long Beach (POLA/POLB) using the automated image-based approach introduced in Section 4.2. The expected 1-second spectral accelerations at each bridge site were obtained using the physics-based approach proposed by the Southern California Earthquake Center [87] for a M_w 7.4 Palos Verdes Fault scenario event, two miles off the port islands as shown in Figure 4.2. Spectral acceleration at 1.0 s is selected as the IM of use in this study due to its high sufficiency and proficiency ratings determined by Shafieezadeh et al. [85] and its ease of use over vector-valued or fractional order IM definitions for representing ground shaking effects (ground shaking is the expected primary driver of seismic damage for the study area). Expected damage probabilities and functionality levels, together with the required recovery time of the bridges, were determined for the computed 1-second spectral accelerations. Figure 4.3 shows the fragility functions computed for two of the bridges modeled for this study. Figure 4.4 shows the road closure map using the proposed method. For the purposes of this study, any bridge with functionality less than 75% was deemed fully closed for traffic, as defined in Gordon et al. [43] (no partial bridge closure condition was considered). This closure map takes into account the information that once a bridge is closed, all road segments feeding traffic into, or underlying, this bridge will also be closed to traffic. In this road closure map, 59 miles of roadway were predicted to be closed the day after the scenario earthquake, 44 miles of roadway remained closed 3 days post-earthquake, 14 miles of roadway remained closed 7 days post-earthquake, 10 miles of roadway remained closed 14 days post-earthquake, and 6 miles of roadway remained closed 30 days post-earthquake. This road closure map is used as the input to the subsequent transportation network analysis.

Transportation Network Analysis

Road Network Data

Road network data for six counties in Southern California represented by the Southern California Association of Governments (SCAG) have been collected from OSMnx [9]. The network is converted into a directed graph representation consisting of 1,444,790 edges and 615,174 nodes where each edge represents a directed road segment and each node represents a road connection or intersection.

Travel Demand Data

Inter-traffic analysis zone (TAZ) origin-destination data in normal situations (i.e., without earthquake damage) was also obtained from SCAG for the following modes: drive alone, shared ride 2 HOV, shared ride 3+ HOV, light-heavy duty trucks, medium-heavy duty trucks, heavy-heavy duty trucks, shared ride 2 No HOV, and shared ride 3+ No HOV. The data does not include transit. Processing this data led to a total of 42,056,426 trips in the entire SCAG region for a typical day composed of 40,814,733 car trips and 1,241,693 truck trips.

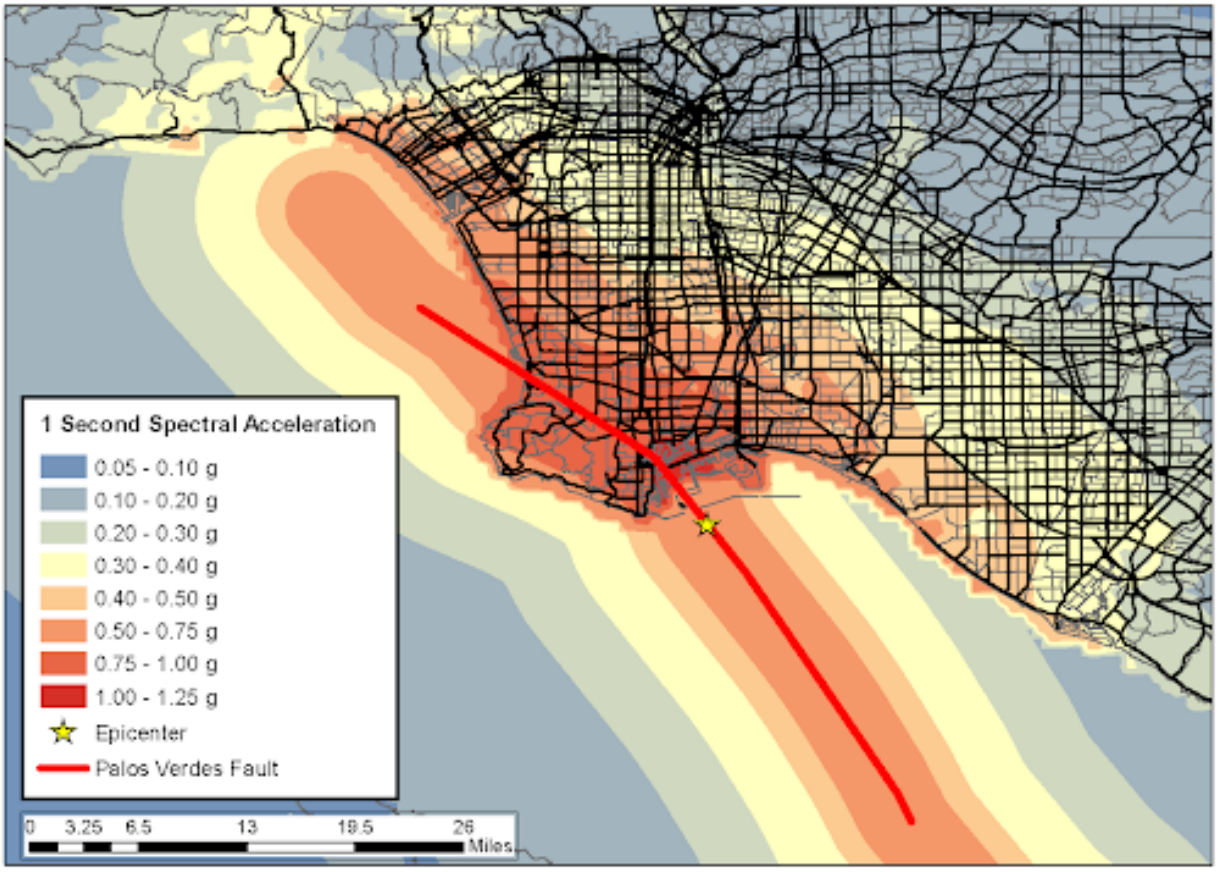


Figure 4.2: Sample earthquake visualization (from Cetiner [15])

Table 4.1 shows the travel demand summary for each time of day, while Figures 4.5a and 4.5b show the visualization of the overall travel demand and the port travel demand.

While Khademi et al. [54] showed that travel demand can shift substantially after an earthquake, estimating such changes is resource-intensive and difficult to generalize. This study instead holds pre-earthquake demand fixed to quantify disruptions to trips that would typically occur under normal conditions. Although this approach does not capture voluntarily canceled trips (e.g., due to fear or closures), it does reflect suppressed demand caused by network disconnections, as captured by the number of unfulfilled trips. These unfulfilled trips serve as a conservative indicator of connectivity loss, and the resulting cost estimates should be interpreted as a lower bound. Results are reported in Section 4.4.

Sampling Due to the computationally intensive requirements of this kind of traffic simulation, the origin-destination data was sampled such that 1 agent represents 5 vehicle trips. The final simulation input is composed of 8,158,000 car agents and 246,218 truck agents for a

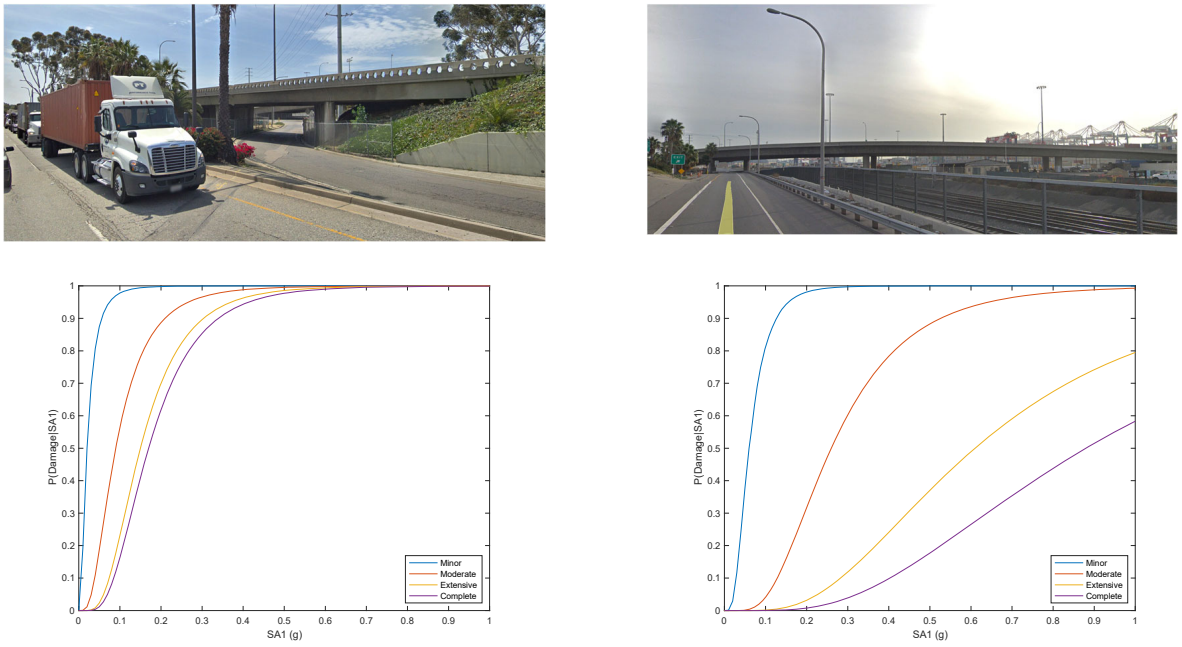


Figure 4.3: Fragility functions computed for two of the modeled bridges

Table 4.1: Travel demand summary

Time of day	# of car trips	# of truck trips	Total trips
6am - 9am	7,396,597	201,815	7,598,412
9am - 3pm	15,146,975	504,754	15,651,729
3pm - 7pm	12,036,376	219,119	12,255,495
7pm - 9pm	3,117,935	69,886	3,187,821
9pm - 6am	3,116,850	246,119	3,362,969

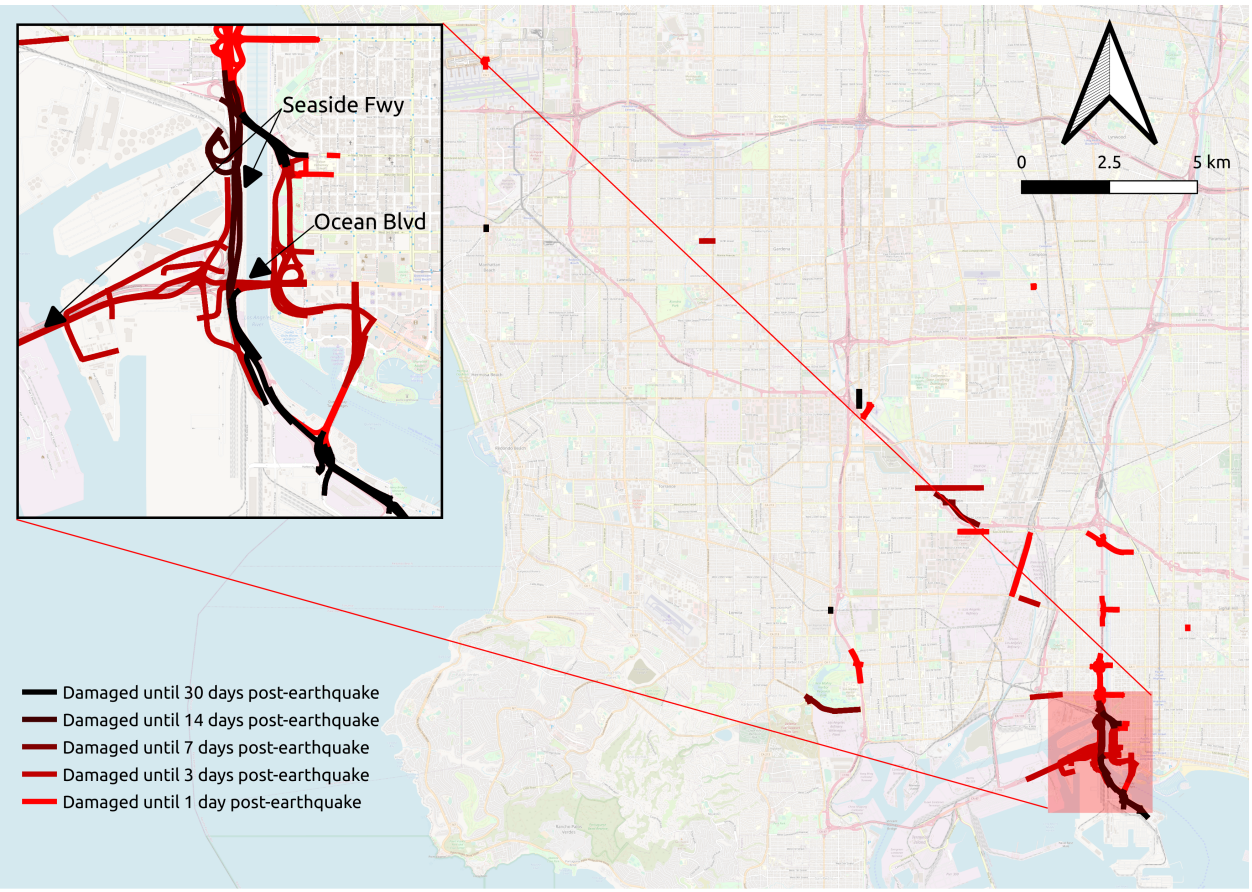


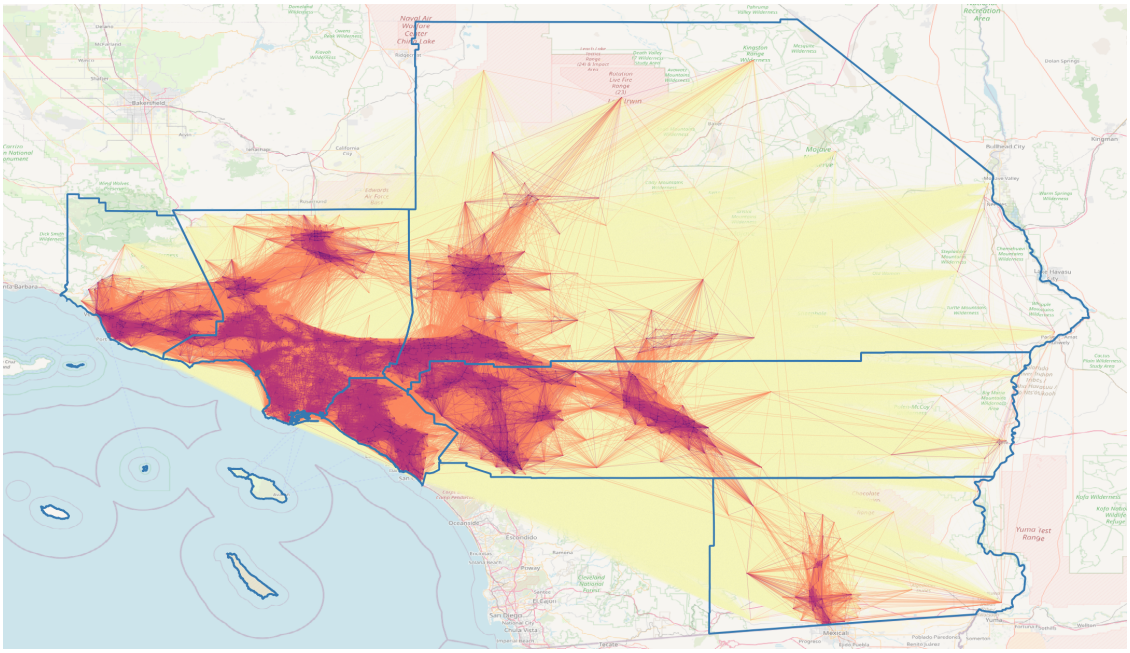
Figure 4.4: Road closure map, which includes the damaged bridges and connecting road/bridge segments assumed to also be closed for inspection.

total of 8,404,218 agents. The output figures are also adjusted accordingly with a factor of 5.

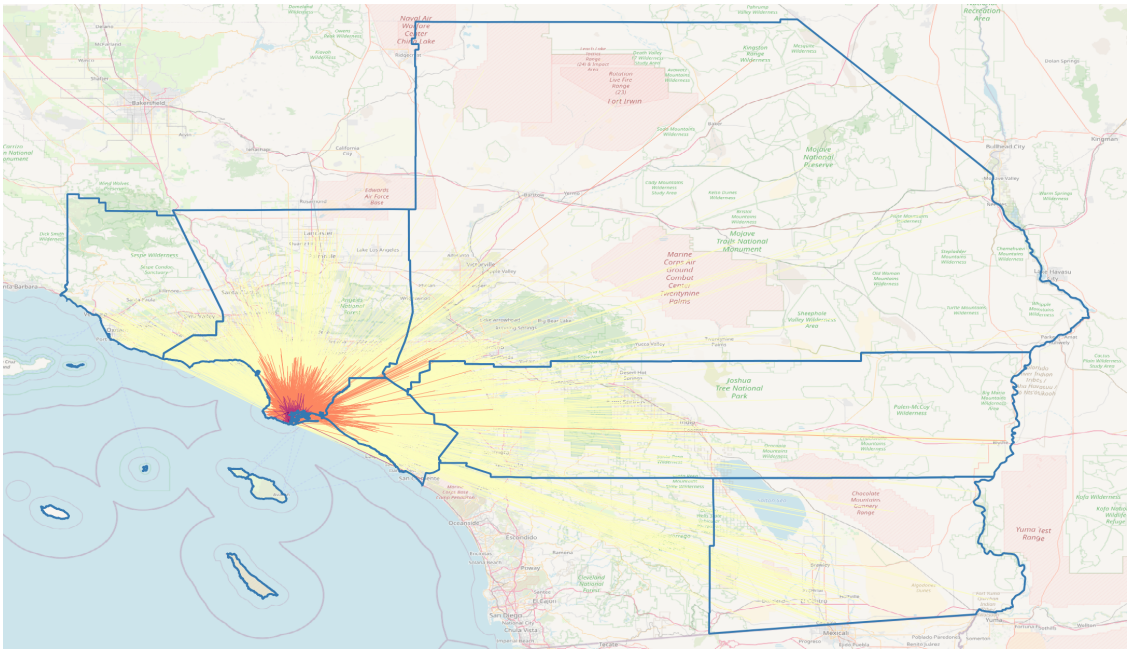
Traffic Simulation

The agent-based semi-dynamic traffic assignment model introduced in Section 4.2 is used to compute the sub-hourly changes in road usage. Each trip is assigned an initial route based on the computed shortest path using contraction hierarchies from origin to destination [39]. Each edge's volume is updated every 15 minutes and each trip's shortest path is recomputed based on the new network congestion status. Trucks were restricted from traveling on residential roads.

Six scenarios were simulated: (1) a base scenario with no road closures, (2) a scenario 1 day post-earthquake, (3) a scenario 3 days post-earthquake, (4) a scenario 7 days post-earthquake, (5) a scenario 14 days post-earthquake, and (6) a scenario 30-days post-earthquake. Each post-earthquake scenario includes road closures from the bridge damage analysis in Section



(a) Overall travel demand



(b) Port travel demand

Figure 4.5: Travel demand data

4.3. Each simulated scenario yields three main outputs: the traffic volume at each link for every 15 minutes of the simulation, the total travel time of each agent, and the total trip distance of each agent.

Due to the bridge modeling output being a deterministic set of bridges for each scenario, the simulations are not expected to produce vastly different results for each run with the same input and scenario parameters. Nevertheless, each scenario was run 10 times to rule out the impact of possible random variations in each run (e.g., sequence in which shortest path is calculated for each agent, selection among multiple shortest paths). For each scenario, the average of metrics such as travel time and travel distance is taken over 10 runs, and these averages are used as the main results for analysis. The variations, or lack thereof, in the results generated from these random repetitions are reported in Section 4.4.

4.4 Results and discussion

Initial verification compared with real-life metrics

To assess the performance of the model framework, the Southern California Association of Governments [89] Transportation Plan included some metrics that are comparable to the model outputs. Some of these key metrics are:

Mean commute time SCAG lists the mean commute time—defined as the average travel time to work—as 32.1 minutes. The input data on travel demand (in Section 4.3) does not have activity labels (work/non-work) but the average travel time computed for the base scenario from the simulation for all trips is 29.4 minutes.

Average distance traveled SCAG lists the average distance traveled as 17.9 miles for work trips and 5.8 miles for non-work trips. The base scenario leads to an overall average travel distance of 15.1 miles, which is within the SCAG range.

Percent of trips less than 3 miles SCAG states that 14.0% of work trips are less than 3 miles, while 40.5% of non-work trips are less than 3 miles. The base scenario computes 26.1% of all trips being less than 3 miles, which is also well within the SCAG range.

From these key metrics, it was concluded that the traffic model resembles the real-life transportation scene in general despite the lack of activity labels on existing data. The availability of activity/trip purpose labels in travel demand inputs can greatly enrich model assessment in future studies.

While the comparison to SCAG travel metrics suggests that the base scenario simulation produces reasonable aggregate values, it is important to note that full empirical validation of the model—particularly under disrupted, post-earthquake conditions—was not possible due to data limitations. Ideally, validation would involve comparing simulated travel time and distance distributions against observed values from real-world seismic events, as well

as using screenline counts (e.g., vehicle volumes across key bridges or corridors) to verify modeled traffic flows at critical bottlenecks. In the absence of such post-disaster data, the presented validation serves primarily as a high-level plausibility check of the base case network performance. Future work could incorporate real-time sensor data or probe vehicle trajectories from actual earthquakes to enable more rigorous calibration and validation of model outputs under disruption.

Robustness to random variations

Average travel time variation across random seeds (base scenario) is largely from 29.32 to 29.37 minutes (around 0.05 minutes or 3 seconds as shown in Figure 4.6), which is much smaller than the increase from the base to Day 1 scenario that can be seen in Figure 4.8c. Therefore, randomness across simulations is not expected to be significant enough to impact the overall results.

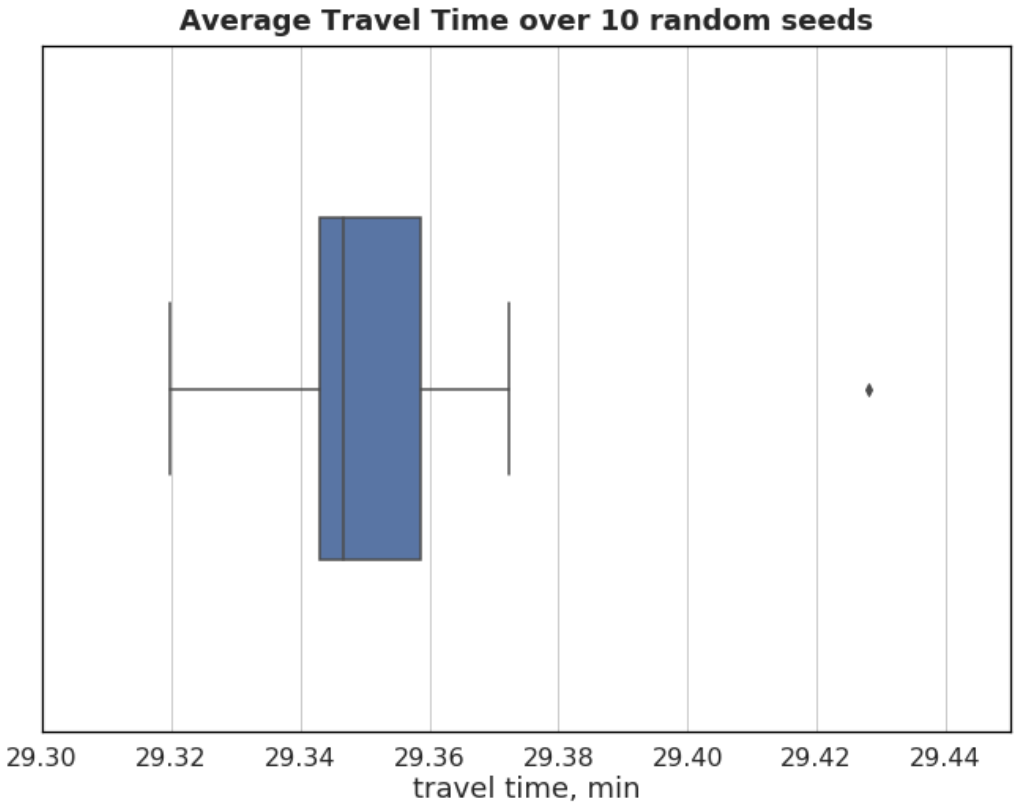


Figure 4.6: Travel time variation over 10 runs

Port area analysis

Focusing on the port area, the trip time and distance outputs for each agent were aggregated to get the overall vehicle hours traveled (VHT), average travel time, and the number of fulfilled & unfulfilled trips for each post-earthquake scenario relative to the base scenario, as shown in Table 4.2. A trip is labeled as *unfulfilled* if the vehicle is unable to travel from its origin to its destination due to damage to the road network.

Figure 4.7 shows the general steps taken to interpret the results obtained for the port area to understand the changes in travel-related metrics at different stages of the earthquake recovery. The primary indicator used to assess the level of impact on the transportation network is the overall vehicle-hours traveled (VHT). Figure 4.8a shows the trend in total VHT for the port area trips. In the base scenario, the VHT is 199,592 vehicle-hours. After the hypothetical earthquake, there is a 10% decrease from Day 0 to Day 1, coinciding with the worst bridge damage and road closure scenario. Despite 14 miles of roadway reopening immediately after Day 1, a small but unexpected 2.5% decrease in VHT happened from Day 1 to Day 3, which makes the VHT to be at the lowest point on Day 3 at 175,272 vehicle-hours, or 12.5% reduction compared to the baseline. From Day 3 on, the VHT starts to recover: a relatively large increase in VHT is observed from Day 3 to Day 7. From Day 7 to Day 30, the VHT plateaus at around 192,843 vehicle-hours, a 4% decrease relative to the base scenario.

To understand the trends in VHT, two components that are influential to VHT are examined: the change in the number of fulfilled trips (completed trips) and the change in the average travel time. The former indicates changes in the connectivity of the road network, as a more severely damaged network would lead to more trips being unable to finish. Figure 4.8b shows the trend in the number of fulfilled trips starting or ending in the port area. There is a steep drop from Day 0 to Day 1 with 15% of port trips unable to be completed; this minimum coincides with the worst bridge damage scenario right after the earthquake, in particular, attributable to 39 bridges and 59 miles of roadway being closed on key access ways within 15 miles of the port. A small recovery in the trip fulfillment rate is observed on Day

Table 4.2: Port area measures

Scenario	[1] Total VHT = [2] * [3]	[2] Average travel time	[3] # of fulfilled trips	[4] # of unfulfilled trips
Baseline (Day 0)	199.59k veh-hrs	48.37 mins	247,565	NA
Day 1	179.75k veh-hrs	51.27 mins	210,335	37,230
Day 3	175.27k veh-hrs	49.19 mins	213,810	33,755
Day 7	191.49k veh-hrs	49.14 mins	233,785	13,780
Day 14	192.21k veh-hrs	48.98 mins	235,455	12,110
Day 30	192.84k veh-hrs	48.45 mins	238,795	8,770

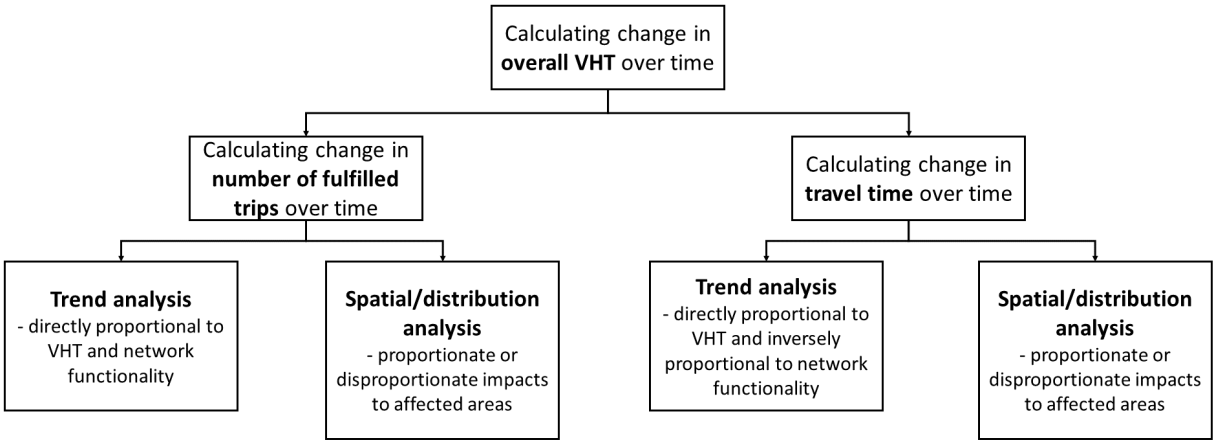
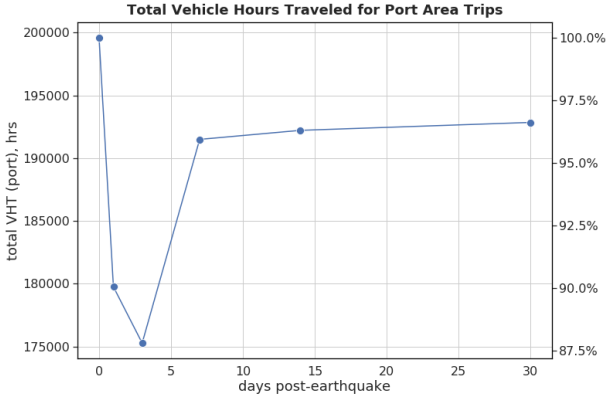


Figure 4.7: Assessing impacts to transportation networks

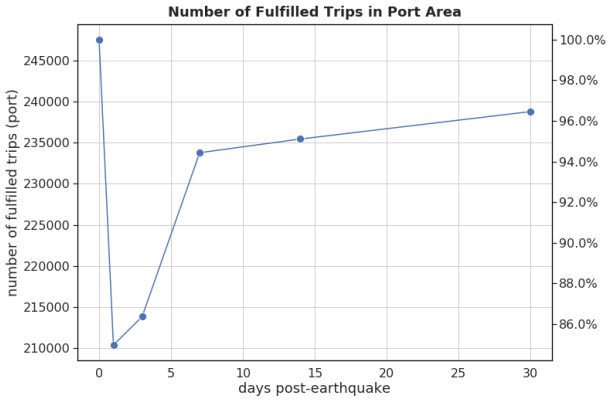
3, due to the recovery of 16 bridges that are mostly external to the port area. The biggest recovery of the trip fulfillment rate happened on Day 7. This large increase in fulfilled trips on Day 7 is due to the reopening of the western portion of the Seaside Freeway bridge that connects the western and eastern sides of the Port of Long Beach and the Port of Long Beach island to the mainland (see Figure 4.4). Slow but steady recovery of the trip fulfillment rate is observed throughout to Day 30 when the number of unfulfilled trips is still about 4% of total port trips a month after the earthquake with 10 bridges and 5.5 miles of roads predicted to be still closed.

On the other hand, changes in the average travel time (calculated only for fulfilled trips) indicate a vehicle's need to detour due to closed roads. Figure 4.8c shows the trend of the average travel time of trips starting or ending in the port area. The average travel time increases by 6% from Day 0 to Day 1, indicating that trips still able to be completed took a longer time to do so, also coinciding again with the worst damage scenario as expected. Average travel time decreases much closer to baseline at Day 3 (with an increase of only 1.7% relative to baseline) when 16 out of 39 damaged bridges are reopened. The average travel time steadily decreases through Day 30 as more bridges are reopened, and it is almost similar to that of the base scenario.

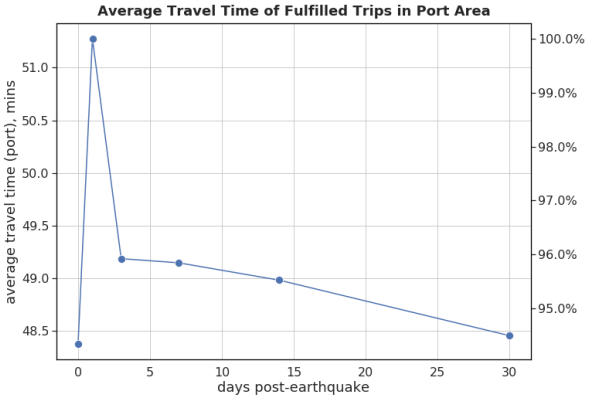
These trends are mostly intuitive, except for the slight drop in the overall VHT from Day 1 to Day 3. Figures 4.8c and 4.8b respectively show that the average travel time decreases on Day 3, but the number of fulfilled trips only increases incrementally. This slight drop in overall VHT, therefore, shows that the change in the travel time component (averaged over 210,335 trips) dominates over the change in fulfilled trips (37,230 unfulfilled trips). This can be attributed to the opening of a road local to the port area that helps the vehicles avoid detours (thus reducing the travel times of trips which can be fulfilled), while roads connecting the port area to the outside area are still closed and only start to open on Day 7. This kind



(a) Change in total VHT



(b) Change in fulfilled trips



(c) Change in average travel time

Figure 4.8: Simulation results

of insight is one that can be made because of the resolution of the traffic simulation and its agent-based nature.

Another observation that stands out is that the increase in average travel time, at worst, is only 3 minutes. While this may seem small, it is important to note that this only takes into account delays due to the road closures because of the earthquake. Any congestion delays already present in the baseline scenario are not separated in this paper, and therefore, the actual delays will be larger than 3 minutes. Furthermore, the averaging of the changes in travel time hides a slightly disproportionate impact on certain trips. Figure 4.9 shows the distribution of travel times of vehicles starting or ending their trips in the port area for Day 0 and Day 1. The shape of the distributions is mostly similar, which indicates that most trip travel times stay the same. To be specific, 75% of Day 1 trips stay within 10% of their Day 0 travel time. However, over 5% of trips (around 5000) have increases of 50% of their Day 0 travel time with some even increasing by a factor of 4 or more. Again, this kind of insight can be made because of the resolution of the traffic simulation and its agent-based nature.

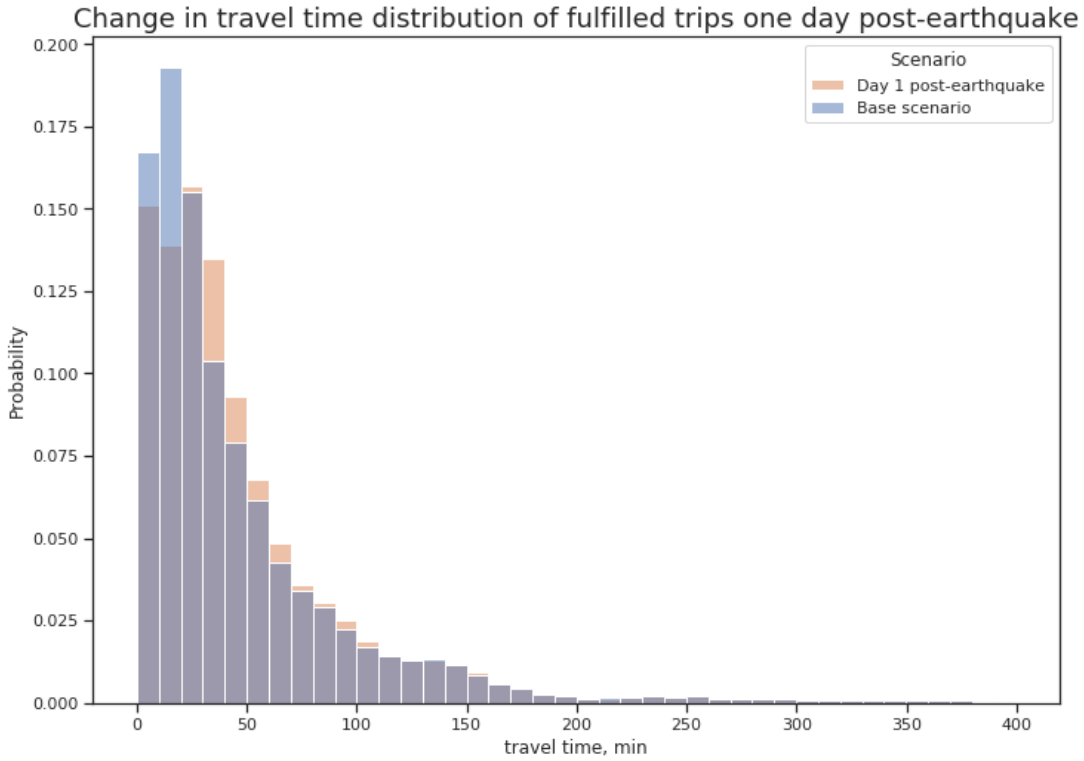


Figure 4.9: Travel time distribution of port area trips

Minimal changes in overall VHT but sizeable decreases in port VHT

Suarez et al. [91] posits that the effect of hazards on VHT and VMT can be ambiguous. VHT, for example, can increase due to vehicles taking less straightforward trips on congested routes due to road closures, but can also reasonably decrease due to the reduced number of trips after a hazard. Figure 4.10 shows the changes in total VHT for the overall study area (orange line) and for trips with origin/destination in the Port of Los Angeles area specifically (blue line). They show that, for this case study in particular, VHT changes negligibly for the overall study area over all of the post-earthquake scenarios. However, port VHT decreases by as much as 12%, indicating a sizeable decrease in productivity in the area. These big differences are attributed to the concentration of bridge damage in the port area, as 31 of the 39 damaged bridges (just under 80%) are within 3 miles of the port boundaries. These findings align with the above findings on changes in travel time.

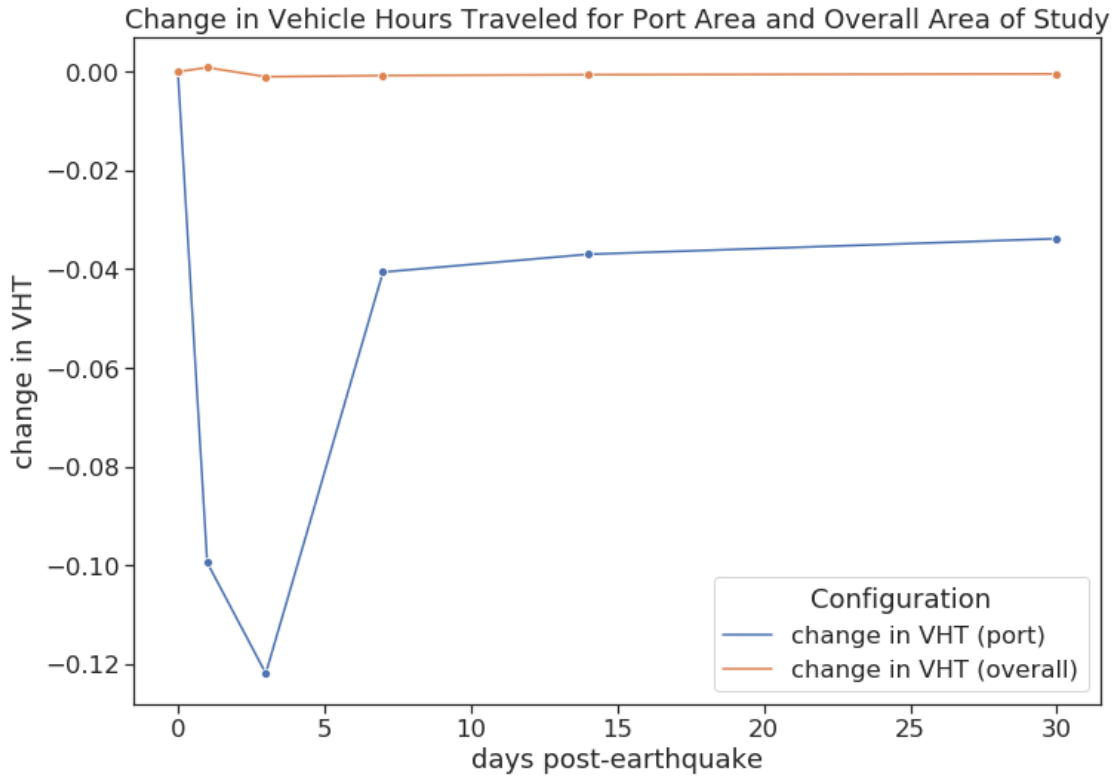


Figure 4.10: Change in VHT (overall area vs port area)

Economic Impact Estimation

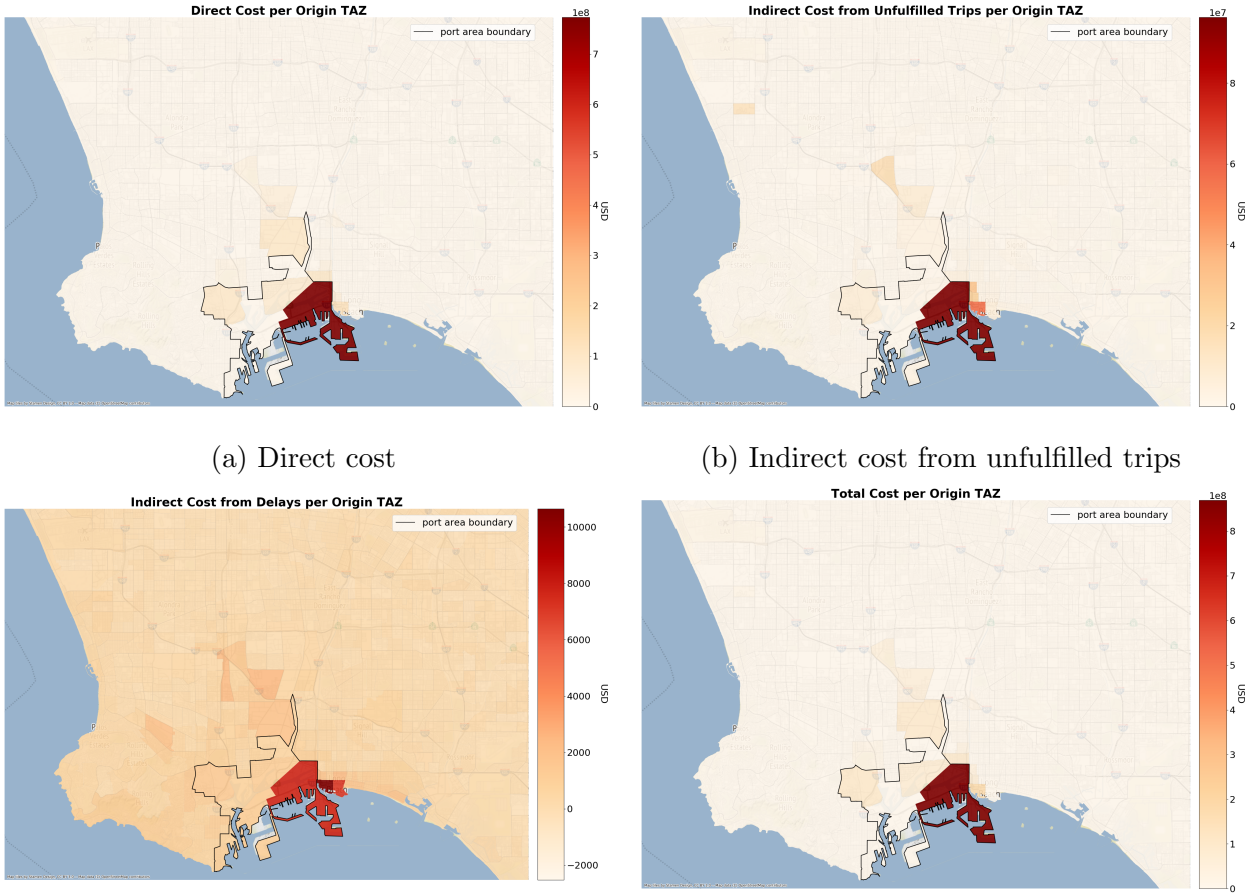
Using the damage maps and simulation outputs from the previous step as inputs to Equations 4.5 through 4.11, the direct and indirect costs related to the transportation system in this hypothetical earthquake scenario are estimated. For direct cost calculations (costs to repair damaged infrastructure), it is assumed that the roads still closed on Day 30 will be repaired by Day 60, and the repair cost ratio in Equation 4.7 is set at 0.68 [34]. For the indirect costs calculations (economic losses due to delays or trip cancellations), the parameters are estimated from the regional economic statistics. For example, for the SCAG area, the median household income in 2018 was $64,989, which translates to an α of around $31 per hour of delay [90] in Equation 4.10. On the other hand, the gross regional product of California was $1,955,856 million in 2020 dollars and the number of labor hours was 25,101 million, which leads to a γ of $78 per hour per lost trip [80] in Equation 4.11. The resulting value from Equation 4.5 indicates the estimated economic impact of the earthquake. The direct cost is calculated to be $1.56 billion, while the indirect cost is calculated to be $768 million (only $121,000 of which is due to traffic delays due to very sparse closure throughout the overall LA region) for a total cost of $2.33 billion. For trips that start or end at the port area, the cost of lost demand dominates and is estimated to be at $476 million, while the delays cost $57,000.

Spatially disproportionate impacts

During hazards such as floods and earthquakes, the number of trips that are able to be completed is always expected to decrease [91]. This is true for this case study with there being as many as 73,845 trips (albeit less than 1% of the total trips) that are unfulfilled in the overall SCAG area one day after the earthquake, 37,230 (or 50% of all unfulfilled trips) of which start or end in the port area. As much as 62% of the total indirect cost is from the port area, showing the spatially disproportionate impact of the earthquake. This aligns with the finding that unfulfilled trips in the port area account for up to 15% of all trips in the port area and is very evident in a spatial visualization of the area as shown in Figure 4.11.

Lost demand over delays

Additionally, the economic cost estimation shows that the impact of delays is dwarfed by that of lost demand (i.e., from the unfulfilled trips), as lost demand accounts for 99.98% of the computed indirect cost. Supporting this observation, Figure 4.12 shows that the economic recovery in the port area and the road restoration trend very similarly with time. Since the lost demand is a proxy indicator for the degradation of road network connectivity, this result shows that road network connectivity is the biggest issue post-earthquake in terms of the economic losses, while economic losses delays due to congestion are relatively negligible.



(a) Direct cost

(b) Indirect cost from unfulfilled trips

(c) Indirect cost from delays

(d) Total cost

Figure 4.11: Cost per origin TAZ

Bridge closure costs versus bridge repair budgets

This study focused only on losses due to disruption of the transportation network, excluding seismic damage impacts to other port structures or buildings. This study also does not look into chain effects due to other sectors outside of transportation also being impacted. Because of this focus on transportation, the computed impacts cannot be directly compared to GDP which is based on a more comprehensive and general perspective of the regional economy. Instead, it is more appropriate to compare the results with budgets, both federal and state levels, allocated for bridge repair.

For 2022, the federal government's Bipartisan Infrastructure Law granted California $574,785,473 under its Bridge Formula Program intended for bridge replacement, rehabilitation, preservation, protection, and construction. This is the first tranche under a five-year program with a budget of $4.2 billion [12]. However, the American Road and Transportation

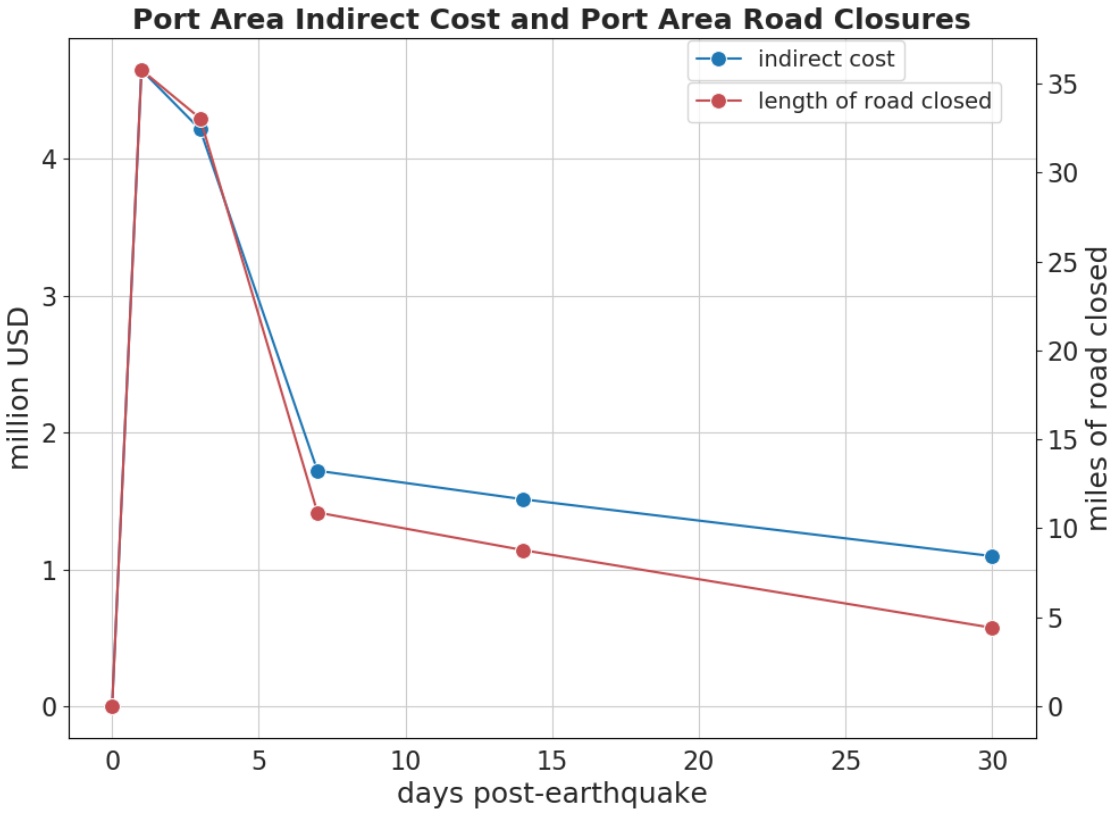


Figure 4.12: Indirect cost and road closures

Builders Association (ARTBA) computes the total repair cost to be at $11.7 billion [2], more than half of which is not in the budget for the next five years. The computed costs of this hypothetical earthquake are a direct cost (due to repair/replacement of bridges) of $1.56 billion and an indirect cost (due to loss of demand and delay) of $768 million for a total of $2.33 billion. In the aftermath of an earthquake, this indirect cost can be taken as the amount of costs incurred by the individuals on top of federal/state bridge repair budgets brought about by a lack of pre-disaster mitigation. In other words, instead of only spending the direct cost of $1.56 billion to preventatively repair bridges before an earthquake, the cost increases by almost 50% post-earthquake which will largely be taken from each individual's personal income on top of taxes paid for the federal and state budgets.

It should be noted carefully, however, that the present study did not consider the direct seismic damage to port structures (wharves, cranes, container yards, etc.) due to ground shaking, or more importantly, the tsunami and inundation hazard, which could potentially close the entire port indefinitely. Impacts to the ports' productivity can also lead to cascading

economic impacts that are more challenging to quantify. In the past years, the COVID-19 pandemic and a subsequent change in consumer behavior led to congestion in the ports and supply chain shortages [50, 93, 29]—the full impacts of which are yet to be studied. In effect, the estimates in this study are still conservative and would likely compound once other factors are considered.

Implications of case study

Figure 4.13 shows a representation of the disaggregated cost based on the results of this study. Due to the finer resolution of the methods used, the presented framework is able to come up with hierarchies of cost, as well as numerical estimates, that can be broken down between direct cost to repair or replace roads as opposed to socio-economic cost to the transportation system and its users. This can further be broken down spatially, for example between the port area and non-port areas, to focus on areas of interest. This can also be further broken down into car trips and truck trips because of the agent-based nature of the traffic model used in this framework. With access to more data, these costs can be further broken down based on trip activity, demographics (such as age, sex, race) and more to analyze whether certain areas, groups, or sectors are affected differently compared to others or compared to the whole, and by extension, decision-makers are able to make more informed policy choices. This model can only improve with more granular information for bridges, roads, and trips.

4.5 Conclusion, limitations, and suggested future work

This chapter presented a highly granular synthesis framework to quantify the robustness of transportation networks to hazards such as earthquakes, including seismic loss and recovery. The framework begins with the characterization of seismic demands and proceeds to assess bridge infrastructure damage by modeling and simulating each bridge's response to produce individual seismic fragility curves. These curves allow for rapid estimation of bridge damage under hypothetical or real events. The resulting damage estimates are then input into a transportation network model that runs a semi-dynamic agent-based traffic assignment over a 24-hour period for both pre- and post-earthquake scenarios. Output metrics such as road usage and agent travel times are used to estimate economic impacts—including both direct (repair) and indirect (delay, trip loss) costs. The resolution and scalability of the framework allow for a holistic and disaggregated assessment of seismic impacts on large-scale transportation systems.

A case study of the Southern California region focused on the Ports of Los Angeles and Long Beach, using a simulated Magnitude 7.4 earthquake and a detailed network with over 1.4 million edges and 8.4 million agents. Simulation results showed consistency with real-world travel time and distance metrics, and the fine resolution of the model enabled spatially detailed analysis of vehicle-hours traveled and trip outcomes. Economic impact analysis revealed that the port area, due to its proximity to the epicenter and reliance on vulnerable

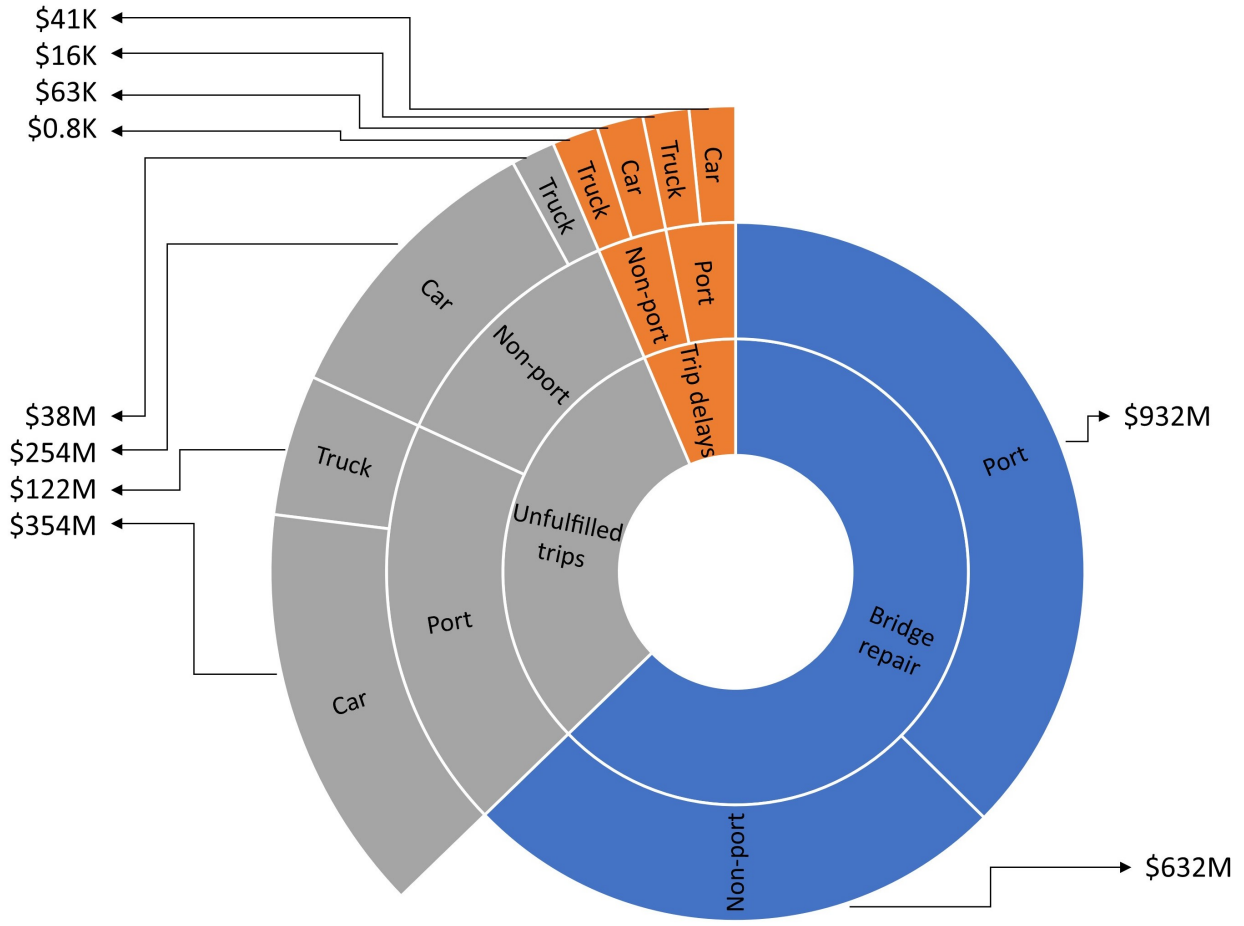


Figure 4.13: Cost estimate visualization

bridges, experienced disproportionate losses. Most of the estimated losses stemmed from direct damage and unfulfilled trips, with minimal contribution from delay-related congestion, as the system retained partial functionality despite reduced capacity.

However, several limitations should be acknowledged. First, travel demand was assumed to remain unchanged immediately after the earthquake. In reality, travel behavior may shift due to school or workplace closures, fear, or disruption of other systems. Conversely, transit disruptions could lead to increased road demand. These behavioral dynamics were not captured. While the assumption of fixed demand enables consistent comparison across scenarios, it may understate or overstate actual demand levels post-earthquake.

Second, the model defines unfulfilled trips strictly as those that could not reach their destination due to blocked links, but does not account for trips that were voluntarily canceled, such as those people avoid due to confusion or safety concerns. Thus, the resulting estimates of lost connectivity reflect a lower bound.

Third, the valuation of delay assumed an hourly wage–equivalent value of time, which may overestimate indirect costs; common practice suggests using 50–65% of hourly wage to reflect non-productive time. Additionally, productivity losses were estimated assuming a full 8-hour workday for each unfulfilled trip, which may overstate foregone economic output if many trips were non-work related.

Finally, validation of post-earthquake conditions was limited by the absence of observed data on travel behavior or traffic volumes, particularly for local roads. Ideal validation would include travel time distributions, screenline counts, or facility throughput comparisons. The current results should therefore be interpreted as internally consistent, but not empirically verified.

To improve the realism and policy relevance of this framework, future work could incorporate dynamic or scenario-based demand models that reflect adaptive behavior, including trip suppression or mode switching. More granular activity-based data (e.g., trip purpose or freight value) would enable more accurate estimates of trip-level and system-wide economic losses. A better understanding of travel behavior under post-disaster conditions, combined with sensor and GPS data from real events, would also allow for more rigorous model calibration and validation. Finally, integrating multimodal systems into the model would provide a fuller picture of regional mobility disruptions and interdependencies.

Chapter 5

Assessing rapidity of recovery of regional transportation systems to seismic hazards: Tokyo case study

5.1 Introduction

A significant portion of resilience research focuses on robustness, which refers to the strength of system components, their likelihood of failure, and the direct impacts of such failures. Equally important, however, is rapidity, defined by Bruneau et al. [11] as a system's ability to contain losses and disruptions to prevent cascading effects. In the context of transportation systems, rapidity reflects how quickly a disrupted network can recover its functionality.

Most existing studies of rapidity focus on identifying optimal link repair strategies to accelerate recovery. For example, Frangopol and Bocchini [40] used optimization to determine the most effective bridge repair sequence over a 24-month horizon for a 13-bridge network in Lehigh Valley, Pennsylvania, while Dong, Frangopol, and Saydam [30] extended the time frame to 30 years, incorporating social, economic, and environmental costs (for a 10-bridge highway network in Orange County, California). Other researchers, such as Sohouenou and Neves [88] and Barati, Yazici, and Almotahari [6], assessed link criticality through simulation-based failure scenarios. Most of these studies use highly simplified networks, often with fewer than 100 links, which makes it difficult to apply their findings to real urban systems with thousands of links and complex redundancy.

More importantly, these models often abstract away from the institutional realities of recovery. In practice, the sequence and timing of link repairs depend not only on technical and economic factors, but also on the governance structures in place. For instance: Who decides which links are repaired first? Are the affected links managed by a single agency or by multiple entities? If multiple agencies are involved, how does institutional fragmentation influence the actual recovery process? These questions underscore the critical role of inter-agency coordination in shaping system rapidity.

In this study, coordination is defined as inter-agency communication during disaster response, with an emphasis on three key aspects: the sharing of (1) strategies, (2) system-level information, and (3) resources. To examine how coordination influences recovery, the Tokyo Metropolitan Area is used as a case study.

Tokyo's expressway system is jointly operated by two main entities: the Metropolitan Expressway Company Limited (MEX), which manages the dense inner-urban network, and the East Nippon Expressway Company Limited (NEXCO), which operates the interurban outer-ring expressways. Although the networks are physically interconnected, the two agencies maintain separate governance frameworks and recovery protocols. MEX has developed its own Disaster Prevention Operations Plan and Business Continuity Plan (BCP), which include structured inspection timelines, communication systems, and coordination procedures for seismic events [66]. NEXCO East, by contrast, maintains formal disaster-response agreements (e.g., with NTT DoCoMo), and independently deploys mobile restoration units and digital traffic-monitoring systems [31, 32]. These distinct institutional arrangements raise important questions about how coordination, or the lack thereof, shapes recovery dynamics.

While Tokyo's governance structure is uniquely complex, it is not an outlier. In the United States, public–private partnerships (P3s) have introduced similar fragmentation. States such as Texas, Indiana, and Virginia have engaged private concessionaires under long-term leases, while Southern California has transitioned some privately developed corridors, like the SR-91 Express Lanes, to public ownership [61, 94]. These institutional arrangements complicate post-disaster recovery, as decision-making authority, resource control, and communication protocols are not always aligned.

Similar dynamics appear in other infrastructure domains, particularly public transit. Tokyo's rail and subway network includes more than a dozen operators. Cities in the UK and Latin America also exhibit multi-operator transit systems, often involving a mix of public, private, and informal providers [49, 44, 47]. Across these contexts, fragmented governance poses serious challenges for coordinated recovery in the face of extreme events.

By using Tokyo as a case study, this chapter examines how different levels of inter-agency coordination affect the rapidity of recovery in a complex, multi-operator highway network. Specifically, the model simulates the recovery of expressway functionality under varying coordination scenarios between MEX and NEXCO, focusing on metrics such as recovery time, area under the recovery curve (AUC), and skewness.

The remainder of this chapter is organized as follows. Section 5.2 defines the rapidity metrics used in this study. Section 5.3 introduces the coordination modeling framework and scenario design. Section 5.4 describes the formulation of the Tokyo case study. Sections 5.5 and 5.6 present the results and discussion, respectively, followed by the conclusions and recommendations in Section 5.7.

5.2 Rapidity metrics

Similar to robustness studies, a key component of rapidity analysis is the definition of cost and the determination of relevant factors to consider during recovery. This can be viewed as defining a performance function over time under varying recovery strategies to evaluate which strategy leads to the fastest return to baseline functionality.

Functional metrics

Functional metrics quantify the system's ability to provide efficient service throughout the recovery process. A common approach is to measure rapidity using the area under the curve (AUC) of a performance function, where a larger AUC indicates a faster and more complete recovery. This foundational concept appears in several studies.

For example, Frangopol and Bocchini [40] defines rapidity (which they refer to as resilience) as:

$$R = \frac{\int_{t_0}^{t_0+t_h} Q(t)\,dt}{t_h} \tag{5.1}$$

where t_0 is the time of the earthquake, t_h is the recovery time horizon, and $Q(t)$ represents the system functionality at time t. They define $Q(t)$ based on a weighted combination of total system travel time (TTT) and total travel distance (TTD):

$$Q(t) = \frac{\Gamma(t) - \Gamma^0}{\Gamma^{100} - \Gamma^0}, \quad Q(t) \in [0,1] \subset \mathbb{R} \tag{5.2}$$

$$\Gamma(t) = \frac{1}{\gamma_T \cdot \mathrm{TTT}(t) + \gamma_D \cdot \mathrm{TTD}(t)}, \quad \Gamma(t) \in \mathbb{R}^+ \tag{5.3}$$

where γ_T and γ_D are unit costs (in min^{-1} and km^{-1}, respectively), and Γ^0 and Γ^{100} correspond to the fully closed and fully open states of the network, respectively. A higher value of R indicates more rapid recovery, as illustrated in Figure 5.1.

Hu et al. [48] also use a recovery curve framework, but normalize performance based on the initial post-earthquake state and full functionality. They define:

$$RL(\zeta) = \frac{F_R(\zeta) - F_I}{F_A - F_I} \tag{5.4}$$

$$RE(\zeta) = \int_0^1 RL(\zeta)\,d\zeta \tag{5.5}$$

Here, ζ is the proportion of restored edges, $RL(\zeta)$ is the recovery level, and $RE(\zeta)$ is the recovery efficiency, which serves as a functional analog to the AUC.

Merschman et al. [65] incorporate functional performance measures based four costs. The first two (C_1 and C_2) are functional metrics while the latter two (C_3 and C_4) are topological

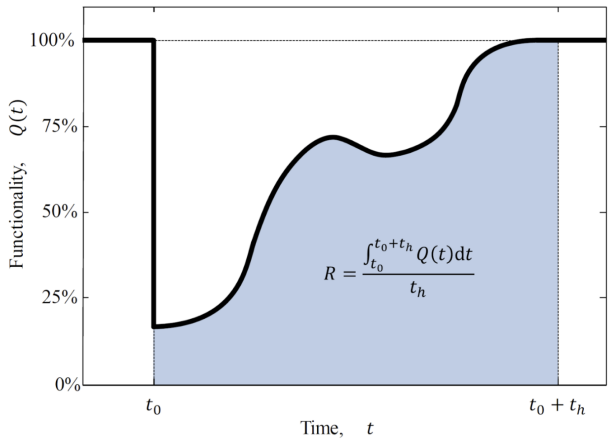


Figure 5.1: Resilience as area under the recovery curve (AUC) (from Frangopol and Bocchini [40])

and social metrics, respectively. C_1 is based on total travel distance and C_2 is based on total travel time which contribute to an aggregated network performance score:

$$NP = \frac{1}{C_1 \times C_2 \times C_3 \times C_4} \tag{5.6}$$

While AUC and recovery duration are useful indicators, Zhang, Wang, and Nicholson [103] argue that they fail to capture differences in recovery trajectory shapes. For instance, two recovery curves may have the same AUC but differ in how quickly functionality is restored in the early versus late stages. To address this, they introduce a complementary metric, trajectory skewness, defined as:

$$\text{Skewness} = \frac{\sum_{i=0}^{k} t_i R(t_i) \Delta t}{\sum_{i=0}^{k} R(t_i) \Delta t} \tag{5.7}$$

where t_i is the time index, $R(t_i)$ is the recovery level at time t_i, and k is the total number of time steps. Optimizing both total recovery time and skewness allows for more nuanced comparisons between recovery strategies.

Topological metrics

Topological metrics assess the structural configuration of the network, independent of actual traffic demand or flow.

Hu et al. [48] measure topological recovery using the fraction of restored edges, where N_R is the total number of restored edges and N_T is the total number of edges:

$$\zeta = \frac{N_R}{N_T} \tag{5.8}$$

This provides a structural measure of how much of the network's connectivity has been reestablished.

Another common topological metric is the use of betweenness. Betweenness centrality quantifies the importance of a node or link in terms of the number of shortest paths that pass through it. It is based on the idea that critical components often serve as bridges or connectors between other parts of the network.

Formally, the betweenness centrality B_i of a node i is defined as:

$$B_i = \sum_{s \neq i \neq t} \frac{\sigma_{st}(i)}{\sigma_{st}} \tag{5.9}$$

where:

- σ_{st} is the total number of shortest paths between node s and node t,
- $\sigma_{st}(i)$ is the number of those paths that pass through node i,
- the summation is taken over all pairs of distinct nodes s and t such that $s \neq t \neq i$.

Similarly, the betweenness centrality of a link (edge) e is given by:

$$B_e = \sum_{s \neq t} \frac{\sigma_{st}(e)}{\sigma_{st}} \tag{5.10}$$

where $\sigma_{st}(e)$ is the number of shortest paths between s and t that pass through link e.

In transportation networks, high-betweenness links or nodes often correspond to routes or intersections that carry a significant portion of through traffic, and their disruption may lead to major system-wide impacts.

Merschman et al. [65] also incorporate topological metrics using a modified betweenness centrality measure (C_3) that prioritizes the shortest path rather than the raw count of traversals, focusing on the network's potential to enable efficient flows.

Social metrics

Social metrics evaluate the recovery process in terms of its impact on populations and access to critical services. These metrics are typically context-dependent and aim to reflect real-world equity concerns.

Dong, Frangopol, and Saydam [30] propose a time-varying sustainability metric $\mathbf{SM}(t)$ that integrates economic, environmental, and social considerations:

$$\mathbf{SM}(t) = \sum_{H} \sum_{LS} \sum_{DS} C_{\text{Cons|DS}}(t) \cdot P_{\text{DS|LS}}(t) \cdot P_{\text{LS}|H}(t) \cdot P_H(t) \tag{5.11}$$

where:

- $C_{\text{Cons|DS}}(t)$ = conditional consequence (economic, social, or environmental) given damage state DS at time t,
- $P_{\text{DS|LS}}(t)$ = conditional probability of a damage state given a structural limit state LS (e.g., yielding, instability) at time t,
- $P_{\text{LS}|H}(t)$ = conditional probability of a structural limit state arising from hazard H at time t,
- $P_H(t)$ = annual mean rate of hazard H.

Different factors of this sustainability metric factor into the maximum expected economic loss. Minimizing this metric combined with minimizing the total retrofit cost is used as the objective in the optimization to determine the optimum sequence to repair a set of 10 bridges.

Merschman et al. [65] define a social metric C_4 based on emergency accessibility, specifically the travel time from each zone to a trauma center compared to pre-disaster conditions. This allows them to factor in the disparate impacts of service disruptions on vulnerable communities and essential services.

Metric selection

Based on the range of rapidity metrics surveyed above, it becomes clear that the selection of an appropriate metric must be aligned with both the modeling framework and the level of resolution being used. While several studies incorporate composite indicators, such as the combination of functional, topological, and social metrics proposed by Merschman et al. [65], or the sustainability-based cost structure from Dong, Frangopol, and Saydam [30], these approaches may not be well-suited for applications involving fine-grained, behaviorally realistic models. Similarly, while the shape-based skewness metric introduced by Zhang, Wang, and Nicholson [103] offers valuable insight into recovery dynamics, and area-under-the-curve (AUC) metrics such as those used by Frangopol and Bocchini [40] provide a holistic summary of system performance over time, their applicability is highly dependent on modeling constraints.

In this study, a semi-dynamic agent-based traffic model is adopted to simulate post-disaster recovery. As elaborated in Chapter 3, this modeling approach enables detailed resolution at the individual vehicle level, avoiding the spatial aggregation inherent in TAZ-level analysis. However, this level of detail also necessitates modeling combined road and highway networks composed of hundreds or thousands of links, which imposes substantial computational demands. As a result, several of the more complex or probabilistic rapidity metrics discussed earlier are impractical to implement in this context.

Given these considerations, this study focuses on functionality-based metrics—specifically, total system travel time—as the primary indicator of network performance during recovery. This approach is consistent with previous work such as Frangopol and Bocchini [40] and

Hu et al. [48], who base performance on time- and cost-weighted travel behavior. System performance $Q(t)$ at time t is defined as:

$$Q(t) = \sum_{j \in V} t_j \tag{5.12}$$

where V is the set of all vehicles in the system and t_j is the travel time of vehicle j.

To evaluate rapidity, two complementary metrics are applied. The first is the total area under the recovery curve (AUC), which quantifies the average system performance over the recovery period as defined in Equation 5.1.

The second metric is the skewness of the recovery trajectory, whether most recovery occurs early or late in the time horizon. This metric is especially useful when different recovery strategies produce similar AUC values but differ in the temporal distribution of performance gains, as highlighted by Zhang, Wang, and Nicholson [103]. Skewness is defined as:

$$\text{Skewness} = \frac{\sum_{i=1}^{n} t_i \cdot R(t_i)}{\sum_{i=1}^{n} R(t_i)} \tag{5.13}$$

where t_i is the time index, $R(t_i)$ is the recovery value at time t_i, and n is the total number of time steps. To allow for comparison across scenarios with different recovery durations with different recovery durations, this value is normalized:

$$\text{Normalized Skewness} = \frac{\text{Skewness}}{T} \tag{5.14}$$

where T is the total recovery duration. A lower normalized skewness indicates that a greater share of recovery occurs earlier, which may be desirable from a service restoration or user-experience perspective.

While this study primarily emphasizes functionality-based metrics due to their compatibility with the chosen traffic model and computational tractability, this does not preclude the incorporation of topological or social dimensions in later steps of the methodology. For example, once optimal recovery strategies are identified based on functional performance, additional criteria, such as accessibility for vulnerable populations or network centrality, can be layered onto the analysis to evaluate outcomes from broader resilience or equity perspectives. This study in particular incorporates topological metrics in the following section.

5.3 Coordination modeling

The behavior of organizations involved in disaster response is a critical component of resilience. While this topic is explored extensively in public policy and organizational management literature, research that intersects these fields with transportation and engineering remains limited. Comfort, Ko, and Zagorecki [27] demonstrates that access to core information significantly enhances both the efficiency of response actions and coordination across the network of responding organizations. Using an agent-based simulation, they test three

scenarios characterized by different levels of information access: (1) no information (blind), (2) time-based information, and (3) severity-based information. They find that access to both timeliness and severity data improves agent response efficiency.

In a related vein, Comfort [26] analyzes three historical cases of inter-organizational conflict during disaster response: the 1987 Ecuador earthquake, the 1988 northern Armenia earthquake, and the 1989 Loma Prieta earthquake in California. In each case, they identify models of inquiry and interaction in post-disaster environments, highlighting pathways to improve information flow and coordination. Key strategies include: (1) investing in prior training and cultivating shared commitment and understanding of responsibilities; (2) establishing a community-wide knowledge system; and (3) fostering exchange relationships supported by timely and accurate information from the disaster environment.

In particular, transportation networks are often managed by multiple agencies or operators, each responsible for a different system component. For example, separate agencies may oversee rail and road networks, urban and regional transit, or even distinct highway systems depending on jurisdictional boundaries. These entities typically operate independently, even during disaster response, despite the interconnected nature of the systems they manage. Although some coordination protocols are established in advance, the effects of varying levels of inter-agency coordination on post-disaster recovery remain underexplored in the engineering and transportation literature.

This work aims to address that gap in two ways: (1) by modeling inter-agency coordination in a post-disaster recovery context, thereby contributing to a bridge between organizational behavior and transportation engineering, and (2) by investigating how different recovery strategies and coordination levels—defined through the sharing of recovery strategies, system-level information, and resources—affect the rapidity of transportation network recovery.

Recovery strategies

In line with the selection of rapidity metrics, it is also necessary to define the recovery strategies under consideration. Hu et al. [48] compare four distinct network recovery strategies: (1) *random recovery*, where damaged links are selected at random at each time step; (2) *greedy recovery*, where the link that maximizes the immediate improvement in network functionality is restored at each step; (3) *periphery recovery*, which prioritizes the link connected to the isolated node with the largest population near the network boundary; and (4) *preferential recovery*, which targets the link connecting the isolated node with the largest population to the functional component of the network. Their results show that strategic approaches outperform random recovery in terms of efficiency and speed.

Similarly, Sohouenou and Neves [88] evaluate four strategies: (1) *optimal recovery*, which is based on identifying the repair sequence that yields the highest resilience indicator (i.e., optimal area under the recovery curve); (2) *average recovery*, derived from averaging results across randomly generated repair sequences; (3) *flow-based recovery*, which prioritizes links with the highest pre-disaster traffic volumes; and (4) *criticality-based recovery*, which restores links in order of decreasing estimated criticality. Criticality is determined by evaluating

the drop in network performance caused by all single-link failure scenarios. Their results show that the criticality-based recovery strategy performs the closest to the optimal recovery strategy.

Ma et al. [60] analyze recovery strategies for a multimodal transportation network, comparing four approaches: (1) *random recovery*; (2) *volume-based recovery*, prioritizing links by pre-disaster traffic volume; (3) *betweenness-based recovery*, which ranks links by their pre-disaster betweenness centrality; and (4) *route-based recovery*. The route-based approach integrates concepts of connectivity and dependency by identifying links belonging to the same route and prioritizing those that restore route-level continuity. If multiple damaged links exist within a route, the strategy prioritizes those connected to functioning components, followed by descending order of pre-disaster volume, capacity, and link length. Among the tested strategies, the route-based method yields the most rapid recovery.

This study adopts a similar set of recovery strategies: betweenness-based, volume-based, and route-based. Given the focus on functionality, specifically total system travel time, as the primary performance indicator, incorporating route- and betweenness-based strategies facilitates consideration of connectivity and interdependency in the recovery process. These strategies are selected to complement the chosen performance metrics and the defined performance curve that focus on functionality.

Levels of coordination

A key limitation of most prior studies, including the multimodal analysis by Ma et al. [60], is the implicit assumption that transportation systems are centrally managed. In practice, different components of a network are typically overseen by distinct agencies or operators, and the degree of coordination among them can significantly influence the speed and efficiency of recovery. One of the few studies to acknowledge this is Comfort, Ko, and Zagorecki [27], which evaluates the role of information access in disaster response performance through agent-based simulation.

To capture these dynamics, this study introduces a stylized framework for modeling inter-agency coordination, consisting of four levels:

1. **Uncoordinated:** Each agency applies a different recovery strategy to its own subnetwork. For example, one agency may adopt a volume-based approach while another uses a betweenness-based one.

2. **Low-level coordination:** Both agencies adopt the same recovery strategy but compute it independently using only their respective subnetworks. This scenario represents minimal communication, such as prior agreement on strategy without real-time data sharing.

3. **Medium-level coordination:** Agencies apply the same strategy, computed using a shared representation of the entire network, but still conduct recovery independently.

For example, betweenness centrality may be computed on the combined network, yet two separate repair sequences are executed in parallel.

4. **High-level coordination:** Agencies fully coordinate by sharing both strategic planning and operational resources. A unified recovery sequence is implemented across both subnetworks, and resource pooling is assumed. Consequently, repair times are reduced; for instance, the time required to repair a link is halved under the assumption of doubled capacity due to joint crew deployment.

This framework enables a structured comparison of how different levels of inter-agency coordination affect the rapidity of recovery. To establish a baseline, these coordinated scenarios are compared to uncoordinated random strategies.

5.4 Tokyo case study formulation

The proposed methodology is applied to the road and highway network of the Tokyo Metropolitan Area. The case study focuses on scenarios involving widespread closures rather than extensive structural damage, i.e., all links are assumed to be restorable at approximately the same rate. This assumption is consistent with the 2011 Great East Japan Earthquake, during which the epicenter was located 373 kilometers northeast of Tokyo. The earthquake, which occurred around 2–3 PM, led to widespread closure of highways and railways due to both structural concerns and precautionary safety inspections. As a result, many travelers were stranded and unable to return home.

Network

Unlike many previous studies that focus solely on highway networks, this research incorporates both local road and highway networks to more realistically capture traffic dynamics, including the redundancy provided by local road infrastructure. However, it is assumed that only highway links experience closures, as these are more likely to be elevated and vulnerable to seismic impacts. The local road network remains fully operational in all scenarios. Network data is obtained from OpenStreetMap, resulting in a network consisting of 3,486,731 links and 1,256,022 nodes.

Tokyo highway network

The Tokyo highway system is jointly managed by two agencies: the Metropolitan Expressway Company, Ltd. (MEX) oversees the inner network, while the Nippon Expressway Company Ltd. (NEXCO) manages the outer network. Figure 5.2 shows this division, with the MEX network in purple and the NEXCO network in green.

This administrative division introduces the potential for inefficiencies and coordination challenges during the recovery process.

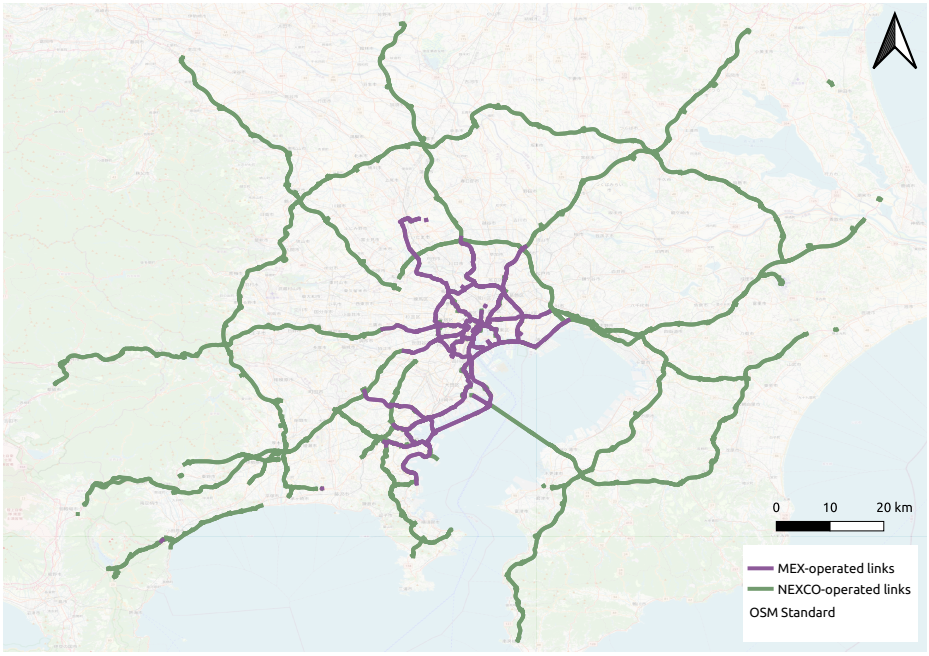


Figure 5.2: Tokyo highway network: MEX (purple) and NEXCO (green)

In total, MEX comprises 23 routes, while NEXCO includes 16. These were grouped into 10 groups for each agency using the following criteria: (1) spatial proximity, (2) comparable group lengths within each agency—approximately 65 km per group for MEX and 200 km for NEXCO, reflecting the latter's larger overall network scale (this helps prevent longer groups from being prioritized in repair sequencing purely due to coverage), and (3) longer routes were split and grouped based on geographic adjacency. More details about the routes and groupings can be found in Appendix A.

The resulting groupings are shown in Figures 5.3 and 5.4.

Travel demand

Travel demand is derived from the 2018 Tokyo Person Trip Survey (`https://tokyo-pt.jp/`), a decennial survey detailing travel behaviors, trip purposes, origins/destinations, and transportation modes. For this study, the number of people outside their residential area at each hour of the day, disaggregated by area of residence, is used to simulate trip demand. Figure 5.5 presents the hourly distribution.

The Person Trip Survey also includes the mode of transportation, so since this work focuses on the local road and highway network, the data is filtered to include only car trips. Figure 5.6 shows the number of car-based trips per hour.

In the event of an earthquake, it is assumed that people who are outside their area of residence will want to make their way back home. The relevant data from the survey is

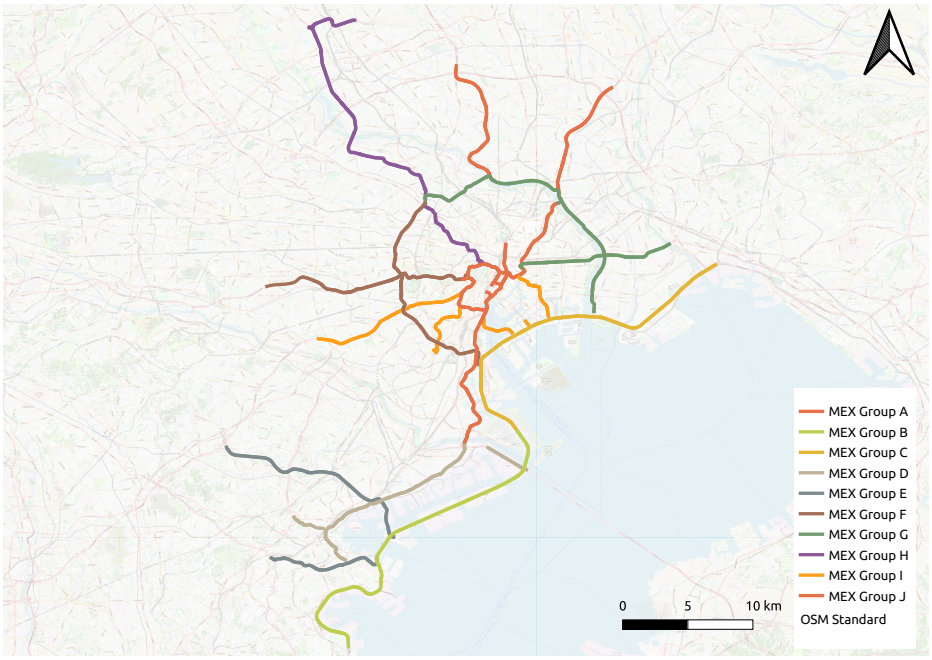


Figure 5.3: MEX route groupings

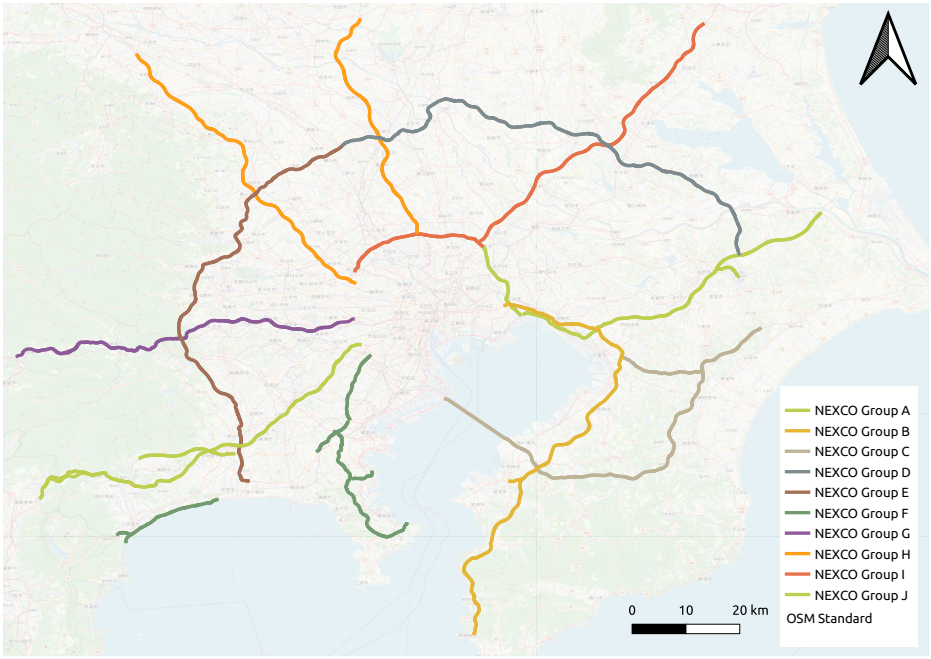


Figure 5.4: NEXCO route groupings

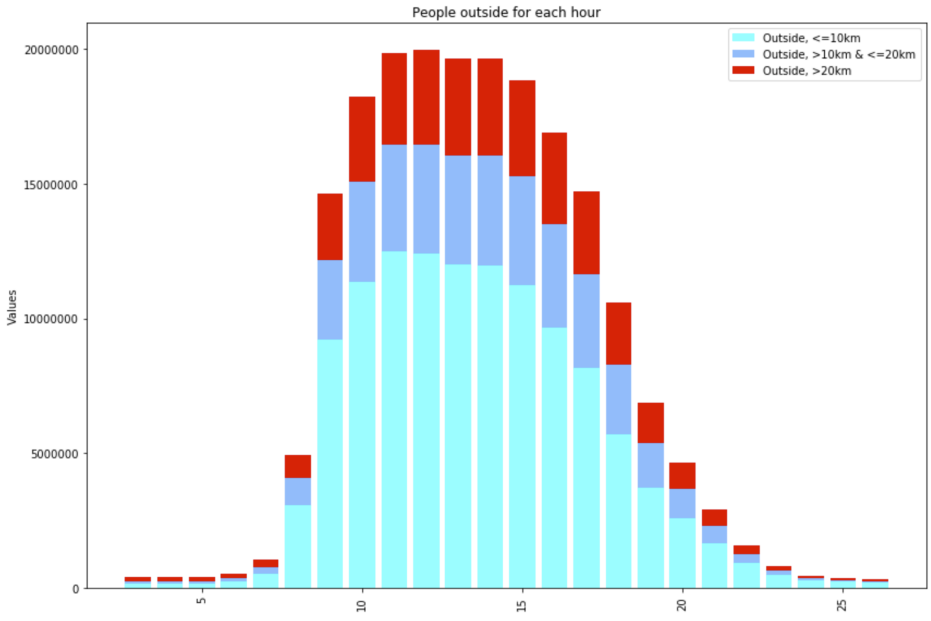


Figure 5.5: Hourly distribution of people outside their area of residence

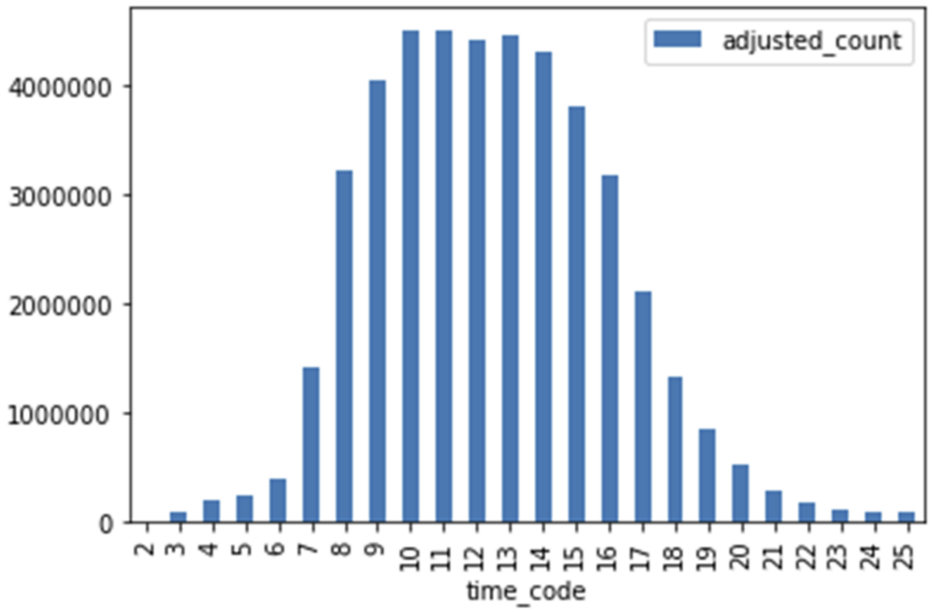


Figure 5.6: Hourly distribution of car trips outside area of residence

processed to arrive at an origin-destination matrix for each area. This research tests the most disruptive scenario, that is, if the seismic event occurs in the middle of a day (around 12PM) when most people are outside. 4,505,657 car trips that want to go back to their area of residence are generated. All trips are assumed to start at the same time.

Traffic model

The semi-dynamic agent-based traffic model described in Chapter 3 and previously implemented in Chapter 4 is also employed here. The model framework is shown in Figure 5.7.

First, the reopening/repair sequence is generated depending on the strategies implemented by each agency. Then a list of closed highway groups is generated for each time step based on the repair sequence. Then simulations are run to produce road usage and trip information output for each time step. Once all time steps are completed, the rapidity metrics are computed for the specific scenario.

Although the traffic model remains largely consistent with the previous chapter, several key modifications are introduced. First, it is assumed that drivers do not reroute during their trip but instead follow the route selected at departure. This change reflects a simplification of driver behavior under disrupted conditions, where real-time information about downstream congestion or closures may be limited. By removing mid-trip rerouting, the model avoids assuming that drivers have perfect knowledge of evolving network conditions. In line with this change, traffic updates are now performed every 30 minutes instead of every 15. Additionally, to improve computational efficiency, each agent is assumed to represent five vehicles.

Actual scenarios

An initial scenario with all roads and highways open is simulated to determine the pre-disaster volumes for each link. For all following scenarios, it is assumed that all highway routes are closed immediately after the earthquake, so each scenario entails generating repair sequences depending on the strategies used by each agency and the corresponding level of coordination:

- **Volume-based**: Links are ranked by pre-disaster volumes. Each group is represented by the link with the highest volume.
- **Betweenness-based**: Uses edge betweenness centrality from NetworkX [45]:

$$c_B(e) = \sum_{s,t \in V} \frac{\sigma(s,t \mid e)}{\sigma(s,t)} \tag{5.15}$$

  where V is the set of nodes, $\sigma(s,t)$ is the number of shortest (s,t)-paths, and $\sigma(s,t \mid e)$ is the number of those paths passing through edge e.

  The same method is performed where each group is ranked based on the link which has the highest edge-betweenness centrality metric to generate the repair sequence.

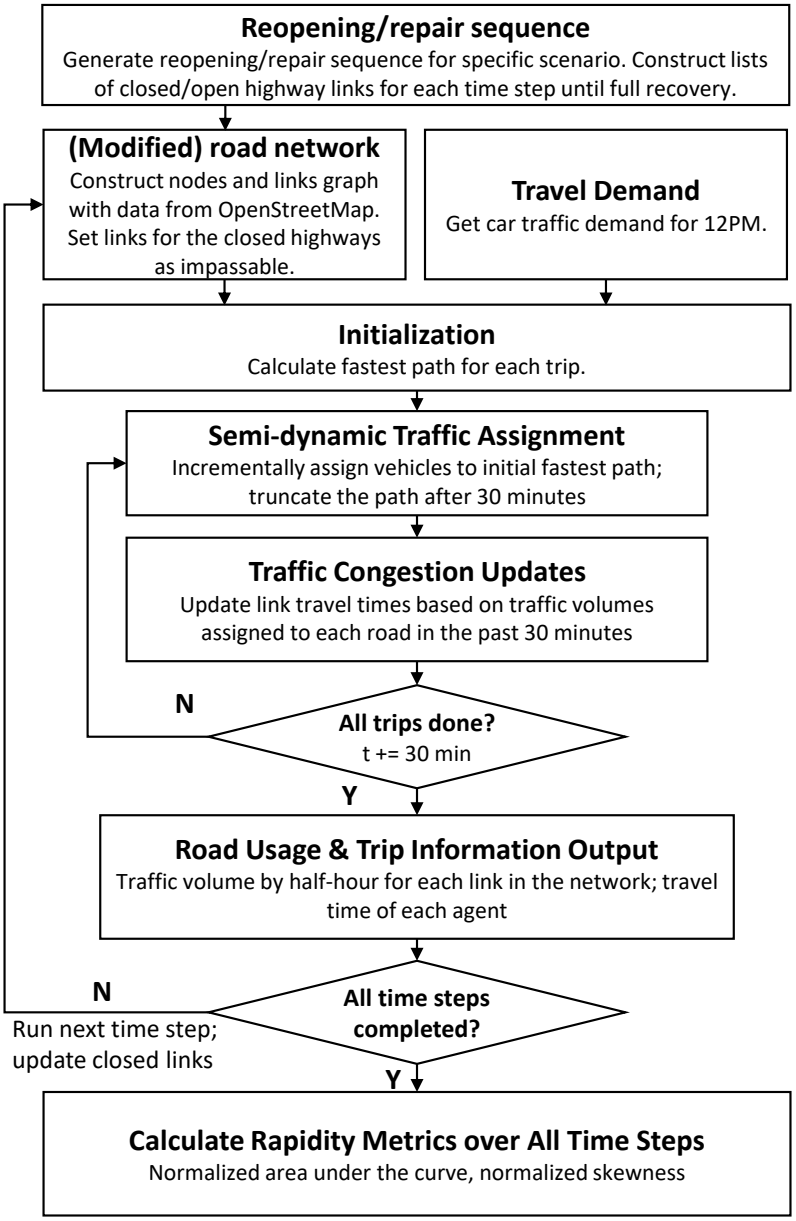


Figure 5.7: Traffic model flowchart

- **Route-based**: Initial group is selected purely by pre-disaster volume. Subsequent groups are selected based on highest pre-disaster volume among those adjacent to opened groups.

Each combination of agency, strategy, and coordination level yields a unique pair of repair sequences (or a single shared sequence in the high-coordination case), totaling 15 scenarios, as shown in Table 5.1. These sequences for each strategy and level of coordination is listed in Appendix B.

To fully simulate each scenario, the sequences for each agency are translated onto generalized time steps that it would take for a hypothetical crew to inspect and reopen each group of routes. The total length and size of the crew are assumed to be the only factors that affect the time it takes to reopen each group of routes. MEX and NEXCO are also assumed to have crews of the same size. Since this work does not attempt to estimate the specific time it takes to inspect and reopen each group, the reopening time is simply defined by a generalized time step. One time step is defined as the time it takes to reopen one MEX group of routes. Since a NEXCO group of routes is three times as long as a MEX group, it would take three time steps for one crew to reopen a NEXCO group. For uncoordinated, low-level, and medium-level coordination scenarios, each highway agency operates independently of each other so MEX groups are being repaired at the same time as NEXCO groups. This leads to 17 subscenarios over 30 time steps for full reopening. Each subscenario requires an individual simulation where the designated MEX and NEXCO groups that are slated to open for that time step are opened cumulatively. The system performance is then determined for each subscenario and is plotted over a recovery curve. For the high-level coordination scenario, since resources (i.e., crews) are assumed to be pooled, there are instead 20 subscenarios over 20 time steps. A comparison of these recovery curves is shown in Figure 5.8.

Upon generating the repair sequences for uncoordinated, low-level, and medium-level coordination scenarios for MEX reopenings, it is found that the repair sequence of the volume-based strategy is exactly the same as the repair sequence for the route-based strategy.

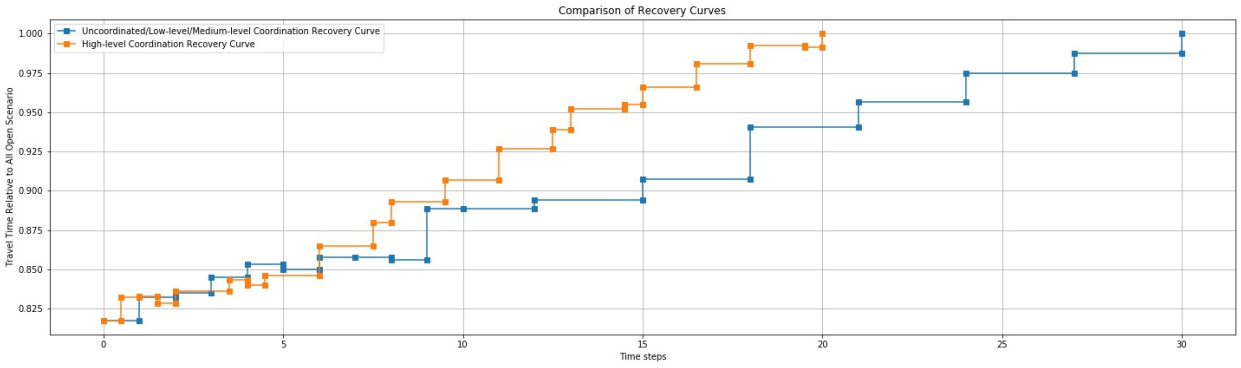


Figure 5.8: Comparison of recovery curves

Table 5.1: Coordination scenarios

	Uncoordinated						Low coordination			Medium coordination			High coordination			
	1	2	3	4	5	6	7	8	9	10	11	12	13	14	15	
VOL	MEX	MEX	NEXCO		NEXCO		MEX, NEXCO			MEX, NEXCO			MEX, NEXCO			
BET	NEXCO		MEX	MEX		NEXCO		MEX, NEXCO			MEX, NEXCO			MEX, NEXCO		
RTE		NEXCO		NEXCO	MEX	MEX			MEX, NEXCO			MEX, NEXCO				MEX, NEXCO

Furthermore, it is found that the low-level and medium-level coordination that adopts the volume-based strategy also generates the same sequences. Coordination scenarios that can be collapsed into one are highlighted in similar colors in Table 5.1. These circumstances reduce the number of scenarios to 11 as shown in Table 5.2. The route group opening sequences for each scenario are detailed in Appendix B.

Lastly, three random scenarios consisting of random recovery sequences for both MEX and NEXCO are also simulated to compare with the scenarios with coordination.

5.5 Case study results

Robustness to random variations

Each scenario is expected to produce stable results with minimal sensitivity to random variation, consistent with findings in Chapter 4. To demonstrate this, each scenario (i.e., with fixed MEX and NEXCO repair sequences) is simulated three times. The mean and standard deviation of the normalized area under the curve (AUC) and skewness metrics are summarized in Table 5.3. A 2-D scatter plot of AUC versus skewness for all scenarios is shown in Figure 5.9.

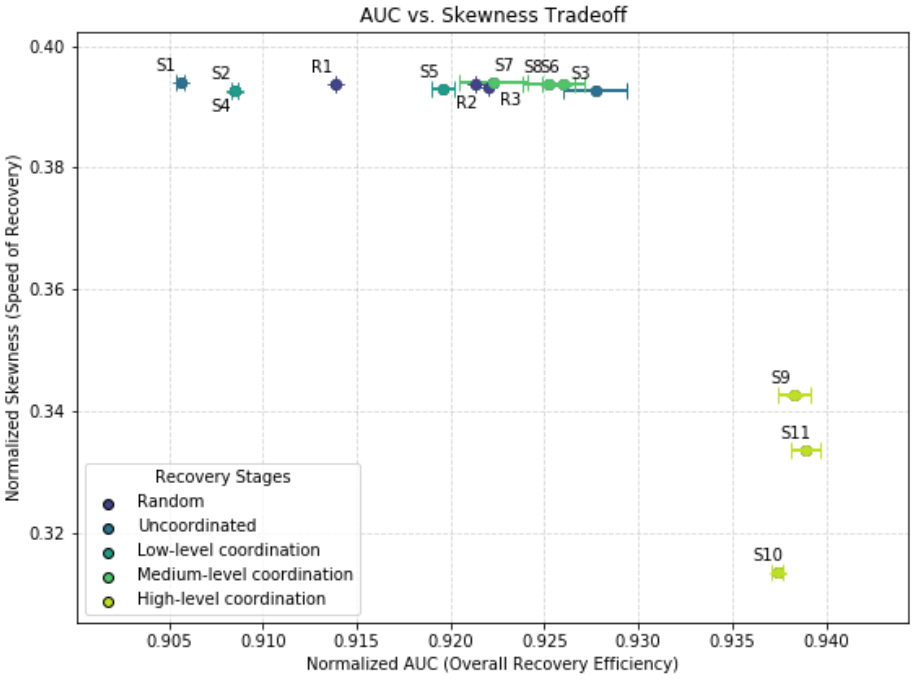


Figure 5.9: Scatter plot of normalized AUC vs. skewness

Table 5.2: Final coordination scenarios

	Uncoordinated			**Low-level**		**Medium-level**			**High-level**		
	1	2	3	4	5	6	7	8	9	10	11
VOL			NEXCO			MEX, NEXCO			MEX, NEXCO		
BET	NEXCO	MEX	MEX	MEX, NEXCO			MEX, NEXCO			MEX, NEXCO	
RTE	MEX	NEXCO			MEX, NEXCO			MEX, NEXCO			MEX, NEXCO

Table 5.3: Normalized AUC and skewness (mean and standard deviation) for each scenario

Level of co-ordination	**Strategy combination**	**Normalized AUC**	**Rank**	**Normalized skewness**	**Rank**
Uncoordinated	**S1**: MEX route-based, NEXCO betweenness-based	0.9056 (0.0002)	11	0.3940 (0.0001)	10
	S2: MEX betweenness-based, NEXCO route-based	0.9085 (0.0002)	9	0.3926 (0.0001)	4
	S3: MEX betweenness-based, NEXCO volume-based	0.9277 (0.0017)	4	0.3928 (0.0001)	6
Low-level	**S4**: MEX & NEXCO betweenness-based	0.9085 (0.0002)	9	0.3926 (0.0001)	4
	S5: MEX & NEXCO route-based	0.9196 (0.0006)	8	0.3931 (0.0001)	7
Medium-level	**S6**: MEX & NEXCO volume-based	0.9260 (0.0011)	5	0.3937 (0.0002)	8
	S7: MEX & NEXCO betweenness-based	0.9223 (0.0018)	7	0.3941 (0.0001)	11
	S8: MEX & NEXCO route-based	0.9252 (0.0014)	6	0.3937 (0.0001)	8
High-level	**S9**: MEX & NEXCO volume-based	0.9383 (0.0009)	2	0.3425 (0.0001)	3
	S10: MEX & NEXCO betweenness-based	0.9374 (0.0003)	3	0.3134 (0.0001)	1
	S11: MEX & NEXCO route-based	0.9389 (0.0008)	1	0.3335 (0.0001)	2

Scenario results

The results from Table 5.3 and Figure 5.9 illustrate the relative performance of all coordination level and strategy combinations. In addition, three randomized scenarios are simulated, where MEX and NEXCO follow separate but random repair sequences. The results of these random scenarios are shown in Table 5.4 and are also included in Figure 5.9 for comparison. Recovery curves for each scenario is included in Appendix C.

Ideally, a scenario would exhibit both high normalized AUC (indicating efficient recovery over time) and low normalized skewness (indicating front-loaded recovery). Therefore, scenarios appearing toward the lower-right quadrant of the scatter plot in Figure 5.9 are considered the most favorable. To facilitate visual comparison, a zoomed-in version of the upper half of the scatter plot is presented in Figure 5.10.

Table 5.4: Normalized AUC and skewness for random scenarios

Level of coordination	**Normalized AUC**	**Normalized skewness**
R1: Random scenario 1	0.9139	0.3937
R2: Random scenario 2	0.9220	0.3932
R3: Random scenario 3	0.9213	0.3938

5.6 Discussion

Impact of coordination

This study investigates whether coordination between highway agencies affects the rapidity of post-earthquake recovery. To explore this, both uncoordinated and randomized scenarios are compared with scenarios featuring varying levels of coordination. As shown in Figure 5.10, the random and uncoordinated scenarios generally exhibit lower AUC values compared to low- and medium-level coordination scenarios. However, the variation in skewness across these scenarios is relatively small, as seen in Figure 5.9, suggesting that the overall shape of the recovery curve does not vary substantially among them. In contrast, high-level coordination scenarios achieve significantly higher AUC and lower skewness values. These results indicate that coordination, particularly at higher levels, substantially improves post-earthquake recovery performance.

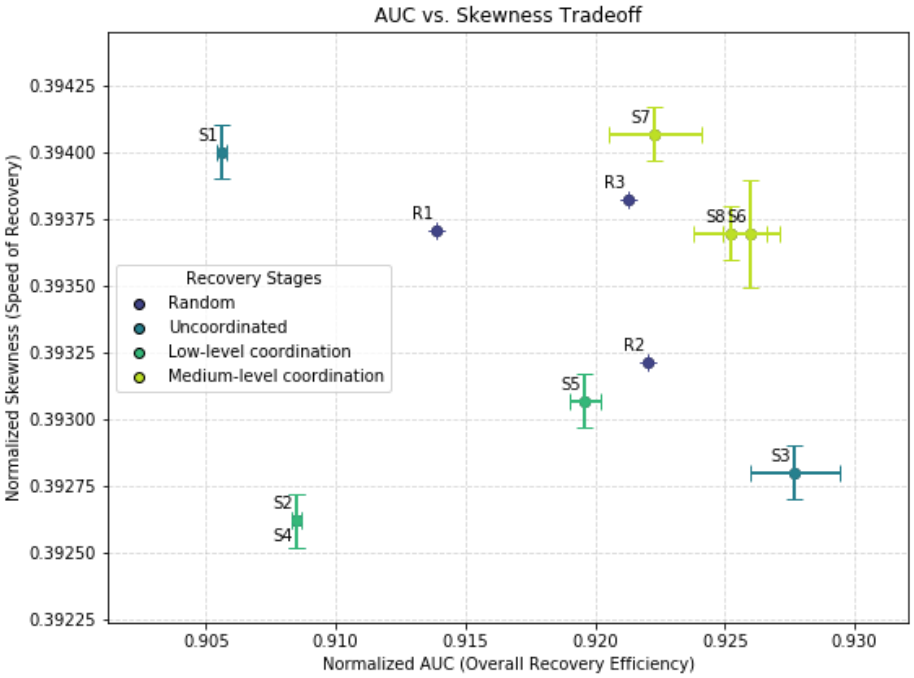


Figure 5.10: AUC-Skewness scatter plot (zoomed in)

Analysis of scenarios

Across levels of coordination

The observed trends align with expectations: uncoordinated < low-level coordination < medium-level coordination < high-level coordination. As the level of shared information and resources increases, recovery performance improves consistently across both metrics. However, two scenarios appear as outliers: S3 (MEX using a betweenness-based strategy, NEXCO using a volume-based strategy, under uncoordinated conditions) and S4 (both MEX and NEXCO using a betweenness-based strategy under low-level coordination).

Although these outcomes may appear unintuitive at first glance, they reflect the nature of the betweenness-based metric. Betweenness performs best when applied to the full network. Applied only to a partial network (e.g., NEXCO's), the edge-betweenness values may not reflect true system connectivity, especially in a circular network such as Tokyo's, with both radial and circumferential components. The MEX network, being more central, provides a more reliable basis for computing betweenness. Therefore, S3 performs better than other uncoordinated cases, while S4 underperforms within its coordination level, clustering closer to uncoordinated scenarios.

To further examine the spatial implications of coordination on rapidity, congestion levels between local roads and highways under low- and high-level coordination, using the

betweenness-based strategy, are compared. A link is classified as congested when its volume-to-capacity ratio is greater than or equal to 1. Figures 5.11, 5.12, and 5.13 compare 2PM local road and highway congestion at time steps 5, 15, and 20. Table 5.5 summarizes the percentage of total congested road length that is on local roads. These results are plotted in Figure 5.14. Given the sharper declines in local road congestion, these results suggest that high-level coordination helps alleviate local road congestion more effectively, likely due to improved recovery sequencing of key highway links that serve as regional connectors as well as due to the sharing of resources to inspect or repair highway routes.

Table 5.5: Percentage of total congested road length on local roads

Coord. level / Time step	Low-level	High-level
5	79%	72%
15	45%	26%
20	31%	20%

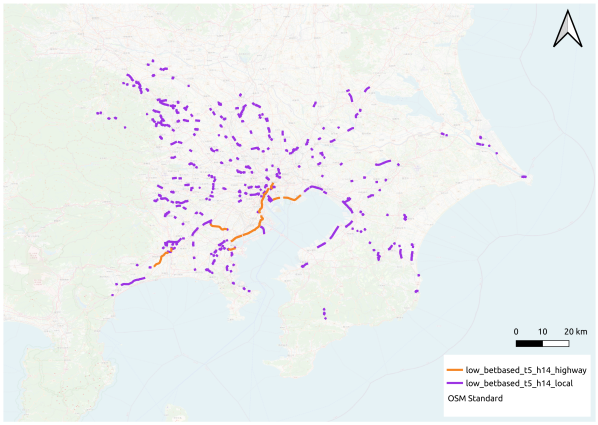
Across strategies

Within each level of coordination, the volume-based strategy generally outperforms the betweenness-based strategy in terms of AUC. For instance, S6 outperforms S4 and S7, and S9 outperforms S10. However, the betweenness-based strategy performs better in terms of skewness under high-level coordination (i.e., S10). This indicates that although it may not maximize overall recovery (AUC), it does front-load system performance—potentially critical in urgent recovery scenarios.

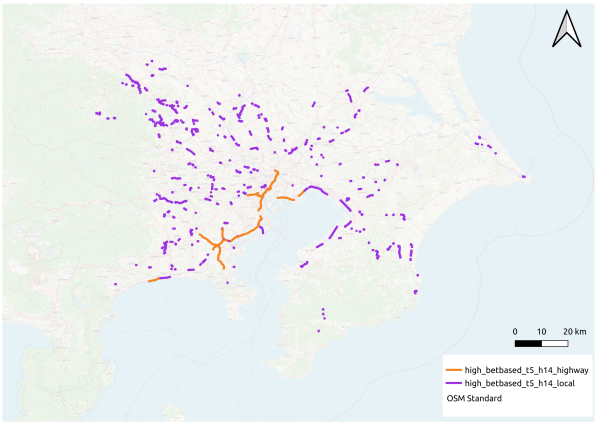
Because this study uses generalized time steps, the true value of steep early recovery (low skewness) may not be fully captured. In real situations where early performance is critical, such as reopening access to hospitals or evacuation routes, strategies that prioritize early gains, such as betweenness-based recovery under high coordination, may be preferred. If urgency is lower, volume- or route-based strategies may be more suitable.

Moreover, results suggest that route-based strategies perform comparably to volume-based ones in terms of AUC under medium- and high-level coordination, and may even outperform them in terms of skewness. This aligns with the findings of Ma et al. [60], who argue that strategies incorporating interdependency—like the route-based approach—yield better performance than those that do not (e.g., volume-based strategies).

While the grouping criteria used in this study were designed to equalize length and proximity, more refined grouping methods may further enhance the effectiveness of route-based strategies. In practice, however, where agreement on grouping or sharing resources is

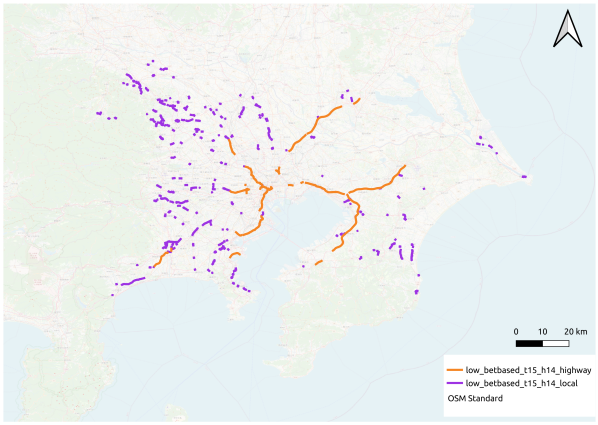


(a) Low-level coordination at timestep 5

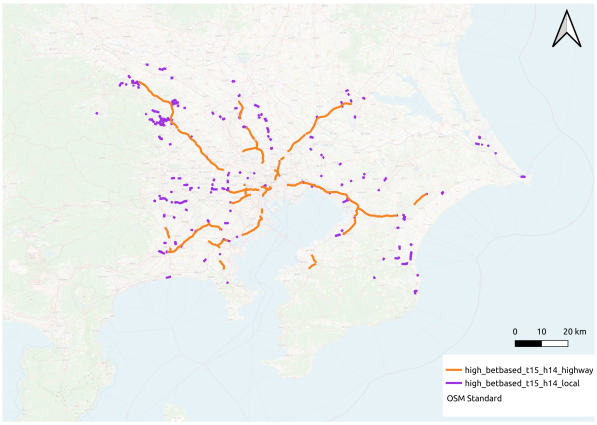


(b) High-level coordination at timestep 5

Figure 5.11: Highway congestion (orange) versus local road congestion (purple) at timestep 5



(a) Low-level coordination at timestep 15



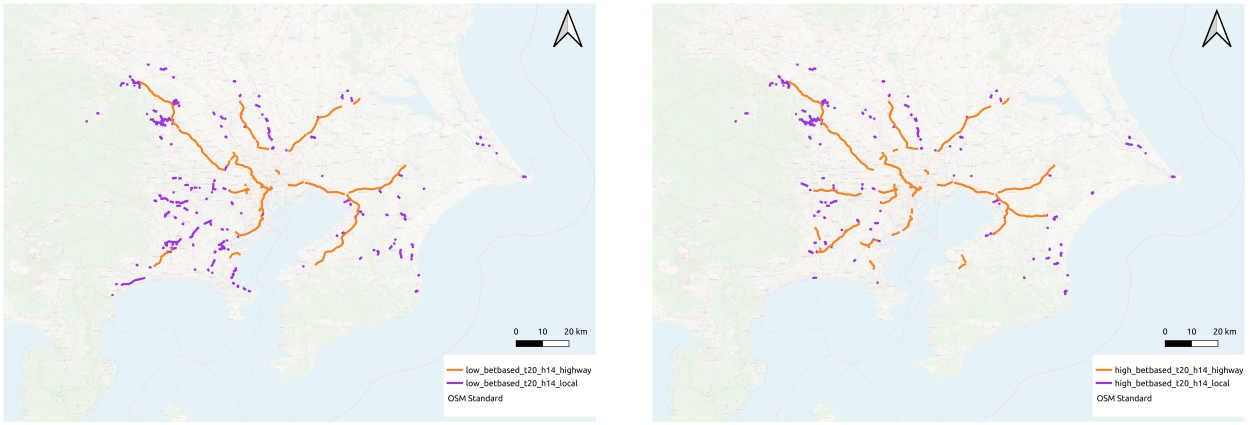
(b) High-level coordination at timestep 15

Figure 5.12: Highway congestion (orange) versus local road congestion (purple) at timestep 15

infeasible, volume-based strategies provide a robust and independently executable baseline, as demonstrated by the relatively strong performance of S6 compared to most uncoordinated or low-level coordination scenarios.

AUC-Skewness tradeoff

Finally, this study proposes and evaluates two performance metrics: normalized area under the curve (AUC) and normalized skewness. The results highlight that trade-offs can exist between these metrics under different strategy–coordination level combinations. While the



(a) Low-level coordination at timestep 20

(b) High-level coordination at timestep 20

Figure 5.13: Highway congestion (orange) versus local road congestion (purple) at timestep 20

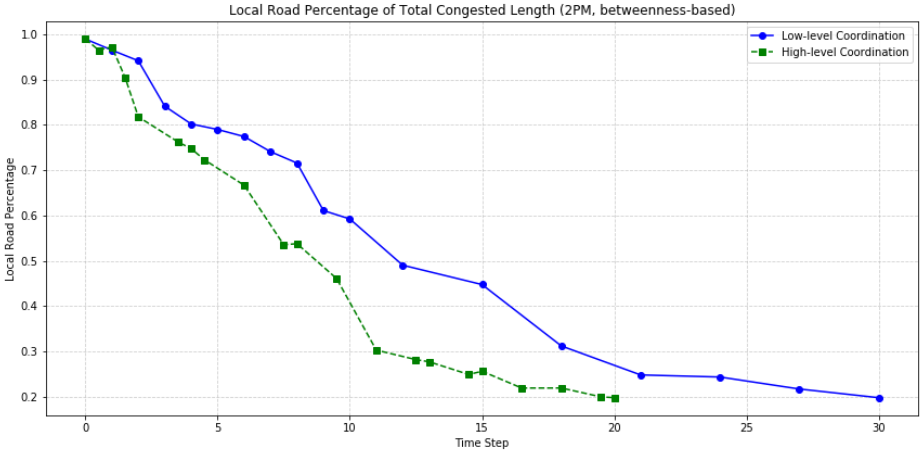


Figure 5.14: Percentage of congested local roads across time steps

model does not attempt to quantify the exact time required to reopen each link (see Misra et al. [67] for more details), the interpretation of generalized time steps provides insight.

For example, if a generalized time step represents 2 hours (e.g., for reopening one MEX group), total recovery would take 60 hours under low- to medium-level coordination. However, if network damage is more severe, a generalized time step might represent 2 days—extending total recovery to 60 days. In such cases, steep early gains become more important. Agencies may prioritize strategies that reach a performance threshold as quickly as possible, or maximize performance within a specific time horizon. This underscores the importance of considering both AUC and skewness simultaneously when evaluating system rapidity.

Broader implications

While this case study focuses on the Tokyo Metropolitan Area, the findings have broader implications for infrastructure governance in other urban contexts. The advantages of stronger coordination, such as faster recovery and reduced congestion spillovers, are relevant in any region where multiple agencies or entities share responsibility for the transportation system. For example, in the United States, such fragmentation is becoming more common due to the growing use of public-private partnerships (P3s) in highway development and operations. In these scenarios, recovery efforts following a disaster could be significantly complicated by institutional boundaries, competing priorities, and lack of shared protocols.

Beyond highways, these coordination challenges are prevalent in public transportation networks. Tokyo's rail and subway system, for example, is operated by over a dozen separate entities. Similar multi-operator dynamics can be found in UK cities with deregulated bus markets and in Latin American cities where BRT systems often co-exist with private or informal operators. The fragmentation across operators—whether public or private—raises the same concerns about recovery planning, real-time communication, and resource mobilization during extreme events. In these contexts, questions around who leads, how decisions are made, and how information is shared become critical.

The results of this study reinforce the importance of incorporating both institutional and operational coordination mechanisms into resilience planning. Policymakers, particularly at the state or national level, may need to develop pre-established frameworks or contractual requirements that facilitate cooperative response and recovery actions across concessionaires or jurisdictions. From a modeling perspective, this chapter demonstrates that coordination is not an abstract governance issue but one with measurable, system-level impacts. Incorporating coordination dynamics into resilience modeling thus offers a valuable tool for anticipating outcomes and informing policy design. As urban infrastructure systems become more fragmented, and as natural and human-made hazards increase in frequency and severity, the urgency of addressing these coordination gaps cannot be overstated.

5.7 Conclusion, limitations, and recommendations

This study implements a semi-dynamic, mesoscopic, regional framework to quantify the impact of inter-agency coordination on the rapidity of highway network recovery following an earthquake. The results indicate that coordinated scenarios (whether low-, medium-, or high-level) consistently outperform uncoordinated and randomized scenarios, particularly in terms of the area under the recovery curve (AUC), which reflects overall recovery efficiency. High-level coordination also achieves significantly lower skewness values, indicating that a larger portion of the recovery occurs earlier in the recovery period—an outcome that may be desirable in time-critical situations.

Among recovery strategies, volume-based approaches serve as reliable baseline strategies in the absence of coordination, offering strong performance without requiring shared information.

Betweenness-based strategies perform marginally worse in terms of AUC but slightly better in terms of skewness, suggesting they are more effective in initiating recovery quickly. Route-based strategies perform comparably to volume-based strategies in AUC but slightly better in skewness. These findings support prior work [60] suggesting that strategies incorporating both network interdependency and demand distribution yield faster recovery trajectories.

Despite its strengths, the proposed framework presents limitations. While it operates at a mesoscopic scale, each subscenario simulation takes approximately 40 minutes to complete. For example, a low-level coordination scenario with 17 subscenarios may require 10–11 hours to run. This computational intensity may constrain the framework's applicability in probabilistic or real-time settings where multiple scenario permutations are needed.

Several components of the traffic model could also be refined. One key area is travel demand modeling. As Kiremidjian et al. [57] observed during the Loma Prieta (1989) and Northridge (1995) earthquakes, travel demand often decreases post-event. Kilanitis and Sextos [56] proposed dynamic demand models that adjust as a function of network operability. While the current study captures partial demand variation by modeling only trips from outside zones returning home, further refinements are possible. These include incorporating trip purposes or activities, integrating public transit options through multi-modal modeling, and modeling temporal shifts in activity patterns.

Driver behavior is another important area for improvement. Assumptions of full network knowledge and static behavior have been widely adopted for simplicity, but they may not reflect real-world post-disaster conditions. As Oyama and Hato [79] argues, driver behavior likely changes across the disaster timeline (pre-, during, and post-event), particularly as spatial knowledge becomes constrained. Empirical progress is hindered by a lack of real-world post-earthquake data, given the rarity of high-magnitude events. While stated preference surveys offer some insight, the most reliable information would come from revealed preference data (e.g., observed driver trajectories collected immediately after a disaster). Oyama and Hato [79] also suggests that post-earthquake, drivers exhibit myopic behavior, relying on limited local knowledge when selecting routes.

In conclusion, while the current framework provides a robust and scalable method to evaluate coordination impacts on traffic network recovery, further work is needed to incorporate dynamic demand models, realistic behavioral assumptions, and scalable computational techniques—especially to extend this framework to broader probabilistic or real-time applications.

Chapter 6

Summary and conclusions

This chapter summarizes the key findings of this dissertation and reflects on how they respond to the study's five core research objectives. These objectives span model development, framework design, case study applications, and evaluation of broader contextual factors influencing transportation system resilience. The chapter is organized accordingly: Section 6.1 summarizes the background of the study, Sections 6.2 to 6.5 correspond to each research objective, and Section 6.6 presents limitations and future directions.

6.1 Overview of seismic resilience of transportation systems

Chapter 1 established the importance of resilience in critical infrastructure systems, particularly transportation networks, which are vulnerable to disruption during seismic events. Aging infrastructure in seismically active regions increases the likelihood of damage, which can significantly impair: (1) evacuation and emergency response operations, and (2) the functionality of interdependent systems such as commerce and logistics.

The literature presents a range of perspectives on seismic resilience. Berdica [7] defined reliability as the complement of vulnerability—a system's susceptibility to incidents that significantly reduce serviceability. Bruneau et al. [11] expanded this with a four-dimensional resilience framework: robustness, resourcefulness, rapidity, and redundancy. Among these, robustness and rapidity are particularly relevant for quantifying seismic impacts and evaluating mitigation and recovery strategies.

Traffic models are commonly used to assess these dimensions, and are characterized by trade-offs in temporal resolution, spatial resolution, and spatial scale. Temporal resolution refers to how frequently the model updates conditions; spatial resolution indicates the granularity of network elements (e.g., TAZ versus node level); and spatial scale ranges from small networks to multi-city regions. These trade-offs are reflected in distinctions such as static versus dynamic models, or macroscopic versus microscopic ones.

Chapter 2 identified two dominant research trends: (1) studies with high spatial resolution but limited spatial scale, and (2) those with coarse resolution but regional scope. Because earthquakes often impact multiple jurisdictions, regional-scale modeling is essential. Yet few studies adopt regional traffic models with high spatial and temporal resolution—an identified research gap this study addresses.

Chapter 2 also distinguished between robustness and rapidity in seismic resilience studies. While robustness studies often address regional impacts, rapidity studies tend to focus on smaller networks due to the computational burden of simulating complex recovery sequences (e.g., through single-link failure analysis). This study aims to bridge this gap through scalable yet detailed modeling approaches.

6.2 Mesoscopic traffic model for resilience assessment

This study began by addressing the need for a scalable, yet behaviorally realistic, traffic simulation framework to model regional transportation systems under seismic disruption. Research Objective 1 focused on developing a mesoscopic, semi-dynamic, agent-based traffic model that strikes a balance between temporal and spatial resolution, computational efficiency, and the ability to represent disaggregated network and traveler behavior.

Chapter 3 introduced the proposed traffic model architecture, which simulates travel across both highway and local road networks at the node-link level. The model uses an agent-based structure where individual agents represent drivers and make route choices based on time-varying travel costs. Unlike traditional static assignment models, the semi-dynamic design allows for periodic updates to link travel times and agent behavior, capturing congestion dynamics over time. At the same time, it avoids the computational burden of fully dynamic assignment, enabling the simulation of large metropolitan regions with millions of trips.

Several key features distinguish this model from prior approaches:

- **Regional scalability**: The model accommodates full-network simulation of large-scale regions such as Southern California and Tokyo, with millions of agents and high spatial resolution.
- **Temporal responsiveness**: By updating link travel times and agent progress at fixed time intervals (e.g., every 30 minutes), the model reflects network dynamics while maintaining manageable runtime.
- **Behavioral flexibility**: The model allows for varying assumptions about driver behavior, including pre-trip versus en-route routing decisions and rerouting frequency. These assumptions can be tuned to reflect empirical findings or scenario-specific constraints.
- **Modularity**: The model structure is designed to support integration with damage models, economic cost estimation modules, and performance metric evaluations for both robustness and rapidity.

This traffic model serves as the computational backbone for the seismic resilience analysis frameworks proposed in subsequent chapters. By addressing the methodological gap between high-resolution but small-scale models and coarse-grained regional models, the proposed model offers a foundation for scalable resilience assessment at the regional level.

6.3 Robustness framework and Southern California case study

Research Objective 2 focused on establishing a modeling framework and defining metrics to quantify the robustness of regional transportation systems following seismic disruption. Building on the mesoscopic traffic model introduced in Chapter 3, this study developed an integrated simulation-based framework to assess system degradation and estimate associated economic impacts. Robustness was defined as the ability of the transportation system to maintain function immediately after an earthquake, measured through changes in travel performance and losses associated with damaged infrastructure.

To evaluate the practical utility of this framework—fulfilling Research Objective 4—it was applied to a regional case study of Southern California under a hypothetical M7.4 earthquake scenario centered on the Palos Verdes Fault. The study area encompassed the Los Angeles and Long Beach ports, two critical freight hubs with high seismic exposure. The implementation combined four components: (1) hazard characterization, (2) infrastructure damage assessment, (3) semi-dynamic traffic simulation, and (4) performance and cost evaluation. This end-to-end pipeline enabled both aggregate and disaggregated assessments of post-earthquake system robustness.

Key findings from the case study include:

- **Widespread but spatially disproportionate economic impacts**: Performance losses extended throughout the region due to network interdependencies but the most severe impacts are to port area trips.
- **Economic losses driven by unfulfilled trips**: Simulation results revealed that the largest share of economic impact came from unfulfilled trips rather than increased travel times. This suggests that access denial, not just delay, is a critical driver of post-earthquake cost.
- **Actionable economic framing**: The integration of a simplified economic model translates technical disruption estimates into monetary terms, enabling direct comparison with retrofit or repair costs to support investment and budgeting decisions.
- **Spatial and activity-based resolution**: The model supports spatial disaggregation by subregion or mode, and allows exploration of robustness impacts across different trip purposes (e.g., freight, commuter, or from certain zones).

The case study demonstrates both the analytical strength and practical feasibility of applying the robustness framework at a regional scale. By combining probabilistic damage modeling with scalable traffic simulation and cost estimation, the approach fills a methodological gap in current resilience assessment practice. It also provides a tool for identifying priority investment areas and for comparing trade-offs between structural retrofits and operational strategies.

6.4 Rapidity framework and Tokyo case study

Research Objective 3 focused on developing a modeling framework and performance-based metrics to evaluate the rapidity of transportation system recovery after disruption. In contrast to robustness, which captures the severity of impacts, rapidity reflects how efficiently a system regains functionality over time. Addressing this objective required modeling not only the evolution of physical repairs but also institutional processes such as coordination and information sharing.

To demonstrate the practical application of this rapidity framework—fulfilling Research Objective 4—a case study was conducted on the Tokyo Metropolitan Area highway network, jointly operated by MEX (inner network) and NEXCO (outer network). The case study evaluated how varying levels of inter-agency coordination and repair prioritization strategies affect recovery trajectories following a major seismic disruption.

The framework introduced in Chapter 5 integrates the mesoscopic traffic model with various link reopening strategies. Two primary metrics were proposed to characterize recovery performance: the *area under the recovery curve* (AUC), reflecting the total efficiency of recovery, and *normalized skewness*, which captures the timing of recovery gains—distinguishing between front-loaded and delayed recovery trajectories.

Four coordination levels were modeled: (1) uncoordinated, (2) low-level coordination (shared strategies applied independently), (3) medium-level coordination (shared strategies and system-level information), and (4) high-level coordination (shared strategies, information, and pooled resources such as repair crews).

Three recovery prioritization strategies were tested across these coordination levels: (1) betweenness-based (topological; focusing on network connectivity), (2) volume-based (functional; prioritizing high-volume links), and (3) route-based (integrating demand and link interdependency).

Key findings from the Tokyo case study include:

- **Stronger coordination yields faster recovery**: Both AUC and skewness metrics improved especially under medium- and high-level coordination, demonstrating the value of institutional collaboration in accelerating recovery.
- **Functional strategies outperform topological ones when coordination is limited**: Volume-based prioritization led to better AUC metrics than betweenness-

based strategies in lower level coordination scenarios, highlighting the relevance of pre-disaster traffic volumes as a recovery heuristic.

- **Integrated (route-based) strategies are consistently effective**: Route-based prioritization performed as well or better than both volume- and betweenness-based approaches across all coordination levels, reinforcing the benefit of blending structural- and demand-based strategies.
- **Complementary insights from AUC and skewness**: While AUC reflected total recovery effectiveness, skewness captured the temporal distribution of gains—emphasizing the need for both metrics to fully characterize rapidity.

The case study illustrates the feasibility of applying rapidity analysis to a large, complex, and institutionally fragmented urban network. By explicitly modeling the influence of coordination structures and repair strategies, the framework extends resilience assessment beyond engineering performance to include governance and organizational factors—highlighting the central role of inter-agency coordination in minimizing disruption and enhancing recovery efficiency.

6.5 Institutional and policy implications

In alignment with Research Objective 5, this dissertation examined how geographic, structural, and institutional factors shape the resilience of transportation systems under seismic disruption. While the primary emphasis was on modeling physical and operational dynamics, both case studies revealed that governance structures and regional context play a critical role in influencing system performance and recovery. These insights extend the relevance of the proposed frameworks beyond technical domains, offering guidance for infrastructure planning, investment prioritization, and policy design.

Insights from Southern California: Prioritizing vulnerable economic corridors

The Southern California robustness analysis showed that seismic disruption near the Ports of Los Angeles and Long Beach would trigger disproportionate economic losses in high-value freight corridors—driven largely by unfulfilled trips rather than congestion delays. This pattern highlights that regional resilience depends not only on the location of physical damage, but on the economic role of the affected corridors in supply chain flows.

From a policy perspective, this finding supports resilience planning that explicitly incorporates freight-specific performance metrics and disaggregated economic loss estimates. Such measures can translate technical simulation results into actionable financial terms, enabling agencies to better justify mitigation projects and to target investments toward corridors where disruption would have the largest regional economic impact. Because these freight

corridors span multiple jurisdictions, metropolitan planning organizations (MPOs) and freight advisory councils are well-placed to coordinate planning and investment strategies across local, regional, and state agencies.

Insights from Tokyo: The role of coordination in system recovery

The Tokyo case study underscored how coordination between independent operators—such as MEX and NEXCO—can significantly affect recovery outcomes. Although this study used a simplified representation of coordination, the results showed that even modest improvements in information sharing and resource pooling can lead to faster and more efficient recovery.

This finding has broader relevance as transportation governance becomes increasingly fragmented through privatization, public–private partnerships, and multi-agency oversight. Similar coordination challenges exist in U.S. highway concessions and in multi-operator public transit systems across cities worldwide. These parallels suggest that future resilience models should integrate more explicit representations of institutional behavior, such as shared response protocols and decision-making mechanisms. Doing so can help bridge the gap between technical resilience modeling and the organizational levers that influence recovery.

Cross-cutting implications

Together, these findings point to the need for integrated resilience planning that accounts for both physical vulnerability and institutional complexity. The proposed frameworks developed in this dissertation can support not only investment prioritization, but also the design of coordination protocols across agencies and sectors. As natural and human-made hazards increase in frequency and severity, addressing governance-related barriers to resilience will be as important as addressing physical ones.

6.6 Limitations and future directions

While this study advances regional-scale modeling of transportation resilience, several limitations remain—primarily related to data availability, model assumptions, and scope of application. These limitations also suggest promising directions for future research.

Model calibration and validation

Model calibration was constrained by limited availability of local road volume data, particularly for the Tokyo case study. Although the mesoscopic model produced plausible results using default parameters and demand scaling, more robust calibration—particularly for local road networks—would improve the reliability of simulation results. Additionally, validation of post-earthquake traffic behavior was limited by the scarcity of empirical data following major seismic events. Access to high-resolution GPS or mobile phone trajectory data from real-world

disruptions would enable more rigorous validation of both routing assumptions and recovery patterns.

Behavioral realism and demand complexity

The simulation framework made simplifying assumptions about driver behavior and demand structure. While the semi-dynamic model allows agents to adapt to changing conditions, rerouting decisions are governed by static or rule-based logic rather than empirical behavioral models. Incorporating post-disaster behavior dynamics [79], such as altered destination choices, evacuation preferences, or risk aversion, remains an area for future improvement. Similarly, richer demand datasets (e.g., disaggregated by purpose or socioeconomic group) would allow more nuanced assessments of equity and access under disruption.

Computational trade-offs and scalability

The semi-dynamic mesoscopic model was selected to balance temporal and spatial resolution and computational efficiency. While it enables simulations at a regional scale, further advances in computing capacity or optimization algorithms may eventually allow for wider use of fully dynamic models. Continued benchmarking of runtime performance, particularly for large-scale recovery scenarios, will help identify the inflection point at which higher fidelity models become practical.

Institutional modeling

This study incorporated coordination mechanisms through an abstracted representation of agency interaction, particularly in the Tokyo case study. While useful for comparative analysis, these assumptions simplify the complex realities of governance, including political, legal, and operational constraints. Future work could explicitly model institutional behaviors, such as prioritization protocols, to better capture the social and organizational dimensions of resilience.

Generalizability and transferability

Finally, while the case studies provide valuable insights, their specificity limits generalizability. Differences in urban form, governance, seismic hazard, and infrastructure condition may yield different outcomes in other regions. Future research could apply the proposed frameworks to additional case studies—especially in developing contexts or multi-hazard environments—to test transferability and further refine the methods.

In sum, this dissertation provides a scalable, integrated approach for assessing transportation system resilience. Addressing the identified limitations would enhance its predictive power, policy relevance, and adaptability to a wider range of regional contexts and hazards.

Bibliography

[1] Alice Alipour and Behrouz Shafei. "Seismic resilience of transportation networks with deteriorating components". In: *Journal of Structural Engineering* 142.8 (2016), p. C4015015.

[2] American Road and Transportation Builders Association. *California 2022 Bridge Profile*. `https://artbabridgereport.org/reports/state/CA.pdf`. Accessed: 2022-11-16. 2022.

[3] ASCE. *2021 Report Card for America's Infrastructure*. Tech. rep. American Society of Civil Engineers (ASCE), 2021.

[4] Jack Baker, Brendon Bradley, and Peter Stafford. *Seismic Hazard and Risk Analysis*. Cambridge University Press, 2021. DOI: 10.1017/9781108425056.

[5] Jack W Baker et al. *New ground motion selection procedures and selected motions for the PEER transportation research program*. Tech. rep. Pacific Earthquake Engineering Research Center, 2011.

[6] Hojjat Barati, Anil Yazici, and Amirmasoud Almotahari. "A methodology for ranking of critical links in transportation networks based on criticality score distributions". In: *Reliability Engineering & System Safety* 251 (2024), p. 110332.

[7] Katja Berdica. "An introduction to road vulnerability: what has been done, is done and should be done". In: *Transport policy* 9.2 (2002), pp. 117–127.

[8] Gitanjali Bhattacharjee and Jack W Baker. "Using global variance-based sensitivity analysis to prioritise bridge retrofits in a regional road network subject to seismic hazard". In: *Structure and Infrastructure Engineering* (2021), pp. 1–14.

[9] Geoff Boeing. "OSMnx: New methods for acquiring, constructing, analyzing, and visualizing complex street networks". In: *Computers, Environment and Urban Systems* 65 (2017), pp. 126–139.

[10] David S Brookshire et al. "Direct and indirect economic losses from earthquake damage". In: *Earthquake Spectra* 13.4 (1997), pp. 683–701.

[11] Michel Bruneau et al. "A framework to quantitatively assess and enhance the seismic resilience of communities". In: *Earthquake spectra* 19.4 (2003), pp. 733–752.

[12] Caltrans. *California to Receive Nearly $850 Million in Initial Funding for Bridge Repair Under Federal Bipartisan Infrastructure Law*. https://dot.ca.gov/news-releases/news-release-2022-001#:~:text=California%20will%20receive%20%24849.4%20million,to%20address%20highway%20bridge%20needs.. Accessed: 2022-11-16. 2022.

[13] Caltrans. *Caltrans Seismic Design Criteria Version 2.0*. State of California Department of Transportation, 2019. 250 pp.

[14] Robert Cervero. "Freeway deconstruction and urban regeneration in the United States". In: (2006).

[15] Barbaros Cetiner. "Image-Based Modeling of Bridges and Its Applications to Evaluating Resiliency of Transportation Networks". PhD thesis. Los Angeles, CA: University of California, Los Angeles, Apr. 2020.

[16] Barbaros Cetiner et al. *NHERI-SimCenter/BRAILS: Release v3.0.0*. Sept. 2022. DOI: 10.5281/zenodo.7132010. URL: https://zenodo.org/record/7132010.

[17] Cy Chan et al. "Quasi-Dynamic Traffic Assignment using High Performance Computing". In: (2021). DOI: 10.48550/ARXIV.2104.12911. URL: https://arxiv.org/abs/2104.12911.

[18] Liang Chang, Amr S Elnashai, and Billie F Spencer Jr. "Post-earthquake modelling of transportation networks". In: *Structure and infrastructure Engineering* 8.10 (2012), pp. 893–911.

[19] Stephanie E Chang and Nobuoto Nojima. "Measuring post-disaster transportation system performance: the 1995 Kobe earthquake in comparative perspective". In: *Transportation research part A: policy and practice* 35.6 (2001), pp. 475–494.

[20] Stephanie E Chang, Masanobu Shinozuka, and James E Moore. "Probabilistic earthquake scenarios: extending risk analysis methodologies to spatially distributed systems". In: *Earthquake Spectra* 16.3 (2000), pp. 557–572.

[21] Liang-Chieh Chen et al. "Encoder-Decoder with Atrous Separable Convolution for Semantic Image Segmentation". In: *CoRR* abs/1802.02611 (2018). arXiv: 1802.02611. URL: http://arxiv.org/abs/1802.02611.

[22] Xifang Chen et al. "Resilience measurement and analysis of intercity public transportation network". In: *Transportation Research Part D: Transport and Environment* 131 (2024), p. 104202.

[23] Yi-Chang Chiu et al. "Dynamic traffic assignment: A primer (transportation research circular e-c153)". In: (2011).

[24] Sungbin Cho et al. "Integrating transportation network and regional economic models to estimate the costs of a large urban earthquake". In: *Journal of Regional Science* 41.1 (2001), pp. 39–65.

[25] Serdar Çolak, Antonio Lima, and Marta C González. "Understanding congested travel in urban areas". In: *Nature communications* 7.1 (2016), p. 10793.

[26] Louise K Comfort. "Turning conflict into cooperation: Organizational designs for community response in disasters". In: *International Journal of Mental Health* 19.1 (1990), pp. 89–108.

[27] Louise K Comfort, Kilkon Ko, and Adam Zagorecki. "Coordination in rapidly evolving disaster response systems: The role of information". In: *American behavioral scientist* 48.3 (2004), pp. 295–313.

[28] James D. Cooper et al. "The Northridge Earthquake: Progress Made, Lessons Learned in Seismic-Resistant Bridge Design". In: *Public roads* 58 (1994), pp. 26–36. URL: http://www.fhwa.dot.gov/publications/publicroads/94summer/p94su26.cfm.

[29] Sam Dean. *Is the ports logjam really getting better? The numbers don't tell the whole story*. Dec. 2021. URL: https://www.latimes.com/business/story/2021-12-03/officials-say-the-ports-logjam-is-easing-but-numbers-dont-tell-the-whole-story.

[30] You Dong, Dan M Frangopol, and Duygu Saydam. "Sustainability of highway bridge networks under seismic hazard". In: *Journal of earthquake engineering* 18.1 (2014), pp. 41–66.

[31] East Nippon Expressway Company Limited. *Expressway Disaster Recovery and Coordination Framework*. https://www.e-nexco.co.jp/en/activity/safety/detail_04.html. Accessed: 2025-07-03. 2020.

[32] East Nippon Expressway Company Limited and NTT DoCoMo. *Agreement on Cooperation for Disaster Recovery*. https://www.e-nexco.co.jp/en/pressroom/head_office/2021/1001/00010358.html. Accessed: 2025-07-03. 2021.

[33] Kenneth J Elwood. "Modelling Failures in Existing Reinforced Concrete Columns". In: *Canadian Journal of Civil Engineering* 31.5 (2004), pp. 846–859. DOI: 10.1139/l04-040. URL: https://doi.org/10.1139/l04-040.

[34] Federal Highway Administration. *Bridge Replacement Unit Costs 2020*. https://www.fhwa.dot.gov/bridge/nbi/sd2020.cfm. Accessed: 2022-11-16. 2022.

[35] Federal Highway Administration. *Recording and coding guide for the structure inventory and appraisal of the nation's bridges*. Tech. rep. Report No. FHWA-PD-96-001. US Department of Transportation, 1995.

[36] FEMA. *Hazus-MH 2.1 Technical Manual: Earthquake Model*. Federal Emergency Management Agency. Washington, DC, 2003.

[37] Kairui Feng, Quanwang Li, and Bruce R Ellingwood. "Post-earthquake modelling of transportation networks using an agent-based model". In: *Structure and Infrastructure Engineering* 16.11 (2020), pp. 1578–1592.

[38] FHWA. *Recording and Coding Guide for the Structure Inventory and Appraisal of the Nation's Bridges*. Tech. rep. Report No. FHWA-PD-96-001, US Department of Transportation, Federal Highway Administration, Office of Engineering Bridge Division, Washington, DC, 1995.

[39] Fletcher Foti, Paul Waddell, and Dennis Luxen. "A generalized computational framework for accessibility: from the pedestrian to the metropolitan scale". In: *Proceedings of the 4th TRB Conference on Innovations in Travel Modeling. Transportation Research Board*. 2012.

[40] Dan M Frangopol and Paolo Bocchini. "Resilience as optimization criterion for the rehabilitation of bridges belonging to a transportation network subject to earthquake". In: *Structures Congress 2011*. 2011, pp. 2044–2055.

[41] Michael Arthur Goldberg. "On the inefficiency of being efficient". In: *Environment and Planning A* 7.8 (1975), pp. 921–939.

[42] Google. *Google Directions API*. `https://developers.google.com/maps/documentation/directions`. 2022.

[43] Peter Gordon et al. "Earthquake Disaster Mitigation for Urban Transportation Systems: An Integrated Methodology that Builds on the Kobe and Northridge Experiences". In: *Modeling Spatial and Economic Impacts of Disasters* (2004), pp. 205–232. DOI: `10.1007/978-3-540-24787-6{\_}11`.

[44] Kenneth Gwilliam. "Bus Transport: Is There a Regulatory Cycle?" In: *Transport Reviews* 28.3 (2008), pp. 357–378. DOI: `10.1080/01441640701642375`.

[45] Aric Hagberg, Pieter J Swart, and Daniel A Schult. *Exploring network structure, dynamics, and function using NetworkX*. Tech. rep. Los Alamos National Laboratory (LANL), Los Alamos, NM (United States), 2008.

[46] Heejoo Ham, Tschangho John Kim, and David Boyce. "Assessment of economic impacts from unexpected events with an interregional commodity flow and multimodal transportation network model". In: *Transportation Research Part A: Policy and Practice* 39.10 (2005), pp. 849–860.

[47] Darío Hidalgo and Pascal Graftieaux. *Bus Rapid Transit Systems in Latin America and Asia: Results and Difficulties*. Tech. rep. Accessed: 2025-07-03. World Bank, 2008. URL: `https://openknowledge.worldbank.org/handle/10986/17405`.

[48] Fuyu Hu et al. "Recovery of infrastructure networks after localised attacks". In: *Scientific reports* 6.1 (2016), p. 24522.

[49] International Association of Public Transport (UITP). *Mobility and the Sustainable Development Goals*. Tech. rep. Accessed: 2025-07-03. 2022. URL: `https://cms.uitp.org/wp/wp-content/uploads/2022/07/Report-TranspAuthorities-JUNE2022-web.pdf`.

[50] Chris Isidore. *Everything you're waiting for is in these containers*. Oct. 2021. URL: https://www.cnn.com/2021/10/20/business/la-long-beach-port-congestion-problem-national-impact/index.html.

[51] Kishor Jaiswal et al. *Hazus® estimated annualized earthquake losses for the United States*. Tech. rep. FEMA P-366. Federal Emergency Management Agency, Apr. 2017.

[52] F. Jalayer and C. A. Cornell. "Alternative non-linear demand estimation methods for probability-based seismic assessments". In: *Earthquake Engineering & Structural Dynamics* 38.8 (2009), pp. 951–972. DOI: https://doi.org/10.1002/eqe.876. URL: https://onlinelibrary.wiley.com/doi/abs/10.1002/eqe.876.

[53] Kazuhiko Kawashima and Ian Buckle. "Structural Performance of Bridges in the Tohoku-Oki Earthquake". In: *Earthquake Spectra* 29.1_suppl (2013), pp. 315–338. DOI: 10.1193/1.4000129. URL: https://doi.org/10.1193/1.4000129.

[54] Navid Khademi et al. "Transportation network vulnerability analysis for the case of a catastrophic earthquake". In: *International journal of disaster risk reduction* 12 (2015), pp. 234–254.

[55] Payman Khalili-Tehrani et al. "Backbone curves with physical parameters for passive lateral response of homogeneous abutment backfills". In: *Bulletin of Earthquake Engineering* 14.11 (Nov. 2016), pp. 3003–3023. ISSN: 15731456. DOI: 10.1007/s10518-016-9934-3.

[56] Ioannis Kilanitis and Anastasios Sextos. "Impact of earthquake-induced bridge damage and time evolving traffic demand on the road network resilience". In: *Journal of traffic and transportation engineering (English edition)* 6.1 (2019), pp. 35–48.

[57] Anne Kiremidjian et al. "Seismic risk assessment of transportation network systems". In: *Journal of Earthquake Engineering* 11.3 (2007), pp. 371–382.

[58] Eyuphan Koc et al. "CRAFT: Comprehensive Resilience Assessment Framework for Transportation Systems in Urban Areas". In: *Advanced Engineering Informatics* 46 (2020), p. 101159. ISSN: 1474-0346. DOI: https://doi.org/10.1016/j.aei.2020.101159. URL: https://www.sciencedirect.com/science/article/pii/S1474034620301300.

[59] Wassily Leontief. *Input-output economics*. Oxford University Press, 1986.

[60] Wenxin Ma et al. "Resilience evaluation and improvement of post-disaster multimodal transportation networks". In: *Transportation Research Part A: Policy and Practice* 189 (2024), p. 104243.

[61] William J. Mallett. *Public-Private Partnerships (P3s) in Transportation Infrastructure*. Tech. rep. R45010. Congressional Research Service, 2020. URL: https://crsreports.congress.gov/product/pdf/R/R45010.

[62] Sujith Mangalathu. "Performance based grouping and fragility analysis of box-girder bridges in California". PhD thesis. Atlanta, GA: Georgia Institute of Technology, 2017.

[63] Lars-Göran Mattsson and Erik Jenelius. "Vulnerability and resilience of transport systems–A discussion of recent research". In: *Transportation Research Part A: Policy and Practice* 81 (2015), pp. 16–34.

[64] Frank McKenna. "OpenSees: A Framework for Earthquake Engineering Simulation". In: *Computing in Science & Engineering* 13.4 (2011), pp. 58–66. DOI: 10.1109/MCSE.2011.66.

[65] Eric Merschman et al. "Postdisaster decision framework for bridge repair prioritization to improve road network resilience". In: *Transportation research record* 2674.3 (2020), pp. 81–92.

[66] Metropolitan Expressway Company Limited. *Earthquake Disaster Prevention and Civil Protection Operations*. https://www.shutoko.co.jp/en/index/about/initiatives/earthquake/. Accessed: 2025-07-03. 2024.

[67] Sushreyo Misra et al. "An expert opinion survey on post-hazard restoration of roadways and bridges: Data and key insights". In: *Earthquake Spectra* 36.2 (2020), pp. 983–1004.

[68] Mohammad Modarres and Behrouz Zarei. "Application of network theory and AHP in urban transportation to minimize earthquake damages". In: *Journal of the Operational Research Society* 53.12 (2002), pp. 1308–1316.

[69] Jack Moehle and Gregory G Deierlein. "A framework methodology for performance-based earthquake engineering". In: *13th world conference on earthquake engineering*. Vol. 679. 2004.

[70] Jack Moehle and Gregory G. Deierlein. "A framework methodology for performance-based earthquake engineering". In: *Proceedings of the 13th World Conference on Earthquake Engineering*. 2004, pp. 3812–3814. DOI: 10.1061/9780784412121.173.

[71] Susendar Muthukumar. "A Contact Element Approach with Hysteresis Damping for the Analysis and Design of Pounding in Bridges". PhD thesis. Georgia Institute of Technology, 2003.

[72] Hitomi Nakanishi, Kojiro Matsuo, and John Black. "Transportation planning methodologies for post-disaster recovery in regional communities: the East Japan Earthquake and tsunami 2011". In: *Journal of Transport Geography* 31 (2013), pp. 181–191.

[73] Ansgar Neuenhofer and Filip C. Filippou. "Evaluation of Nonlinear Frame Finite-Element Models". In: *Journal of Structural Engineering* 123.7 (1997), pp. 958–966. ISSN: 0733-9445. DOI: 10.1061/(asce)0733-9445(1997)123:7(958).

[74] Bryant G Nielson. *Analytical fragility curves for highway bridges in moderate seismic zones*. Georgia Institute of Technology, 2005.

[75] Nariman Nikoo, Mohsen Babaei, and Afshin Shariat Mohaymany. "Emergency transportation network design problem: Identification and evaluation of disaster response routes". In: *International journal of disaster risk reduction* 27 (2018), pp. 7–20.

[76] Nobuoto Nojima and Masata Sugito. "Simulation and evaluation of post-earthquake functional performance of transportation network". In: *Proceedings of the 12th world conference on earthquake engineering*. New Zealand Society for Earthquake Engineering Upper Hutt. 2000.

[77] Saeed Nozhati. "A resilience-based framework for decision making based on simulation-optimization approach". In: *Structural Safety* 89 (2021), p. 102032.

[78] OpenStreetMap. *OpenStreetMap*. `https://www.openstreetmap.org`. 2022.

[79] Yuki Oyama and Eiji Hato. "A discounted recursive logit model for dynamic gridlock network analysis". In: *Transportation Research Part C: Emerging Technologies* 85 (2017), pp. 509–527.

[80] Sabrina Pabilonia et al. "BLS publishes experimental state-level labor productivity measures". In: *Monthly Labor Review* (June 2019). DOI: 10.21916/mlr.2019.12. URL: https://doi.org/10.21916/mlr.2019.12.

[81] Jamie E Padgett, Reginald DesRoches, and Emily Nilsson. "Regional seismic risk assessment of bridge network in Charleston, South Carolina". In: *Journal of Earthquake Engineering* 14.6 (2010), pp. 918–933.

[82] Xing Pan et al. "Resilience model and recovery strategy of transportation network based on travel OD-grid analysis". In: *Reliability Engineering & System Safety* 223 (2022), p. 108483.

[83] Harold J Payne. "FREFLO: A macroscopic simulation model of freeway traffic". In: *Transportation Research Record* 722 (1979).

[84] Karthik Ramanathan, Jamie E. Padgett, and Reginald DesRoches. "Temporal evolution of seismic fragility curves for concrete box-girder bridges in California". In: *Engineering Structures* 97 (Aug. 2015), pp. 29–46. ISSN: 0141-0296. DOI: 10.1016/J.ENGSTRUCT.2015.03.069. URL: https://www.sciencedirect.com/science/article/pii/S0141029615002229.

[85] Abdollah Shafieezadeh et al. "Fractional order intensity measures for probabilistic seismic demand modeling applied to highway bridges". In: *Earthquake Engineering & Structural Dynamics* 41.3 (2012), pp. 391–409. DOI: https://doi.org/10.1002/eqe.1135. URL: https://onlinelibrary.wiley.com/doi/abs/10.1002/eqe.1135.

[86] Pedro F. Silva, Sami Megally, and Frieder Seible. "Seismic Performance of Sacrificial Exterior Shear Keys in Bridge Abutments". In: *Earthquake Spectra* 25.3 (Aug. 2009), pp. 643–664. ISSN: 8755-2930. DOI: 10.1193/1.3155405. URL: http://journals.sagepub.com/doi/10.1193/1.3155405.

[87] Patrick Small et al. "The SCEC Unified Community Velocity Model Software Framework". In: *Seismological Research Letters* 88.6 (Sept. 2017), pp. 1539–1552. ISSN: 0895-0695. DOI: 10.1785/0220170082. eprint: https://pubs.geoscienceworld.org/ssa/srl/article-pdf/88/6/1539/3950255/srl-2017082.1.pdf. URL: https://doi.org/10.1785/0220170082.

[88] Philippe YR Sohouenou and Luis AC Neves. "Assessing the effects of link-repair sequences on road network resilience". In: *International Journal of Critical Infrastructure Protection* 34 (2021), p. 100448.

[89] Southern California Association of Governments. *Connect SoCal - The 2020-2045 Regional Transportation Plan/Sustainable Communities Strategy*. Tech. rep. Southern California Association of Governments, 2020.

[90] Southern California Association of Governments. *Profile of the City of Anaheim*. http://www.anaheim.net/DocumentCenter/View/13049/SCAG-Demographic-Profile-for-Anaheim?bidId=. Accessed: 2022-06-29. 2019.

[91] Pablo Suarez et al. "Impacts of flooding and climate change on urban transportation: A systemwide performance assessment of the Boston Metro Area". In: *Transportation Research Part D: transport and environment* 10.3 (2005), pp. 231–244.

[92] Hirokazu Tatano and Satoshi Tsuchiya. "A framework for economic loss estimation due to seismic transportation network disruption: a spatial computable general equilibrium approach". In: *Natural Hazards* 44.2 (2008), pp. 253–265.

[93] The White House. *Recent Progress and Actions on Port Congestion*. Nov. 2021. URL: https://www.whitehouse.gov/briefing-room/blog/2021/11/10/recent-progress-and-actions-on-port-congestion/.

[94] Federal Highway Administration U.S. Department of Transportation. *Report on Highway Public–Private Partnership Concessions in the United States*. Tech. rep. Accessed: 2025-07-03. 2016. URL: https://www.fhwa.dot.gov/ipd/pdfs/p3/p3-toolkit_report_on_highway_p3s_122916.pdf.

[95] US Census Bureau. *Tiger/line shapefiles*. Dec. 2021. URL: https://www.census.gov/geographies/mapping-files/time-series/geo/tiger-line-file.html.

[96] US Cybersecurity & Infrastructure Security Agency. *Infrastructure Security*. https://www.cisa.gov/infrastructure-security. 2022.

[97] USBPR. *United States Bureau of Public Roads Traffic Assignment Manual for Application with a Large, High-speed Computer*. Vol. 2. 1964.

[98] Francisco Vasconcelos, João P. Barreto, and Edmond Boyer. "Automatic Camera Calibration Using Multiple Sets of Pairwise Correspondences". In: *IEEE Transactions on Pattern Analysis and Machine Intelligence* 40.4 (2018), pp. 791–803. DOI: 10.1109/TPAMI.2017.2699648.

[99] Michael Benedict Virtucio et al. "A granular framework for modeling the capacity loss and recovery of regional transportation networks under seismic hazards: A case study on the Port of Los Angeles". In: *International Journal of Disaster Risk Reduction* 100 (2024), p. 104164.

[100] AM Wein et al. "Spatial Analysis of Industries, Employment, and Commute Flows in Areas of Concentrated Damage from the HayWired Earthquake Scenario, Chap. V5". In: *The HayWired Earthquake Scenario—Societal Consequences: US Geological Survey Scientific Investigations Report 2017–5013–R–W, 57 P* (2020).

[101] Jidong Wu et al. "Regional indirect economic impact evaluation of the 2008 Wenchuan Earthquake". In: *Environmental Earth Sciences* 65 (2012), pp. 161–172.

[102] Yangyang Wu, Guangyang Hou, and Suren Chen. "Post-earthquake resilience assessment and long-term restoration prioritization of transportation network". In: *Reliability Engineering & System Safety* 211 (2021), p. 107612.

[103] Weili Zhang, Naiyu Wang, and Charles Nicholson. "Resilience-based post-disaster recovery strategies for road-bridge networks". In: *Structure and Infrastructure Engineering* 13.11 (2017), pp. 1404–1413.

[104] B. Zhao et al. "Agent-Based Model (ABM) for City-Scale Traffic Simulation: A Case Study on San Francisco". In: *International Conference on Smart Infrastructure and Construction 2019 (ICSIC)*. ICE Publishing, 2019, pp. 203–212. DOI: 10.1680/icsic.64669.203. eprint: https://www.icevirtuallibrary.com/doi/pdf/10.1680/icsic.64669.203. URL: https://www.icevirtuallibrary.com/doi/abs/10.1680/icsic.64669.203.

[105] Yichao Zhou, Haozhi Qi, and Yi Ma. "End-to-End Wireframe Parsing". In: *ICCV 2019*. 2019.

[106] Youwei Zhou, Swagata Banerjee, and Masanobu Shinozuka. "Socio-economic effect of seismic retrofit of bridges for highway transportation networks: a pilot study". In: *Structure and Infrastructure Engineering* 6.1-2 (2010), pp. 145–157.

Appendix A

MEX and NEXCO route groupings

The highways that MEX and NEXCO manage are divided into several predefined routes.

A.1 MEX routes

MEX has a total of 23 routes. These are:

- Circumferential routes
  - C1 Inner Circular Route
  - C2 Central Circular Route
  - Y Yaesu Route
  - B Bayshore Route
- Radial routes
  - No. 1 Ueno Route & Haneda Route
  - No. 2 Meguro Route
  - No. 3 Shibuya Route
  - No. 4 Shinjuku Route
  - No. 5 Ikebukuro Route
  - No. 6 Mukojima Route & Misato Route
  - No. 7 Komatsugawa Route
  - No. 9 Fukagawa Route
  - No. 10 Harumi Route
  - No. 11 Daiba Route
- Kanagawa routes

  - K1 Yokohane Route
  - K2 Mitsuzawa Route
  - K3 Kariba Route
  - K5 Daikoku Route
  - K6 Kawasaki Route
  - K7 Yokohama North Route & Yokohama Northwest Route
- Saitama routes
  - S1 Kawaguchi Route
  - S2 Saitama Shintoshin Route
  - S5 Omiya Route

These routes are shown in Figure A.1.

A.2 NEXCO routes

NEXCO has a total of 16 routes in the Tokyo Metropolitan Area. These are:

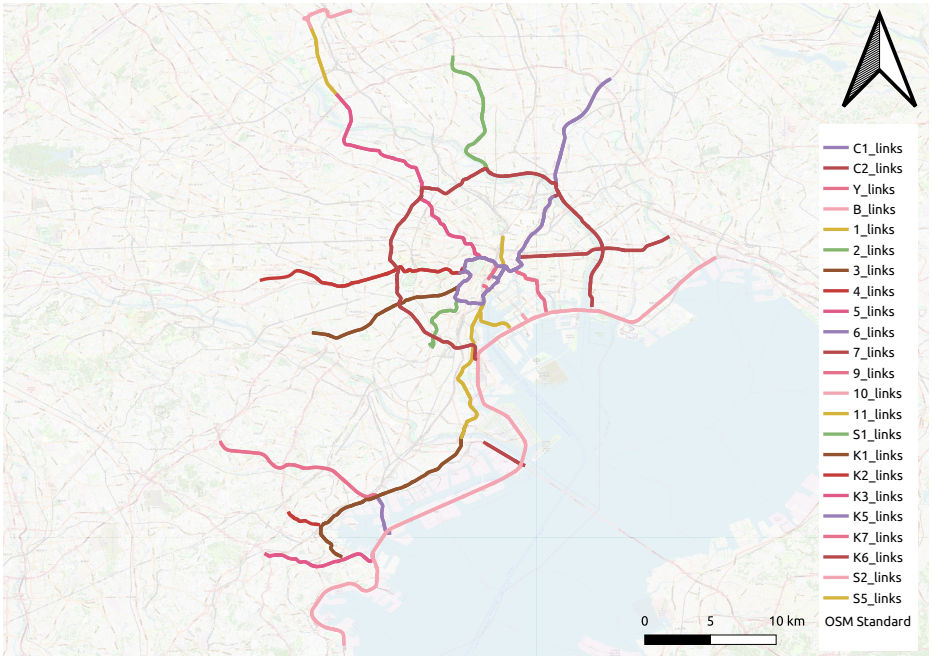


Figure A.1: MEX routes

- E1 Tōmei Expressway
- E1A Shin-Tōmei Expressway
- E4 Tōhoku Expressway
- E6 Jōban Expressway
- E14 Keiyō / Tateyama Expressway
- E16 Yokohama–Yokosuka Expressway
- E17 Kan-Etsu Expressway
- E20 Chūō Expressway
- E51 Higashi-Kantō Expressway
- E65 Shin-Kūkō Expressway
- E82 Chiba–Tōgane Road
- E83 Daisan-Keihin / Yokohama-Shindō
- E84 Seishō By-pass
- C3 Tokyo-Gaikan Expressway
- C4 Ken-Ō Expressway
- CA Tokyo-Wan Aqua-Line

These routes are shown in Figure A.2.

A.3 Grouping criteria

As mentioned in Chapter 5, the above routes were grouped into 10 groups for each agency using the following criteria: (1) spatial proximity, (2) similar total length per group—approximately 65 km for MEX and 200 km for NEXCO, given NEXCO's larger network scale (this is to ensure that a group is not ranked higher on the repair sequence simply because it is longer and has more coverage), and (3) longer routes were split and grouped based on geographic adjacency. The resulting groups are described in the following sections.

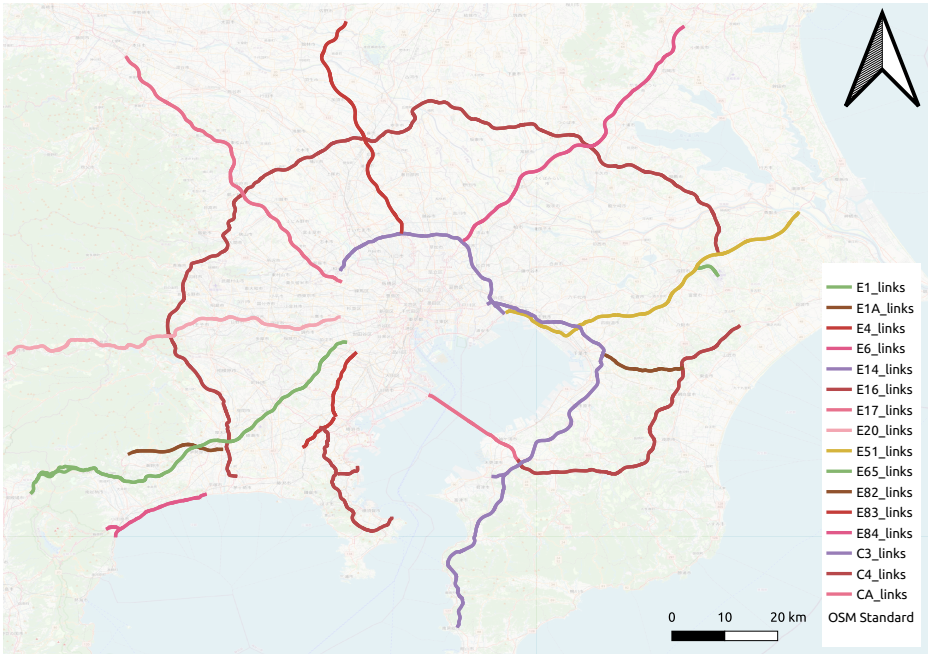


Figure A.2: NEXCO routes

A.4 MEX groups

- Group A: C1, Y, 1
- Group B: B (southern half)
- Group C: B (northern half)
- Group D: K1, K2, K6
- Group E: K3, K5, K7
- Group F: C2 (western half), 4
- Group G: C2 (eastern half), 7
- Group H: 5, S2, S5
- Group I: 2, 3, 9, 10, 11
- Group J: 6, S1

These groups are shown in Figure 5.3.

A.5 NEXCO groups

- Group A: E1, E1A
- Group B: E14
- Group C: CA, E82, C4 (southeastern part)
- Group D: C4 (northeastern part)
- Group E: C4 (western part)
- Group F: E16, E83, E84
- Group G: E20
- Group H: E4, E17
- Group I: C3 (northern part), E6
- Group J: C3 (eastern part), E51, E65

These groups are shown in Figure 5.4.

Appendix B

Recovery/reopening sequences

Route groups are ranked based on the strategy and level of coordination chosen by each agency. This essentially means that the criteria is applied either to individual highway systems or as one whole system. This leads to the following sequences for MEX and NEXCO for each strategy:

1. Volume-based (computed as separate systems)
    - MEX sequence
        a) G
        b) J
        c) H
        d) F
        e) A
        f) I
        g) D
        h) C
        i) E
        j) B
    - NEXCO sequence
        a) H
        b) B
        c) A
        d) I
        e) F
        f) J
        g) C

h) G
i) E
j) D

2. Betweenness-based (computed as separate systems)

- MEX sequence
  a) C
  b) A
  c) D
  d) E
  e) J
  f) I
  g) G
  h) F
  i) B
  j) H
- NEXCO sequence
  a) E
  b) D
  c) J
  d) B
  e) I
  f) H
  g) A
  h) F
  i) C
  j) G

3. Route-based (computed as separate systems)

- MEX sequence
  a) G
  b) J
  c) H
  d) F
  e) A
  f) I

g) D
h) C
i) E
j) B

- NEXCO sequence
  a) H
  b) I
  c) J
  d) B
  e) C
  f) E
  g) A
  h) G
  i) D
  j) F

4. Volume-based (computed as unified system)
   a) NEXCO H
   b) MEX G
   c) NEXCO B
   d) MEX J
   e) NEXCO A
   f) MEX H
   g) MEX F
   h) MEX A
   i) NEXCO I
   j) MEX I
   k) NEXCO F
   l) MEX D
   m) NEXCO J
   n) NEXCO C
   o) NEXCO G
   p) MEX C
   q) NEXCO E

r) MEX E
s) NEXCO D
t) MEX B

5. Betweenness-based (computed as unified system)

a) MEX C
b) MEX J
c) MEX D
d) MEX A
e) NEXCO F
f) MEX G
g) MEX I
h) NEXCO A
i) NEXCO B
j) MEX E
k) NEXCO I
l) NEXCO H
m) NEXCO C
n) MEX F
o) NEXCO E
p) MEX B
q) NEXCO G
r) NEXCO J
s) NEXCO D
t) MEX H

6. Route-based (computed as unified system)

a) NEXCO H
b) MEX J
c) MEX G
d) NEXCO B
e) MEX H
f) MEX F

g) MEX A
h) NEXCO I
i) MEX I
j) NEXCO A
k) MEX D
l) NEXCO F
m) NEXCO J
n) NEXCO C
o) NEXCO G
p) MEX C
q) NEXCO E
r) MEX E
s) NEXCO D
t) MEX B

The above sequence for each strategy and level of coordination translate to the following recovery/reopening sequence for each of the 15 final coordination scenarios:

- S1: Uncoordinated; MEX route-based, NEXCO betweenness-based
  - Time step 1: Open MEX G
  - Time step 2: Open MEX J
  - Time step 3: Open MEX H, NEXCO E
  - Time step 4: Open MEX F
  - Time step 5: Open MEX A
  - Time step 6: Open MEX I, NEXCO D
  - Time step 7: Open MEX D
  - Time step 8: Open MEX C
  - Time step 9: Open MEX E, NEXCO J
  - Time step 10: Open MEX B
  - Time step 12: Open NEXCO B
  - Time step 15: Open NEXCO I
  - Time step 18: Open NEXCO H
  - Time step 21: Open NEXCO A

  - Time step 24: Open NEXCO F
  - Time step 27: Open NEXCO C
  - Time step 30: Open NEXCO G

- S2: Uncoordinated; MEX betweenness-based, NEXCO route-based
  - Time step 1: Open MEX C
  - Time step 2: Open MEX A
  - Time step 3: Open MEX D, NEXCO E
  - Time step 4: Open MEX E
  - Time step 5: Open MEX J
  - Time step 6: Open MEX I, NEXCO D
  - Time step 7: Open MEX G
  - Time step 8: Open MEX F
  - Time step 9: Open MEX B, NEXCO J
  - Time step 10: Open MEX H
  - Time step 12: Open NEXCO B
  - Time step 15: Open NEXCO I
  - Time step 18: Open NEXCO H
  - Time step 21: Open NEXCO A
  - Time step 24: Open NEXCO F
  - Time step 27: Open NEXCO C
  - Time step 30: Open NEXCO G

- S3: Uncoordinated; MEX betweenness-based, NEXCO volume-based
  - Time step 1: Open MEX C
  - Time step 2: Open MEX A
  - Time step 3: Open MEX D, NEXCO H
  - Time step 4: Open MEX E
  - Time step 5: Open MEX J
  - Time step 6: Open MEX I, NEXCO B
  - Time step 7: Open MEX G
  - Time step 8: Open MEX F
  - Time step 9: Open MEX B, NEXCO A

  - Time step 10: Open MEX H
  - Time step 12: Open NEXCO I
  - Time step 15: Open NEXCO F
  - Time step 18: Open NEXCO J
  - Time step 21: Open NEXCO C
  - Time step 24: Open NEXCO G
  - Time step 27: Open NEXCO E
  - Time step 30: Open NEXCO D

- S4: Low-level coordination; MEX & NEXCO betweenness-based
  - Time step 1: Open MEX C
  - Time step 2: Open MEX A
  - Time step 3: Open MEX D, NEXCO E
  - Time step 4: Open MEX E
  - Time step 5: Open MEX J
  - Time step 6: Open MEX I, NEXCO D
  - Time step 7: Open MEX G
  - Time step 8: Open MEX F
  - Time step 9: Open MEX B, NEXCO J
  - Time step 10: Open MEX H
  - Time step 12: Open NEXCO B
  - Time step 15: Open NEXCO I
  - Time step 18: Open NEXCO H
  - Time step 21: Open NEXCO A
  - Time step 24: Open NEXCO F
  - Time step 27: Open NEXCO C
  - Time step 30: Open NEXCO G

- S5: Low-level coordination; MEX & NEXCO route-based
  - Time step 1: Open MEX G
  - Time step 2: Open MEX J
  - Time step 3: Open MEX H, NEXCO H
  - Time step 4: Open MEX F

  - Time step 5: Open MEX A
  - Time step 6: Open MEX I, NEXCO I
  - Time step 7: Open MEX D
  - Time step 8: Open MEX C
  - Time step 9: Open MEX E, NEXCO J
  - Time step 10: Open MEX B
  - Time step 12: Open NEXCO B
  - Time step 15: Open NEXCO C
  - Time step 18: Open NEXCO E
  - Time step 21: Open NEXCO A
  - Time step 24: Open NEXCO G
  - Time step 27: Open NEXCO D
  - Time step 30L Open NEXCO F

- S6: Medium-level coordination; MEX & NEXCO volume-based
  - Time step 1: Open MEX G
  - Time step 2: Open MEX J
  - Time step 3: Open MEX H, NEXCO H
  - Time step 4: Open MEX F
  - Time step 5: Open MEX A
  - Time step 6: Open MEX I, NEXCO B
  - Time step 7: Open MEX D
  - Time step 8: Open MEX C
  - Time step 9: Open MEX E, NEXCO A
  - Time step 10: Open MEX B
  - Time step 12: Open NEXCO I
  - Time step 15: Open NEXCO F
  - Time step 18: Open NEXCO J
  - Time step 21: Open NEXCO C
  - Time step 24: Open NEXCO G
  - Time step 27: Open NEXCO E
  - Time step 30: Open NEXCO D

- S7: Medium-level coordination; MEX & NEXCO betweenness-based
  - Time step 1: Open MEX C
  - Time step 2: Open MEX J
  - Time step 3: Open MEX D, NEXCO F
  - Time step 4: Open MEX A
  - Time step 5: Open MEX G
  - Time step 6: Open MEX I, NEXCO A
  - Time step 7: Open MEX E
  - Time step 8: Open MEX F
  - Time step 9: Open MEX B, NEXCO B
  - Time step 10: Open MEX H
  - Time step 12: Open NEXCO I
  - Time step 15: Open NEXCO H
  - Time step 18: Open NEXCO C
  - Time step 21: Open NEXCO E
  - Time step 24: Open NEXCO G
  - Time step 27: Open NEXCO J
  - Time step 30: Open NEXCO D
- S8: Medium-level coordination; MEX & NEXCO route-based
  - Time step 1: Open MEX J
  - Time step 2: Open MEX G
  - Time step 3: Open MEX H, NEXCO H
  - Time step 4: Open MEX F
  - Time step 5: Open MEX A
  - Time step 6: Open MEX I, NEXCO B
  - Time step 7: Open MEX D
  - Time step 8: Open MEX C
  - Time step 9: Open MEX E, NEXCO I
  - Time step 10: Open MEX B
  - Time step 12: Open NEXCO A
  - Time step 15: Open NEXCO F

  - Time step 18: Open NEXCO J
  - Time step 21: Open NEXCO C
  - Time step 24: Open NEXCO G
  - Time step 27: Open NEXCO E
  - Time step 30: Open NEXCO D

- S9: High-level coordination; MEX & NEXCO volume-based
  - Time step 1.5: Open NEXCO H
  - Time step 2: Open MEX G
  - Time step 3.5: Open NEXCO B
  - Time step 4: Open MEX J
  - Time step 5.5: Open NEXCO A
  - Time step 6: Open MEX H
  - Time step 6.5: Open MEX F
  - Time step 7: Open MEX A
  - Time step 8.5: Open NEXCO I
  - Time step 9: Open MEX I
  - Time step 10.5: Open NEXCO F
  - Time step 11: Open MEX D
  - Time step 12.5: Open NEXCO J
  - Time step 14: Open NEXCO C
  - Time step 15.5: Open NEXCO G
  - Time step 16: Open MEX C
  - Time step 17.5: Open NEXCO E
  - Time step 18: Open MEX E
  - Time step 19.5: Open NEXCO D
  - Time step 20: Open MEX B

- S10: High-level coordination; MEX & NEXCO betweenness-based
  - Time step 0.5: Open MEX C
  - Time step 1: Open MEX J
  - Time step 1.5: Open MEX D
  - Time step 2: Open MEX A

  - Time step 3.5: Open NEXCO F
  - Time step 4: Open MEX G
  - Time step 4.5: Open MEX I
  - Time step 6: Open NEXCO A
  - Time step 7.5: Open NEXCO B
  - Time step 8: Open MEX E
  - Time step 9.5: Open NEXCO I
  - Time step 11: Open NEXCO H
  - Time step 12.5: Open NEXCO C
  - Time step 13: Open MEX F
  - Time step 14.5: Open NEXCO E
  - Time step 15: Open MEX B
  - Time step 16.5: Open NEXCO G
  - Time step 18: Open NEXCO J
  - Time step 19.5: Open NEXCO D
  - Time step 20: Open MEX H

- S11: High-level coordination; MEX & NEXCO route-based
  - Time step 1.5: Open NEXCO H
  - Time step 2: Open MEX J
  - Time step 2.5: Open MEX G
  - Time step 4: Open NEXCO B
  - Time step 4.5: Open MEX H
  - Time step 5: Open MEX F
  - Time step 5.5: Open MEX A
  - Time step 7: Open NEXCO I
  - Time step 7.5: Open MEX I
  - Time step 9: Open NEXCO A
  - Time step 9.5: Open MEX D
  - Time step 11: Open NEXCO F
  - Time step 12.5: Open NEXCO J
  - Time step 14: Open NEXCO C

- Time step 15.5: Open NEXCO G
- Time step 16: Open MEX C
- Time step 17.5: Open NEXCO E
- Time step 18: Open MEX E
- Time step 19.5: Open NEXCO D
- Time step 20: Open MEX B

Appendix C

Coordination scenario recovery curves

Each coordination scenario was run three times with different random seeds. The following figures show the three recovery curves generated for each coordination scenario. The metrics calculated in Table 5.3 are based on these recovery curves.

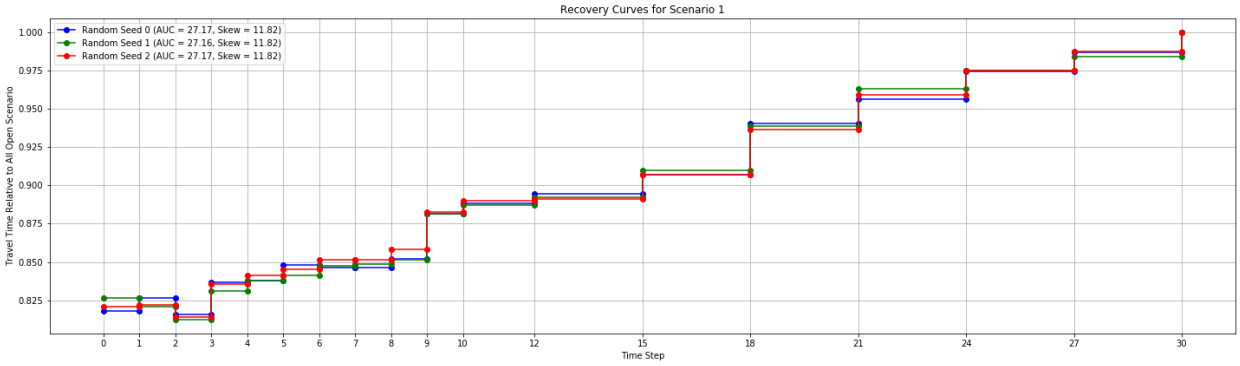


Figure C.1: Recovery curves for Scenario 1

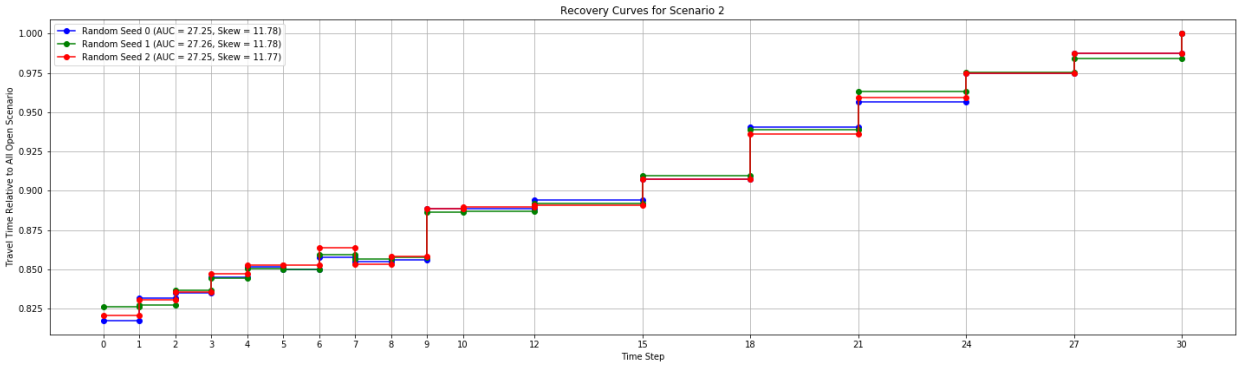


Figure C.2: Recovery curves for Scenario 2

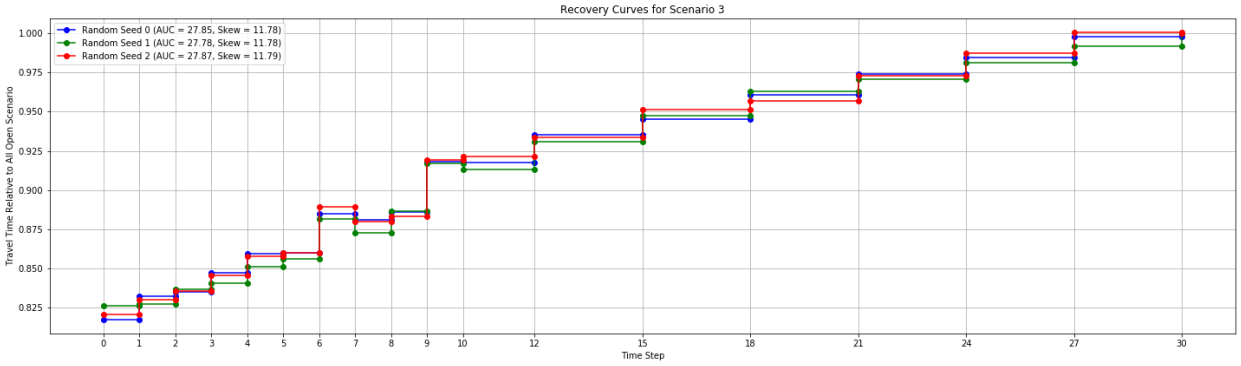


Figure C.3: Recovery curves for Scenario 3

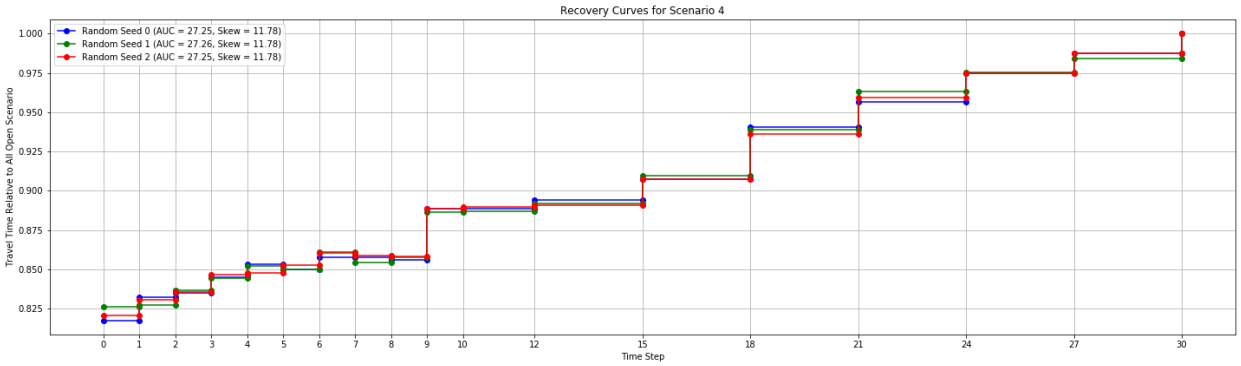


Figure C.4: Recovery curves for Scenario 4

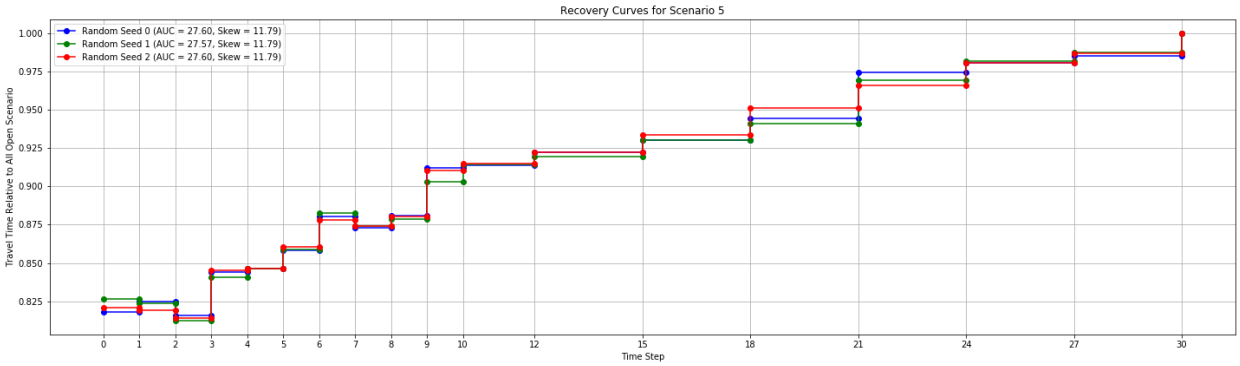


Figure C.5: Recovery curves for Scenario 5

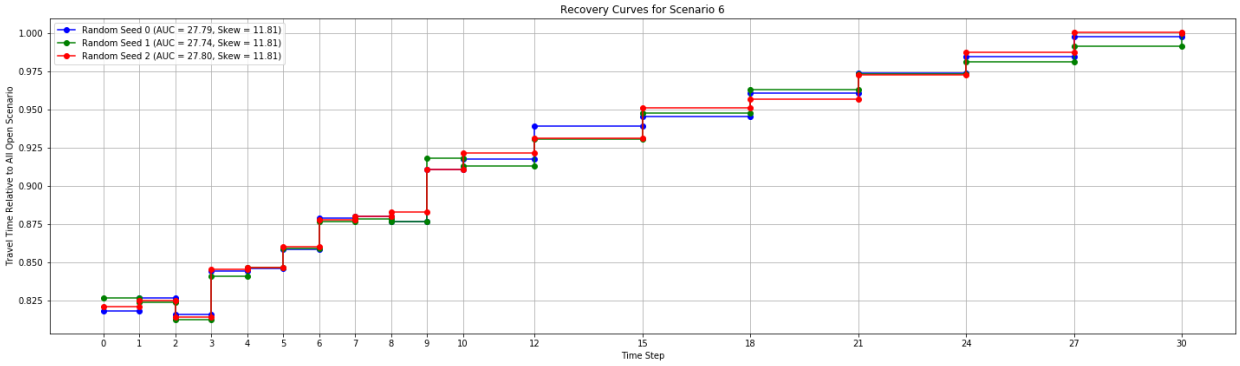


Figure C.6: Recovery curves for Scenario 6

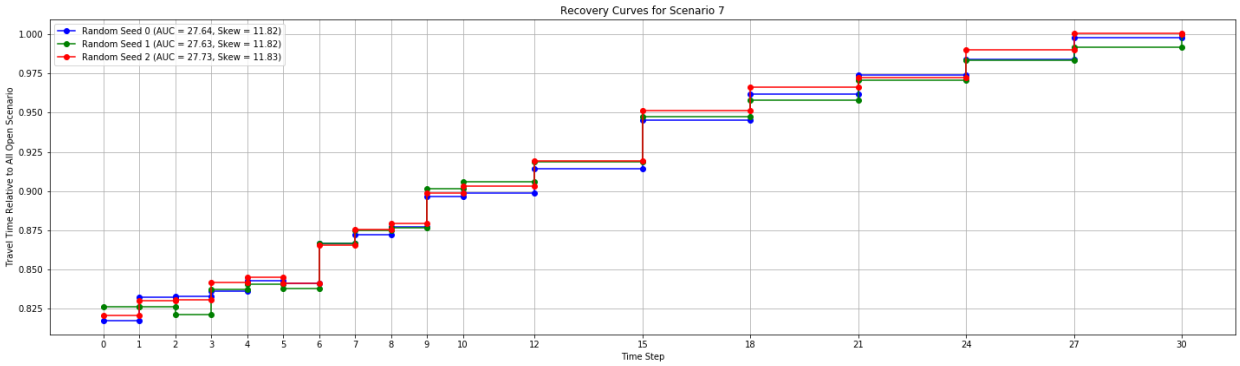


Figure C.7: Recovery curves for Scenario 7

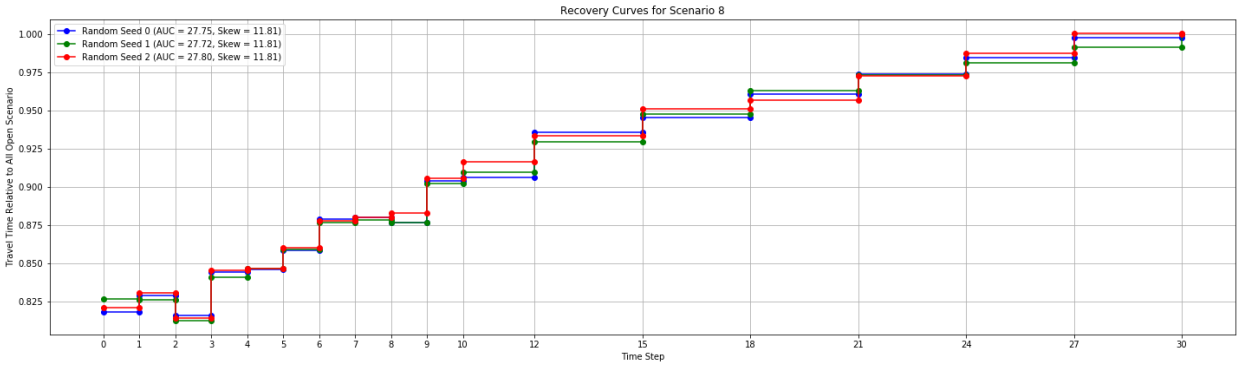


Figure C.8: Recovery curves for Scenario 8

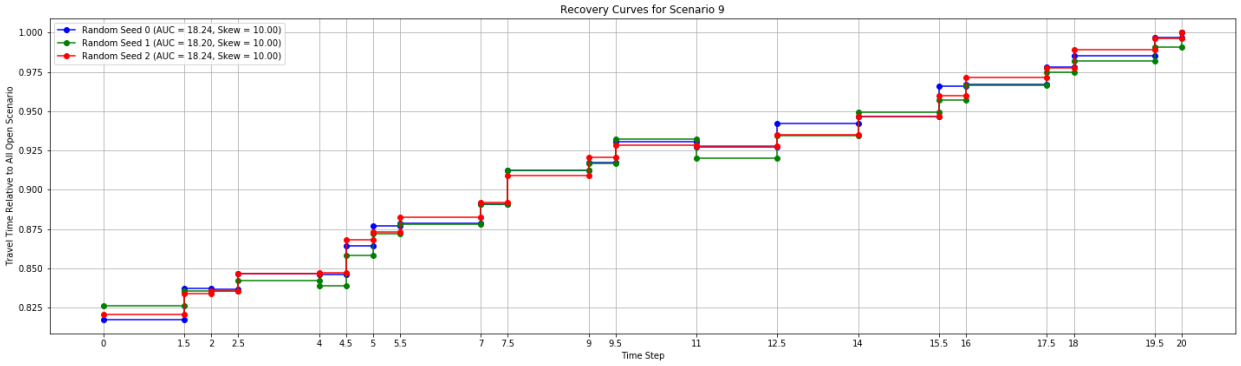


Figure C.9: Recovery curves for Scenario 9

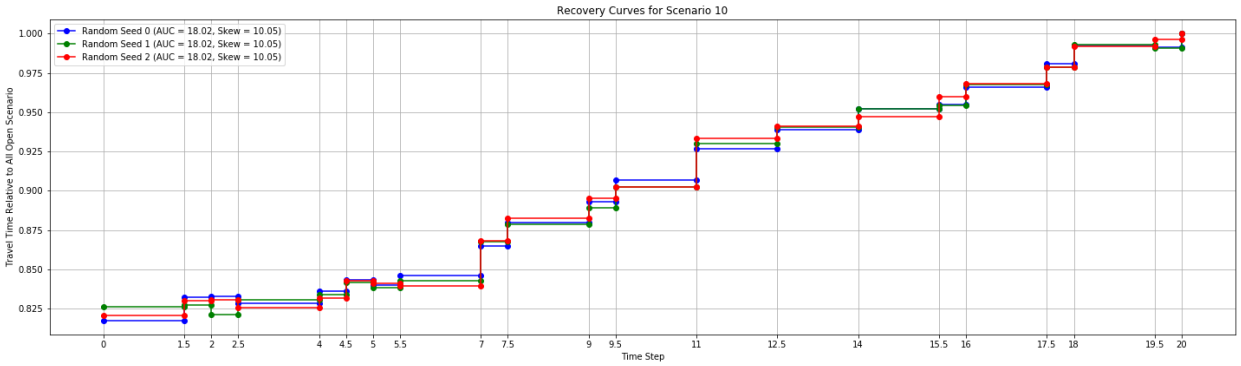


Figure C.10: Recovery curves for Scenario 10

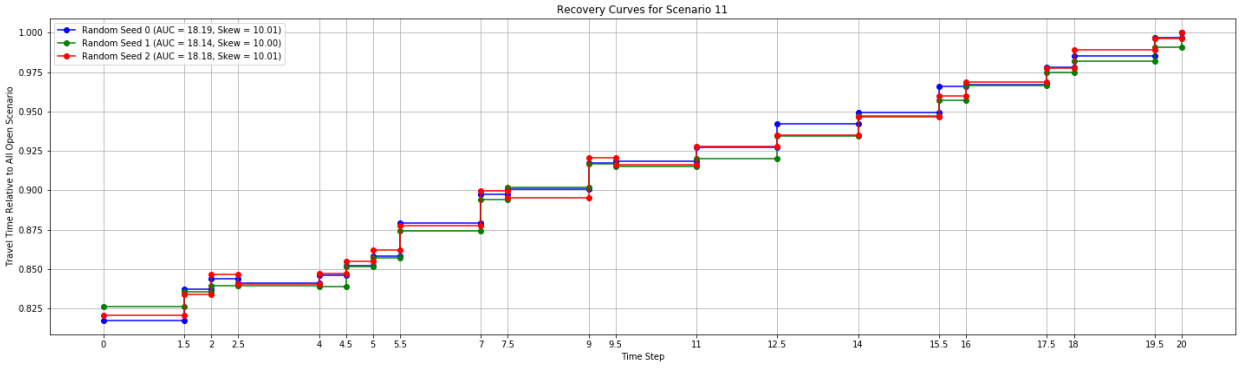


Figure C.11: Recovery curves for Scenario 11

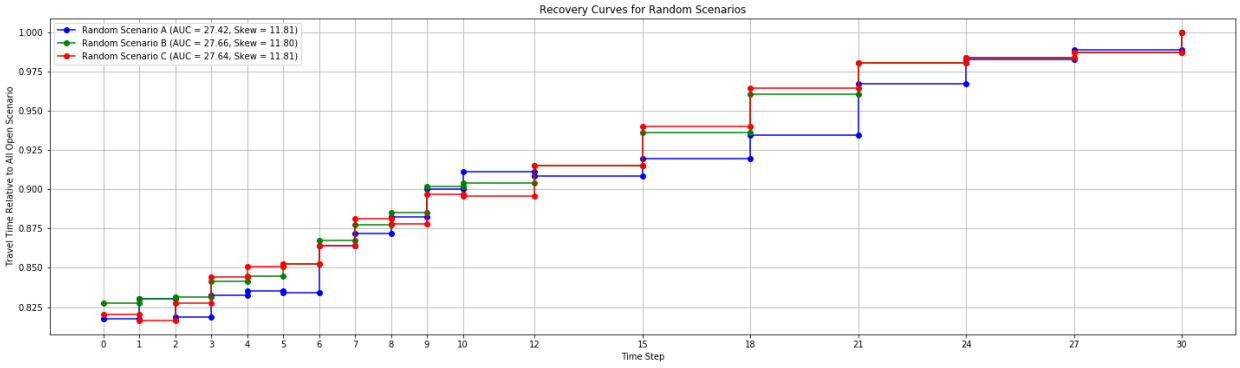


Figure C.12: Recovery curves for random scenarios